Titre: Title:	Design and realization of all-fiber mode separating couplers
Auteur: Author:	Yuanxin Shou
Date:	1999
Type:	Mémoire ou thèse / Dissertation or Thesis
Référence: Citation:	Shou, Y. (1999). Design and realization of all-fiber mode separating couplers [Ph.D. thesis, École Polytechnique de Montréal]. PolyPublie. https://publications.polymtl.ca/8646/

Document en libre accès dans PolyPublie
Open Access document in PolyPublie

URL de PolyPublie: PolyPublie URL:	https://publications.polymtl.ca/8646/
Directeurs de recherche: Advisors:	Jacques Bures
Programme: Program:	Unspecified

UNIVERSITÉ DE MONTRÉAL

DESIGN AND REALIZATION OF ALL-FIBER
MODE SEPARATING COUPLERS

YUANXIN SHOU

DÉPARTEMENT DE GÉNIE PHYSIQUE
ET DE GÉNIE DES MATÉRIAUX
ÉCOLE POLYTECHNIQUE MONTRÉAL

THÈSE PRÉSENTÉE EN VUE DE L'OBTENTION
DU DIPLÔME DE PHILOSOPHIÆ DOCTOR (Ph.D)

(GÉNIE PHYSIQUE)

AVRIL, 1999

Your file Votre référence

Our file Notre référence

0-612-48894-2

Canada

UNIVERSITÉ DE MONTRÉAL

ÉCOLE POLYTECHNIQUE DE MONTRÉAL

Cette thèse intitulée:

DESIGN AND REALIZATION OF ALL-FIBER
MODE SEPARATING COUPLERS

présenté par : SHOU Yuanxin

en vue de l'obtention du diplôme de : Philosophiæ Doctor

a été dûment acceptée par le jury d'examen constitué de :

M. FAUCHER Guy, D.Sc., président

M. BURES Jacques, D.Sc., membre et directeur de recherche

Mme. LACROIX Suzanne, D.Sc., membre

M. OUELLETTE François, Ph.D., membre

To My parents
Gao Shou and Juhong Hu

Acknowledgments

I sincerely thank my supervisor, Prof. Jacques Bures, for his excellent supervision and guidance throughout the course of this thesis work. His kindness, patience and encouragement during my full four years studying at Ecole Polytechnique deserve my deepest gratitude.

I am also very grateful to Prof. Suzanne Lacroix for her invaluable suggestions, warm encouragement and technical help through this Ph.D research program.

I thank Dr. Xavier Daxhelet for his wonderful cooperation, fruitful discussion and indispensable assistance on many simulation programs during this study.

I thank Dr. François Gonthier, Mr. Nicolas Godbout and Mr. René Ghosh for numerous valuable discussions and constant assistance at various stages.

I appreciate the kind cooperation from Mr. Emmanuel Marin, Mr. Denis Ricard, Mr. Arnaud Symon, and Mr. Lilian Martineau.

Finally, I wish to express my special gratitude to my wife Erlian for her love, understanding and unyielding encouragement during the good and the difficult times encountered along the way.

Summary

In optical communication systems, the time division multiplexing (TDM) and wavelength division multiplexing (WDM) are the common techniques employed to transmit more channel signals in a single fiber. Mode division multiplexing (MDM) as an innovative technique has been proposed to be used in local area network (LAN) and metropolitan area networking (MAN) to add more channels. The key component in MDM is the mode separating coupler (MSC) used to separate the signals carried by each mode. The mode separating coupler is also used in two-mode fiber optical sensor systems to measure the intensity variation of the LP_{01} and LP_{11} modes simultaneously. An external perturbation, such as strain or temperature, can be observed by comparing the intensity difference between the LP_{01} and LP_{11} modes, and this is more precise than the conventional measurement of the far-field pattern.

In this present thesis, I investigate the possibility of fabricating an all-fiber mode separating coupler by using the polishing method, fusion and tapering method and other various methods. A supermode analysis from a model for the single mode fiber couplers into two-mode fiber couplers was developed and the transmission properties of two-mode couplers were obtained. The finite difference method was used in the simulation for the polished mode separating couplers case. Both uniform and parabolic coupler structures were considered. The results show that it is possible to fabricate a mode separating coupler by polishing circular core fibers, but the fabrication requirements are very

rigorous. However, using polished elliptical core fiber has certain advantages, such as the large tolerance and simpler mode separation conditions.

Fusion and tapering couplers have been studied for more than a decade, but most of the research is concentrated on the single mode fiber couplers. In this dissertation, special attention is given to fusion and tapering two-mode fiber couplers. First, the longitudinal shapes of the coupler were modeled with various flame widths and flame sweep distances. Then, the effective indices of the supermodes were calculated with the fiber mode expansion method (FMEM). Finally, the transmission was obtained by the transfer matrix method. In addition, the beat lengths, the birefringence and the adiabatic criteria for the two-mode fiber coupler case were studied. In contrast to single mode fiber couplers, the transmission properties of two-mode fiber couplers are more sensitive to the fiber core shape and the relative index difference profile.

In order to depict the transmission precisely, three hypotheses based on experimental measurements were used for the simulation process. First, the cross section of the fiber core evolves from a circle into an ellipse after heating the two parallel fibers; second, the refractive index difference between the core and cladding decreases as a linear function of inverse taper ratio (ITR) (defined as the ratio of coupler transversal dimension over the double fiber initial diameter), due to dopant diffusion during the fusion process; third, after heating, the index profile evolves from a step to a graded profile. However, for simplicity, the equivalent step profile is used.

Pre-etching and prepolishing methods were first used to fabricate the flat spectrum response asymmetric couplers. Here, these techniques were introduced in the fabrication of two-mode couplers to satisfy the adiabatic condition. The simulation results demonstrated that using the pre-etching and prepolishing methods has certain advantages,

especially, for the couplers made of elliptical core fibers. This is because that the pre-etching and prepolishing method could help to realize the mode separating with a short elongation and a short flame sweep distances, making the adiabatic conditions are more easily satisfied. Besides, highly elliptical core and thermally expanded core fibers are considered to be used in the fabrication of mode separating couplers. The numerical results show that these kinds of fibers are good for the fabrication of mode separating couplers, especially, highly elliptical core fibers make the mode separation conditions much simpler because only the LP_{01} and even LP_{11} modes propagate in it.

The all-fiber mode separating coupler was first realized by the fusion and tapering method in this dissertation. Compared with a mode separating coupler consisting of a polished fiber stacked on a prism, the all-fiber mode separating coupler has better mechanical stability, and can be fabricated quickly at less cost. During the fabrication process, the LP_{11} mode excitation and stripping, were respectively implemented by offset splices and wound fiber coils of small radius. The proper offset distance and fiber coil radius were calculated and executed in practice. For a MSC, the transfer efficiency of the LP_{11} mode depends on the beat synchronization of two orientation LP_{11} modes at certain elongation points. This beat synchronization can be adjusted by fusion time and flame sweep distance and is more sensitive to the latter. The best packaged samples demonstrated for these kinds of mode separating couplers had a high transfer efficiency of 92.3% and low excess loss of 0.2 dB. Finally, a numerical analysis based on the experimental parameters and the above three hypotheses was done. The calculation results are in good agreement with the experimental results, therefore confirming the validation of the analysis method used in this dissertation.

In conclusion, all-fiber mode separating couplers were successfully realized by using the fusion and tapering method, with a mode transfer efficiency as high as 92.3%. The numerical analysis is in very good agreement with the experimental results taking into account the variation of fiber core shape and refractive index profile. Furthermore, improvements for fabricating mode separating couplers in the future are proposed.

Abstract

The mode separating coupler is a key component for mode division multiplexing (MDM) techniques and two-mode fiber sensor systems. The existing mode separating couplers are made of a polished fiber stacked on a prism, which is unstable and has high insertion loss. The aim of the work described in this dissertation was to develop an all-fiber mode separating coupler that has good mechanical and thermal stability, low loss and compatible in optical fiber systems.

Using scalar supermode formalism as the basis, the finite difference and fiber mode expansion methods were used to study the feasibility of the fabrication of the all-fiber mode separating coupler with polishing, fusion and tapering method, and other various methods. For the polishing method, the coupler structure could be uniform or parabolic according to the fiber polishing ways and the fiber could have a circular or an elliptical core. The simulation results show that it is possible to make a mode separating coupler with both uniform and parabolic structures. However, using circular core fibers requires precise polished depth and coupling length that may be difficult to realize in practice. Elliptical core fibers have certain advantages and make the fabrication of the mode separating couplers relatively easy. For the fusion and tapering method, both the circular and elliptical core fiber couplers were modeled and the numerical results show that both circular and elliptical core fused couplers are able to act as mode separating couplers if their structure is properly designed. In order to relax the fabrication requirements and

realize adiabatic couplers, some improvements such as pre-etching and prepolishing techniques as well as thermally expanded core fibers and highly elliptical core fibers are proposed.

An all-fiber mode separating coupler was realized by the fusion and tapering method for the first time. The LP_{11} mode transfer efficiency reaches as high as 92.3% and the excess loss is as low as 0.2 dB. A numerical simulation that takes into account the variation of core shape and relative refractive index is in very good in agreement with the experiment al results, which confirms our theoretical understanding of the mode separating coupler.

Condensé en Français

Dans les systèmes de communications, pour transmettre plus d'un signal temporel ou plus d'une longueur d'onde, les techniques de multiplexage sont couramment utilisées. Toutefois, une méthode appelée technique de multiplexage des modes, peut être appliquée en plus des techniques conventionnelles pour augmenter la capacité de transmission des réseaux déjà implantés ou à venir. En 1992, Schmauss et al. [1] ont démontré la réussite d'une transmission réalisée avec deux modes codés. Dans cette technique, le composant le plus important est le séparateur de modes qui permet à la sortie d'avoir accès au signal transporté par chaque mode.

Récemment, de nombreuses recherches ont été publiées sur les fibres à deux modes et leurs composants, comme les coupleurs modaux [2-5], les accéléromètres [6], les jauges de contraintes [7], les composants pour déplacer la fréquence [8, 9], les compensateurs de dispersion [10], les détecteurs à quadrature de phase [11]. Ces composants ont des avantages distincts par rapport à leurs homologues réalisés avec des fibres monomodes, liés à leurs immunités à certains paramètres et à leurs grandes sensibilités à d'autres. Par example, des capteurs fabriqués avec des fibres bimodales basées sur l'interférence entre le mode LP_{01} et le mode LP_{11} propagatifs ont montré leurs avantages sur les conventionnels interféromètres à deux bras, par leurs simplicités et leurs stabilités ouvrant des possibilités attractives pour les capteurs de contraintes [12-14] de stress [15], de température [7], et de tension [16]. A présent les capteurs réalisés avec des fibres

bimodales sont considérés comme les plus appropriés pour réaliser de intelligent structures.

Pour les capteurs réalisés avec des fibres bimodales la méthode d'analyse standard implique une mesure de la puissance optique échangée entre les deux distributions d'intensité des champs lointains dans le cas où l'on veut déterminer la nature de la perturbation externe. Plusieurs techniques de détection pour ces capteurs ont été suggérées. Une technique élémentaire est de placer un démodulateur spatial dans un petit trou, lequel échantillonne seulement une partie du champ lointain [17]. Une technique de traitement du signal optique utilise une barrette de CCD pour analyser le champ lointain à la sortie de la fibre multimode qui supporte les capteurs; elle a été démontrée dans la référence [18]. La plupart de ces méthodes requièrent un système permettant de visualiser la répartition du champ lointain en sortie de fibre. Ceci n'est pas une solution optimale pour des capteurs mobiles pour lesquels la région sensible peut être un environnement hostile. Murphy et al. [13] ont utilisé une épissure avec décalage entre la fibre bimodale et une fibre unimodale, et ainsi en mesurant l'intensité en sortie de celle-ci ils déterminent la contrainte. Toutefois, ces méthodes sont toutes basées sur la mesure de la puissance optique, laquelle peut conduire à un rapport signal sur bruit petit et donc une possible limitation du capteur. En utilisant les séparateurs de modes dans le système de mesure, il est possible de détecter l'intensité des modes LP_{01} et LP_{11} simultanément. La différence de phase due à la perturbation externe peut-être obtenue en comparant les valeurs des intensités mesurées au même instant. La mesure de l'intensité de chaque mode est plus facile, plus stable et plus précise que celle de la répartition spatiale.

Le séparateur de modes peut-être réalisé par un coupleur optique directionnel utilisant les champs évanescents pour coupler entre les deux fibres parallèles ou utilisant battement entre les supermodes dans la partie fusionnée et effilée. Les coupleurs directionnels à

fibres peuvent êtres fabriqués par une de trois méthodes suivantes: soit par attaque chimique, soit par polissage, soit par fusion-étirage. Dans la première méthode [19-23], la gaine optique des fibres est attaquée chimiquement dans un petit récipient afin de réduire son diamètre pour se rapprocher de celui du cœur, donnant ainsi une intégrale de recouvrement des champs dans la gaine optique suffisante pour coupler la puissance. Ces coupleurs sont délicats et peu robustes, donc uniquement utilisables dans les conditions de laboratoire. Les pertes par insertion de tels coupleurs sont de l'ordre du dB.

Dans la seconde méthode pour produire les coupleurs directionnels à fibre, chaque fibre est collée dans une rainure incurvée faite dans un bloc de silice et ensuite une partie de la fibre est enlevée soit en meulant, soit par polissage ou soit en rodant [24-29]. Le coupleur directionnel est alors réalisé en plaçant un des blocs par-dessus l'autre avec une fine couche de liquide d'indice entre eux [30, 31]. Une autre méthode utilisée pour polir est celle de la roue en rotation [32], laquelle conduit à une structure uniforme de la section polie. Pendant la fabrication des coupleurs polis, la distance entre les surfaces polies, donc les cœurs, est un paramètre important car il détermine le taux de couplage réalisable [31, 33, 34]. Les coupleurs directionnels à fibres polies présentent peu de pertes, une grande directivité et permettent d'obtenir tous les taux de couplages désirés. Toutefois, il faut des fixations élaborées pour maintenir le couplage stable même pour de courts temps d'utilisation.

La troisième et la plus importante technique pour fabriquer les coupleurs directionnels à fibres monomodes est la méthode de fusion-étirage. Deux fibres préalablement dégainées sont placées en contact parallèlement l'une à l'autre et chauffées par un arc électrique, une micro-torche, un micro-four ou un laser CO_2. Puis les deux fibres sont étirées, les puissances transmises et échangées sont visualisées sur un écran en temps réel. Si la zone étirée bi-conique a une pente douce, la puissance en sortie du coupleur change

périodiquement comme une fonction de l'élongation et peut être observée. L'étirage est arrêté quand le taux désiré dans chaque branche est atteint [35-39]. Des articles faisant l'état de l'art sur la technologie des coupleurs à fibres monomodes fusionnés ont été publiées par Kawasaki et al. [40] et Ragdale et al. [41].

Ce phénomène de transfert de puissance dans les coupleurs fusionnés-étirés a été expliqué pour la première fois par Bures et al. [42, 43] avec le concept de supermode; d'autres auteurs ont aussi contribué [44-48]. Pour les coupleurs directionnels réalisés par fusion-étirage, la fusion de deux guides unimodaux pour donner un guide plus grand (c'èst-à-dire. multimodal) et les dimensions des cœurs rendues petites par l'étirage (par conséquent la valeur de la fréquence normalisée V), entraînent que le champ électromagnétique propagé dépend de la totalité du profil d'indice de réfraction de la section transversale du coupleur. Au centre du coupleur, les cœurs sont pratiquement inexistants et le transfert de puissance peut s'expliquer en termes de battement de deux supermodes du guide d'onde formé par la gaine optique et le milieu extérieur.

Les techniques de fabrication des coupleurs fusionnés-étirés bi-coniques ont été décrites dans plusieurs articles [28, 44, 49-52]. Ils peuvent être réalisés rapidement et simplement. Ils n'ont pas beaucoup de pertes et ont une bonne stabilité thermique et mécanique. Un montage automatique pour fabriquer des coupleurs fusionnés-étirés a été décrit par Kopera et al. [53], Yokahama et al. [54], Takeuchi et al. [55-57] et Donati et al. [58]. Un bon contrôle des paramètres de fabrication comme le degré de fusion et le profil longitudinal, permet de réaliser de nombreux composants. Ceci inclut les diviseurs de puissance [36, 42, 49, 53, 54], les multiplexeurs en longueur d'onde [59-61], et les séparateurs de polarisation [62-66]. La dernière application est considérée dans cette thèse car les principes de bases sont similaires à ceux mis en jeu dans les séparateurs de modes. Le premier séparateur de polarisation a été réalisé par Yakati et al. [51] et Bricheno et al. [62]

en utilisant de très longs coupleurs fusionnés-étirés, la longueur de la région de couplage était de plus de 100 mm, les fibres utilisées étaient non biréfringentes. Yokohama et al. [64, 65] ont fabriqué leur séparateur de polarisation en employant des fibres biréfringentes PANDA ou dans ce cas-là la longueur de la région de couplage était d'environ 20 mm.

Des méthodes pour analyser les séparateurs de polarisation ont été proposées par Love et al. [67], Payne et al. [68], Snyder [69], et Yokohama et al. [65]. La biréfringence étant due soit à la non-circularité de la gaine optique des coupleurs à fibres non-biréfringentes, soit à la nature même de la fibre pour le cas des coupleurs à fibres PANDA. Ceci entraîne une différence entre les constantes de propagation des deux premiers supermodes ($\beta_{01}{}^x$-$\beta_{11}{}^x \neq \beta_{01}{}^y$-$\beta_{11}{}^y$), ou autrement dit, les longueurs de battements correspondant à $LP_{01}{}^x$ et $LP_{11}{}^x$ sont différentes dans la polarisation x et dans la polarisation y. Donc des puissances transmises $I_x = \cos^2[\int (\beta_{01}^x - \beta_{11}^x)dz \, / \, 2]$ qui dépendent de la différence d'accumulation des phases tout au long du coupleur sont différentes pour la polarisation x et la polarisation y. Si les conditions $\int (\beta_{01}^x - \beta_{11}^x)dz = 2m\pi$ et $\int (\beta_{01}^y - \beta_{11}^y)dz = (2m+1)\pi$ sont satisfaites, le mode polarisé x sortira par une branche tandis que le mode polarisé y sortira par l'autre branche, et ce coupleur se comportera comme un séparateur de polarisation.

Ce principe peut être utilisé dans le cas des séparateurs de modes. Les longueurs de battements étant différentes, elles entraînent une différence de constantes de propagation des modes individuels comme LP_{01} et LP_{11}. Quelques recherches ont été menées sur le couplage modal. En 1986, Sorin et al. [70] ont publié la fabrication d'un filtre modal, constitué de deux fibres à cœurs circulaires permettant de coupler dans le mode LP_{11} de la fibre bimodale par l'intermédiaire des champs évanescents, le coupleur était réalisé en polissant et en collant la fibre monomode et la fibre bi-modale. En 1990, Kumar et al. [71] ont simulé un filtre modal constitué de deux fibres bimodales à cœur elliptique par la méthode des perturbations. En 1994, Thursby et al. [72] ont présenté un séparateur de

modes réalisé en polissant une fibre à cœur elliptique et en la collant sur un prisme. Le mode LP_{11} est couplé dans le prisme par l'intermédiaire du champ évanescent et est collecté par une autre fibre collée au prisme. En 1995, Barcelos et al. [73] ont démontré l'excitation sélective du mode LP_{11} en utilisant les plasmons de surface et Pechstedt et al. [74] ont montré le couplage sélectif d'un mode d'une fibre particulière en utilisant les modes guidés de Bloch propagés à la surface d'une structure diélectrique multicouche. La plupart des recherches effectuées sur ces composants "en-ligne" n'ont jamais été compatibles pour les systèmes de capteurs tout-fibre ou ont occasionné d'importantes pertes d'insertions. En outre, tous les composants fabriqués par la technique de polissage sont limité par la longueur de couplage, la stabilité mécanique et ne peuvent être utilisés qu'en laboratoire.

L'objectif de cette thèse est de réaliser un séparateur de modes avec un coupleur codirectionnel fusionné-étiré, lequel aura une bonne stabilité mécanique et sera plus facile à fabriquer. Premièrement, nous utiliserons la théorie des supermodes dans l'approximation scalaire, la méthode de décomposition sur les modes d'une fibre et la méthode des différences finies, afin de simuler les coupleurs directionnels réalisés soit par polissage, soit par fusion-étirage, soit par pré-attaque chimique et par pré-traitement thermique. Nous étudions l'influence du profil longitudinal du coupleur ainsi que la condition d'adiabaticité sur la possibilité de réaliser un séparateur de modes. Puis, nous essayerons de fabriquer un prototype de séparateur de modes fait par fusion-étirage. L'influence du temps de fusion et de la longueur de balayage de la flamme sur l'efficacité de transfert sera aussi étudiées.

Dans le premier chapitre, nous présentons la théorie des supermodes dans l'approximation scalaire, qui élargit la théorie des coupleurs entre guides unimodaux à celle des coupleurs entre guides bi-modaux. Nous introduisons aussi, les principes d'opération des

séparateurs de modes et les méthodes numériques utilisées dans la simulation comme la méthode de décomposition sur la base des modes de la fibre, la méthode des différences finies et la méthode itérative inverse. Le principe d'opération d'un séparateur de modes est le suivant: dans un coupleur à guide bimodal, il y a six supermodes dans une direction de polarisation qu'on nomme SLP_{01}, SLP_{11}^{impair}, SLP_{11}^{pair}, SLP_{02}, SLP_{12}, SLP_{21}. Seuls les supermodes provenant du même mode individuel peuvent battre ensemble, donc il y a trois longueurs de battements. Si la structure du coupleur fait que le battement entre les supermodes SLP_{01} et SLP_{11}^{impair} (correspondant au mode individuel LP_{01}) est in-phase et dans le même temps le battement entre SLP_{21} et SLP_{11}^{pair} et SLP_{02} et SLP_{12} (correspondant au mode individuel LP_{11}) sont en quadrature pour la même élongation, il en résultera que le mode LP_{01} restera dans la fibre originale et les deux orientations du mode LP_{11} iront dans l'autre fibre, ceci réalisant les fonctions de séparateur de modes.

Dans le deuxième chapitre, nous nous concentrerons sur les séparateurs de modes fabriqués par la méthode de polissage. Bien que Kumar et al. [71] aient simulé le cas de fibres avec des cœurs elliptiques, leurs résultats sont trop généraux et le modèle pris pour le coupleur est trop simple pour pouvoir concevoir un séparateur de modes. Nous nous basons sur deux types de profil longitudinal que l'on peut obtenir par le procédé de polissage: d'une part, le profil parabolique et d'autre part une structure uniforme. Par la méthode des différences finies, nous calculons la transmission comme une fonction de la longueur de couplage pour les structures uniformes et comme une fonction du rayon de courbure pour les structures paraboliques. Il est à noter que les longueurs de battement des deux orientations du mode LP_{11} sont très différentes. La valeur pour le mode LP_{11}^{impair} est beaucoup plus petite que celle du mode LP_{11}^{pair}, ce qui veut dire que l'interaction entre SLP_{02} et SLP_{12} est plus forte que celle entre SLP_{11} et SLP_{21}. Ceci peut s'expliquer intuitivement par le raisonnement physique suivant: la distribution du champ

SLP_{11}^{pair} s'annulant dans les cœurs et l'orientation du supermode SLP_{21}, entraînent que l'intégrale de recouvrement entre ces deux supermodes est plus petite que celle entre SLP_{02} et SLP_{12}. La comparaison des résultats numériques des deux structures nous permet de dire : pour le coupleur uniforme, la longueur de couplage peut être courte si les deux fibres sont très proches ; tandis que pour le coupleur parabolique, la longueur de couplage reste grande même si les deux fibres sont proches au waist. La tolérance du coupleur parabolique est plus large que celle du coupleur uniforme. De plus, une technique contrôlée par ordinateur a été développée pour réaliser des rayons incurvés dans des substrats, ceci permet d'obtenir les rayons de courbure désirés et de changer les autres paramètres plus facilement en modifiant le programme, donc il permet de garantir un bon contact optique pour les coupleurs avec un profil parabolique. Le coupleur à profil parabolique est plus facile à fabriquer et a des tolérances plus grandes. Toutefois, la technique de fabrication requise pour les séparateurs de modes réalisés avec la méthode de polissage est encore trop limitative. Une solution est d'utiliser des fibres à cœurs elliptiques qui supportent seulement les modes LP_{01} et LP_{11}^{pair}, le mode LP_{11}^{impair} étant coupé. Dans ce cas, la condition de séparation des modes devient simple et donc le composant peut être facilement réalisé. L'autre solution est d'utiliser la méthode de fusion-étirage.

Dans le troisième chapitre, nous étendons l'étude à des profils longitudinaux plus généraux pour modéliser le fait que la largeur de la flamme et la position peuvent varier, nous prendrons que la distribution de la température le long de la fibre est approximativement comme l'intégration d'une fonction gaussienne, ceci pour tenir compte dans le cas d'une recette de fabrication générale de toutes les formes de zones effilées raisonnables. Puis nous calculons les indices effectifs des six premiers supermodes dans le cas de cœurs circulaires et elliptiques pour les coupleurs fusionnés-étirés par la méthode

de décomposition sur les modes de la fibre. En s'assurant que dans les deux cas, circulaire et elliptique, le cœur de la fibre a la même aire et la même différence relative d'indice de réfraction, il est à noter que les indices effectifs des quatre supermodes SLP_{11}^{pair}, SLP_{21}, SLP_{12} et SLP_{02} sont dégénérés à l'entrée et à la sortie du coupleur et séparés presque simultanément pour un taux de réduction inverse TRI = 0.75 pour des cœurs circulaires; dans le cas des cœurs elliptiques les indices effectifs sont dégénérés deux à deux à l'entrée et à la sortie SLP_{11}, SLP_{21} et SLP_{02}, SLP_{12} qui se séparent respectivement à TRI = 0.71 et TRI = 0.8. Finalement, nous obtenons la transmission comme une fonction de l'élongation pour respectivement, les coupleurs à cœurs circulaires et elliptiques. Les résultats numériques montrent que lorsque la longueur de balayage est petite, les courbes de transmission pour les cœurs circulaires se séparent plus doucement que celles obtenues pour les cœurs elliptiques. Pour obtenir un maximum de transfert dans le mode LP_{11}, les deux pics des deux LP_{11} (pair et impair) doivent coïncider à la même élongation. Ce qui veut dire qu'il faut une plus grande distance de balayage dans le cas des cœurs circulaires. Du point de vue de la fabrication, quand la largeur de la flamme est fixée, nous préférons avoir une élongation et une longueur de balayage petites car les petits coupleurs sont plus faciles à fabriquer et à emballer. Aussi, les fibres à cœurs elliptiques sont préférées dans la fabrication des séparateurs de modes. D'un autre coté, nous avons aussi étudié l'influence des longueurs de battement, de la biréfringence et des conditions d'adiabaticité. Dans le cas des fibres à cœurs circulaires, en augmentant le TRI la différence des longueurs de battements entre z_{b11-21} et z_{b02-12} reste petite tandis que dans le cas des fibres elliptiques elle devient grande. Ceci coïncide avec les courbes de transmissions des deux modes LP_{11} qui se séparent plus lentement dans le cas circulaire. Dans les deux cas, circulaire et elliptique, pour des coupleurs ayant des

fusions complètes et des TRI moyens, comme ceux des séparateurs de modes, la biréfringence est petite.

Dans le quatrième chapitre, les techniques de pré-attaques chimique et de pré-polissage et le pré-traitement thermique intense pour obtenir de cœurs elliptiques à partir de cœurs circulaires, sont introduites afin de réaliser des coupleurs adiabatiques et de réduire la distance de balayage de la flamme ainsi que la longueur d'élongation pour fabriquer des coupleurs plus facilement. Les conditions d'adiabaticité pour les coupleurs à cœurs elliptiques, calculés dans le troisième chapitre, ne sont pas complètement satisfaites. Pour résoudre le problème, la distance entre les deux cœurs des fibres doit être diminuée afin de réduire les pentes de la partie effilée. Pour atteindre ce but, quelques travaux préparatoires sur les fibres sont nécessaires comme la pré-attaque chimique, le pré-polissage et le pré-traitement thermique d'expansion des cœurs. D'un autre coté, ces techniques peuvent aussi réduire la longueur de battement des supermodes, donc peut être celle des coupleurs. Pour simplifier, les coupleurs fabriqués par ces méthodes sont appelés coupleurs améliorés et les précédents coupleurs normaux. Au point d'élongation où il y a séparation des modes, les coupleurs améliorés ont un TRI au waist qui sera plus grand que les coupleurs normaux, donc la biréfringence pour les coupleurs améliorés sera plus petite. Une autre méthode pour simplifier les séparateurs de modes est d'utiliser des fibres avec des cœurs très elliptiques, qui ne guident que le mode LP_{11}^{pair} entraînant que les conditions de séparations des modes deviennent plus simples.

Dans le cinquième chapitre, le séparateur de modes qui a été pour la première fois réalisé par la méthode de fusion-étirage est présenté dans ce mémoire. En comparant avec les séparateurs de modes existants réalisés par la méthode de polissage, ce type de séparateur de modes a une bonne stabilité mécanique, il peut être fabriqué rapidement et à faible coût. Pendant le processus de fabrication, l'excitation des modes LP_{11} et le dénudage ont été

pris en compte par une épissure avec décalage et en entourant la fibre autour d'une tige de petit rayon de courbure. La distance de décalage et le rayon d'enroulement de la fibre ont été convenablement calculés et réalisés en pratique. L'efficacité de transfert du mode LP_{11} dépend du synchronisme des battements des deux orientations du mode LP_{11} à certains points d'élongation. Ce synchronisme peut être ajusté par le temps de fusion et la distance de balayage de la flamme, l'ajusterrent étant plus sensible à ce dernier paramètre. Par un choix approprié des paramètres de fabrication, deux types de séparateurs de modes ont été réalisés. Le premier dont la longueur d'emballage est petite et avec un petit temps de fusion offrant seulement une efficacité de transfert de 81,5 %. Le deuxième dont la longueur d'emballage et le temps de fusion sont relativement plus longs ayant un taux de transfert de 92,3 %. Les deux séparateurs de modes n'apportent pas plus de 0,2 dB de pertes. Finalement, l'analyse numérique basée sur les paramètres expérimentaux et avec juste trois hypothèses en plus, donnent des résultats en accord avec les résultats expérimentaux, cet accord justifiant la méthode d'analyse utilisée dans ce mémoire.

Bien que le complet succès de la modélisation et de la fabrication des séparateurs de modes ait été démontré dans ce mémoire, l'écart entre le potentiel et les caractéristiques obtenues montre que les capacités de ces composants n'ont pas été totalement épuisées. Quelques améliorations pourraient être amenées dans le futur. Premièrement, la variation de la différence d'indice de réfraction avec le temps de fusion est très importante pour déterminer la transmission. Cette variation est causée par une diffusion des dopants de la région du cœur et donc il n'est pas possible d'obtenir des bonnes solutions pour toute les nombreuses situations possibles. Dans ce mémoire, on a pris la différence d'indices les valeurs typiques mesurées expérimentalement. Afin de permettre de concevoir plus généralement des séparateurs de modes il est nécessaire de connaître précisément la différence d'indice. Cette étude serait très intéressante. Deuxièmement, la forme de la

section transverse des cœurs des fibres après fusion est un autre facteur qui affecte la transmission. La forme a été mesurée expérimentalement, montrant qu'elle ressemble à une ellipse qui doit être reliée à la position de la flamme et au temps de fusion. Le mécanisme physique et le contrôle de la forme reste encore à explorer. Troisièmement, la fibre utilisée pendant la fabrication des séparateurs de modes de ce mémoire est la SMF28 qui a un cœur circulaire. Etant donné que les simulations montrent de bon taux de séparation avec des fibres à cœurs elliptiques, et bien que les cœurs circulaires puissent devenir elliptiques après fusion, l'ellipticité est encore petite. Alors si les séparateurs de modes pouvaient être directement fabriqués avec des fibres dont les cœurs ont une grande ellipticité, spécialement celle qui propage uniquement les modes LP_{01} et LP_{11} pair, la séparation des modes serait plus aisée.

En conclusion, les séparateurs de modes réalisés par la méthode de fusion-étirage apportent de nombreux avantages pour l'amélioration des systèmes de capteurs à fibre optique et joueront un rôle de plus en plus important dans les systèmes de communication de demain. Suite à ces progrès dans la modélisation et la fabrication, les séparateurs de modes deviendront encore plus compétitifs.

Table of Contents

List of Figures

List of Tables

List of Symbols and Abbreviations

A_∞	infinite cross section
A_{lm}	normalization constant
a_e, b_e	minor and major semi-axes of the elliptical fiber core
a_j	individual modal amplitude
b_i	supermode modal amplitude
C_{jk}	coupling coefficient between supermode j and k
$\overline{C}_{jk}$	normalized coupling coefficients
d_{cl}	depth of polish part of fiber
d_e	distance between the cores of the completely fused coupler
d_0	minimum distance in the coupler waist
$d(z)$	distance between the two cores
d_{poli}	distance between two fiber cores of the prepolished and completely fused couplers
dl	elongation of a element section of fiber
$d\rho$	radius reduction of the coupler
E	electric field
E_{rad}	radiation electric field
FMEM	Fiber Mode Expansion Method
$F(z), F'(z), G(z)$	relative temperature distribution of heat source
f	fusion degree
f_R	the radius correction factor

G	number of the supermodes
$\boldsymbol{H}$	magnetic field
$\boldsymbol{H}_{rad}$	radiation magnetic field
$\mathbf{H}_f$	band matrix
$H(x)$	Heaviside function
h	half distance difference between $d(z)$ and d_0.
$\mathbf{I}$	identity matrix
ITR	Inverse Taper Ration
J_l, K_l	Bessel functions
K	proportional constant
k	free space wavenumber
L	length of a fiber
l_o	lateral dimension of the coupler before fusion
l_{min}	minimum lateral dimension of the coupler after fusion
l_t	real lateral dimension of the coupler after fusion
$|p_j^{(u)}\rangle$	jth individual mode of waveguide u in Dirac symbol
M	number of the individual fiber modes
MSC	Mode Separating Coupler
$\mathbf{N}$	non-orthogonal coefficient matrix
N_j	mode normalization
n_{co}	refractive index of core
n_{cl}	refractive index of cladding
$n(x,y)$	index profile of a waveguide
$n(r)$	index profile of a fiber

P	passage matrix between the basis of individual fiber modes and supermodes
$\mathbf{P^T}$	transposed of **P**
$P(z)$	power detected in bend fiber
$P(0)$	power entering the bend fiber
P_i	total power in the ith mode
$P_d(r)$.	detected power
P_{cl}	total power received by the detector
p	polish degree
Q_z	magnitudes of birefringence
R	curvature radius of the coupler
R_b	effective bend radius
R_{exp}	actual bend radius
R_o	critical bend radius
R_c	radius of the completely fused coupler
R_p	radius of the prepolished and completely fused couplers
r	distance from the fiber core axis
S	phase matrix
$|SLP_i>$	supermode in Dirac symbol
S_a	cross section of the polished fiber
T	transfer matrix
TEC	Thermally Expanded Core
V_f	normalized eigenvector
W	constant volume
Z_b	beat length between supermodes

z_0	half length of the coupler
$\hat{z}$	unit vector parallel to the waveguide
z_f	central position of the flame
α	angle
α_{ij}^{x}	accumulated phase with x polarization direction
α_{ij}^{y}	accumulated phase with y polarization direction
α_i	supermode-accumulated phase
α_B	conventional bend loss
α_{BL}	bend loss of the coated fiber
β	propagation constant
Γ	power loss coefficient
γ_i	scalar coefficients
∇_t^2	Laplacien vector
∇_t	gradient transverse vector
Δn	index difference between the core and cladding of fiber
δL	total elongation of a coupler
ε	dielectric constant
ε_o	dielectric constant of free space
ζ	launching efficiency
η	power transfer efficiency of LP_{11} mode
θ_{max}	the maximum angle defined by the input aperture
θ_{min}	the minimum angle defined by the opaque disk
λ	wavelength of light in free space
μ_o	magnetic permeability of free space
ξ	portion of power injected with an x direction polarization

Π	oscillation number during one envelope cycle
ρ_{co}	core radius of fiber
ρ_{cl}	cladding radius of fiber
ρ_o	original radius of couplers before tapering
$\rho(z)$	longitudinal profile after tapering
ρ_e	cladding radius of etched fiber
τ	initial estimate eigenvalue
ψ	scalar field
ψ	scalar field distribution of mode
Ω_w	normalized taper slope

Introduction

In optical communication systems, time or wavelength division multiplexing techniques are commonly used to transmit more than one channel in a single fiber. However, a method called mode division multiplexing can be applied in addition to conventional multiplexing techniques to increase the transmission capacity in planned and existing local area data networks. In 1992, Schmauss *et al.* [1] successfully demonstrated a transmission system with two-mode coded channels. The key component in this technique is the mode separating coupler (MSC) at the output end to separate the signal carried on each mode.

Recently, a considerable amount of research has been reported on two-mode fibers and devices made with them, such as intermodal couplers [2-5], accelerometers [6], strain gauges [7], frequency shifters [8, 9], dispersion compensator [10], and quadrature phase detectors [11]. These devices have certain distinct advantages over their single mode fiber counterparts such as their immunity to certain parameters and high sensitivity to others. For example, two-mode optical fiber sensors based on the interference between the LP_{01} and the LP_{11} modes propagating in a two-mode fiber have advantages over conventional two-arm interferometers because of their simplicity and stability, making them attractive for sensing strain [12-14], stress [15], temperature [7], and voltage [16]. At present, two-mode fiber sensors are being considered as one of the most appropriate candidates for the realization of smart structures.

For two-mode optical fiber sensors, the standard analysis method involves a measurement of the power exchange between the two lobe far-field intensity distribution, to determine

the nature of the external perturbation. Several detection techniques for two-mode fiber sensors have been suggested. An elementary technique involves the placement of a spatial demodulator in the form of a pinhole, which samples only part of the far-field pattern [17]. An optical signal processing technique using a CCD array to analyze the far-field pattern at the output of a multimode fiber sensor has been demonstrated [18]. Most such methods require the output fiber to display the far-field pattern on a monitoring system. This is not optimal for remote sensing system in which the sensing region may be restricted to a hard-to-reach environment. Murphy *et al.* [13] used an offset splices two-mode fiber to a single mode fiber and measured the single mode fiber intensity at the output end to determine the strain. However, this method reduces the optical power, which could lead to a smaller signal-to-noise ratio and possibly restricts the sensitivity of the sensor. Alternatively, using the mode separating couplers in the sensing system, one could detect the LP_{01} and LP_{11} modes intensity simultaneously. The phase difference caused by an external perturbation can be obtained by comparing their intensity values measured at the same time. The measurement of each mode intensity is easier, more stable and more precise than that of spatial patterns.

Mode separation could be realized by an optical directional coupler made with either the evanescent field coupling between two parallel fibers, or the beating between supermodes in fused and tapered fibers. Fiber directional couplers can be fabricated by one of three different methods: by etching, by polishing, or by fusion-tapering. In the first method [19-21], the plastic coating is stripped from two single mode fibers, which are then twisted together. The claddings of the fibers are etched with a solution of HF in a small container to a diameter close to that of the cores, giving an overlap of the evanescent fields in the cladding that is sufficient for power coupling. The coupling efficiency of these so called "bottle couplers" can be adjusted after the completion of etching by turning a

threaded cap to control the number of twists between the two etched fibers as well as their separation. The first bottle couplers were filled with index matching oil. In more recent versions of the etching technique, the fibers were embedded in a suitable room temperature vulcanized silicone [22] or in a gel glass [23]. Etched couplers are delicate, non-ruggedized components, which are only suitable for use under laboratory conditions. The insertion loss of bottle couplers is of the order of 1 dB.

In the second method for producing fiber directional couplers, each fiber is cemented in a fused silica block with a curved groove cut in it and part of the cladding is removed by grinding, polishing, and lapping [24-29]. The directional coupler is then realized by placing one block on top of the other and filling a thin film of index matching liquid between the two blocks. The coupling can be tuned by sliding one block laterally from the other. In a modification of the method, the fiber is embedded before polishing into a substrate glass having a low melting temperature [30]. This method reduces the drift of coupling ratio with aging. Another improvement is to polish the fibers by a grinding wheel [31], which leads to a uniform structure in the polished section. During production of a polished coupler, the distance between the polished surface and the core axis is an important parameter, since it determines the achievable coupling ratio. It is difficult to measure this distance using standard optical and mechanical instruments. Instead, the distance is measured by observing the attenuation of the half-coupler when a droplet of liquid of appropriate refractive index is placed on the polished fiber region [31, 33, 34]. Polished fiber directional couplers exhibit low loss, high directivity, and can be tuned to any required coupling ratio. However, an elaborate fixture is required to maintain a stable coupling ratio even for a short time. An asymmetric polished directional coupler has also been made with a single mode fiber and a multimode fiber [75]. Power can be coupled effectively from the single mode fiber into the multimode fiber, but only a very small part

of the power transmitted through the multimode fiber can be coupled into the single mode fiber.

The third and most important technique for making the single mode directional coupler is the fusion and tapering method. The two cladding stripped fibers are placed parallel, in contact, and heated by an arc, a micro torch flame, microheater or a CO_2 laser; then the two fibers are pulled (refereed to as tapering) while the transmitted and coupled power are monitored. If the biconical taper gradient is low, it can be observed that the power exchanges periodically at the output end of the coupler as a function of the elongation. Tapering is stopped when the desired splitting ratio is obtained [35-39]. Reviews of fused single mode coupler technologies have been published by Kawasaki et al . [40] and Ragdale et al . [41].

This phenomenon of power transfer in fusion and tapering couplers was first explained by Bures et al. [42, 43] with supermode concepts and other authors contributed to this also [44-48]. For fusion and tapering directional couplers, the fusion makes the two single mode waveguide into a wider waveguide that is no longer a single mode structure, and the tapering makes the core diameter and local fiber parameter V at the waist of the coupler so small that the electromagnetic field propagates in a waveguide consisting of the entire coupler cross section. In the coupler waist, the core region then becomes insignificant and the power transfer can be explained in terms of the beating of two supermodes on a waveguide formed by the fiber cladding and the medium surrounding the fused fibers.

The techniques of fabrication of fused biconical tapered couplers have been described in a number of papers [28, 44, 49-52]. Fusion and tapering single mode fibers can be manufactured quickly and simply. They have low excess loss, and good thermal and mechanical stability. An automatic set up to produce the fused and taper coupler has been

described by Kopera *et al.* [53] Yokohama *et al* . [54], Takeuchi *et al.* [55-57], and Donati *et al.* [58]. By carefully controlling the fabrication parameters such as the fusion degree and the longitudinal profile, many kinds of components based on the fusion and tapering technique are realizable. These include power splitters [36, 42, 49, 53, 54], wavelength multiplexers [59-61], and polarization beam splitters [62-66]. The last application is considered in this thesis because these components and the mode separating couplers are based on similar principles. The first polarization beam splitter has been fabricated by Yakati *et al.* [51] and Bricheno *et al.* [62] by using a very long fusion and tapering coupler with the coupling region length of over 100 mm composed of nonbirefringent fibers. Yokohama *et al.* [64, 65] fabricated their polarization beam splitter by employing birefringent PANDA fibers wherein the length of the coupling region was about 20 mm. Methods for analysis of the polarization beam splitter have been proposed by Love *et al.* [67], Payne *et al.* [68], Snyder [69], and Yokohama *et al.* [65]. Due to the form birefringence of the noncircular cladding of nonbirefringent fiber couplers or the stress birefringence of PANDA fiber couplers, the propagation constant difference between the fundamental and the first high order supermode is different, or equivalently, the beat length corresponding to LP_{01}^x and LP_{01}^y is different in x-polarization and y-polarization. Therefore, the power transmission that depends on the accumulated propagation constant difference along the coupler is different for x-polarization and y-polarization. If the accumulated phase difference is in-phase in x-polarization and out-of-phase in y-polarization, the x-polarization mode will stay in the original branch, while the y-polarization mode will go to the other output branch; thus the coupler acts as a polarization beam splitter.

This principle can be used in the mode separating coupler. In this case, the beat length differences are caused by the different propagation constants of individual modes such as

LP_{01} and LP_{11}. Some relative modes selective coupling researches were done. In 1986, Sorin *et al.* [70] reported the fabrication of a modal filter consisting of two circular core fibers in which the power in the LP_{11} mode of a two-mode fiber is coupled through its evanescent field by polishing and gluing it to a single mode fiber. In 1990, Kumar *et al.* [71] simulated a mode filter consisting of two-mode elliptical core fibers by a perturbation method. In 1994, Thursby *et al.* [72] presented an in-line mode separating coupler made by polishing an elliptical core fiber in contact with a prism. The LP_{11} mode is coupled into the prism through its evanescent field and recollected by another fiber bonded on the prism. In 1995, Barcelos *et al.* [73] demonstrated the selective excitation of the LP_{11} mode using surface plasmons and Pechstedt *et al.* [74] show that the selective coupling of a particular fiber mode with the use of surface guided Bloch modes supported by dielectric multilayer stacks. Most of past studies were on in-line components that are neither compatible to all fiber sensing systems or have high insertion loss. Besides, all the devices fabricated by the polishing method are restricted by requirements on the coupling length, mechanical stability, and they can only be used in the laboratory.

The objective of the work described in this dissertation was to develop an all-fiber mode separating coupler that has good mechanical stability, low insertion loss and is easier to fabricate. First, the supermode analysis based on the scalar mode approximation was developed from a model of single mode fiber coupler into a two-mode fiber coupler. The numerical techniques such as the fiber mode expansion method and the finite difference method were used to design the mode separating couplers that were made by polishing method, fusion and tapering method, pre-etching fiber, prepolishing fiber, and highly elliptical core and thermally expended core fibers. The influence of the coupler longitudinal profile on its transmission and the adiabatic condition was studied. Then, the prototype of the mode separating coupler was fabricated by the fusion and tapering

method. The influence of fusion time and flame sweep distance on transfer efficiency was studied. A few samplers were packaged and their characteristics were measured. This dissertation is organized as followings.

In Chapter one, it will present the scalar mode approximation, the supermode analysis, the principle of operation of mode separating coupler and the numerical method used in the simulations such as fiber mode expansion method, finite difference methods and power reverse iteration method.

In Chapter two, the mode separating coupler made by the polishing method will be presented. Although Kumar *et al* . [71] have simulated the elliptical core fiber case, their results are too general and their coupler model is so simple that can not be used in the design of mode separating coupler. Based on the practical polishing process, two kinds of coupler structure were given: one is parabolic and the other is the uniform. By the finite difference method, MSC were designed under various polishing degrees for the above two kinds of structures.

In Chapter three, the fusion and tapering couplers were simulated by the FMEM. The longitudinal profiles formed with various flame widths and flame sweep distances were modeled. The MSC were designed for the cases of circular and elliptical core fibers. In addition, the characteristics of two-mode fiber coupler such as the beat lengths, birefringence and adiabatic conditions were studied.

In Chapter four, results from MSC's made with pre-etching and pre-polishing fibers, highly elliptical core fibers, and thermally expended core fibers will be presented. These methods as alternatives could make the manufacture of an adiabatic MSC more easily.

In Chapter five, the LP_{11} mode excitation by offset splice and the LP_{11} mode stripper made by a small fiber loop will be discussed. Moreover, the LP_{11} mode coupling in the two-mode fiber coupler is confirmed. Results of influence of fusion time and flame sweep distance on the transmission will be presented. By properly choosing the fabrication parameter, two kinds of mode separating coupler were constructed. One package length is short, as well as the fusion time, but the transfer efficiency is only about 81.5%. For the other one, the package length and fusion time are relatively longer but the transfer efficiency reaches 92.3%. Excess losses of both mode separating couplers are less than 0.2 dB. Numerical analysis based on the experimental parameters and taking into account the core shape deformation and the refractive index difference reduction were done. The theoretical results are in good agreement with the experimental results. They explain the power transfer process in the mode separating coupler.

Chapter 1

Basic Concepts

1.1 Maxwell Equations

When a beam of light propagates in a waveguide, the electromagnetic field spatial distributions are determined by Maxwell equations. If a waveguide is homogeneous and far from any source, the electromagnetic fields have an implicit time dependence $\exp(-i\omega t)$. The current density, and charge densities are equal to zero, therefore we write the source-free Maxwell's equations:

$$\nabla \times \mathbf{E} = ik\sqrt{\frac{\mu}{\varepsilon_o}}\mathbf{H}$$

$$\nabla \times \mathbf{H} = -ikn^2\sqrt{\frac{\varepsilon_o}{\mu}}\mathbf{E} \qquad (1.1)$$

$$\nabla \cdot (n^2\mathbf{E}) = 0$$

$$\nabla \cdot \mathbf{H} = 0$$

Where $\mathbf{E}$ is the electric field and $\mathbf{H}$ is the magnetic field. ε is the dielectric constant that is related to the refractive index n by $\varepsilon = n^2\varepsilon_o$, where ε_o is the dielectric constant of free space. For the optical waveguide consisting of nonmagnetic materials, the magnetic permeability μ is very nearly equal to the free space value μ_o. $k = 2\pi/\lambda$ is the free space wavenumber, and λ is the wavelength of light in free space.

If a waveguide refractive index profile is translationally invariant, *i.e.*, its refractive index profile does not vary with distance z along the waveguide, the electromagnetic fields of the waveguide are expressible as a superposition of fields with the separable form.

$$E(x,y,z) = e(x,y)\exp(i\beta z)$$
$$H(x,y,z) = h(x,y)\exp(i\beta z)$$

(1.2)

where β is the propagation constant. We decompose these fields into longitudinal and transverse components, parallel to and orthogonal to the waveguide axis, respectively, and denoted by subscript z and t, where

$$E(x,y,z) = (e_t + e_z\hat{z})\exp(i\beta z)$$
$$H(x,y,z) = (h_t + h_z\hat{z})\exp(i\beta z)$$

(1.3)

and $\hat{z}$ is the unit vector parallel to the waveguide. If we substitute the Eq. (1.3) into the Maxwell's equations (1.1) and compare longitudinal and transverse components, we obtain

$$e_z = \frac{i}{kn^2}\sqrt{\frac{\mu_o}{\varepsilon_o}}\hat{z}\cdot\nabla_t\times h_t$$

$$h_z = -\frac{i}{k}\sqrt{\frac{\mu_o}{\varepsilon_o}}\hat{z}\cdot\nabla_t\times e_t$$

(1.4)

If the transverse electromagnetic field and refractive index of waveguide are given, we can obtain the longitudinal component. Thus, we only concentrate on the transverse electromagnetic field. If we eliminate either the electric or magnetic fields from Maxwell's equations (1.1), we obtain the vector wave equation

$$(\nabla_t^2 + k^2n^2 - \beta^2)e_t = -\nabla_t(e_t\cdot\nabla_t\ln n^2)$$
$$(\nabla_t^2 + k^2n^2 - \beta^2)h_t = (\nabla_t\times h_t)\times\nabla_t\ln n^2$$

(1.5)

where $n=n(x,y)$, and ∇_t^2 is the Laplacian vectorial operator and ∇_t is the gradient transverse vectorial operator. If the waveguide refractive index profile $n(x, y)$ is given, these equations can be resolved by eigenfunction, or modal methods. The eigenvalues and eigenvectors corresponding to the bound modes, evanescent modes, radiation modes, and various combination of all these modes represent the electromagnetic field of the waveguide. Actually, a waveguide always has some loss caused by the modal radiation, so the electric and magnetic field vectors E and H include two parts: one part representing the power that is guided without attenuation along the waveguide, and the remaining part representing the power that is radiated from the waveguide. The guided portion is expressed as a finite sum of bound modes, which are solutions of Maxwell's equations for the waveguide, given by

$$E = \sum_j a_j E_j(x,y,z) + E_{rad}(x,y,z)$$

$$H = \sum_j a_j H_j(x,y,z) + H_{rad}(x,y,z)$$

(1.6)

where $j=1,2...M$, a_j is the modal amplitude, and the subscript rad denotes the radiation fields.

1.1.1 Orthogonality and Normalization

In order to determine the amplitude a_j of a bound mode in the expression of Eq. (1.6), we require an orthogonality condition. This condition is derived from the reciprocity theorem of Maxwell's equation [76]. Assuming that the waveguide is nonabsorbing, the modal fields of the jth and kth forward propagating modes obey the vector orthogonality condition

$$\int_{A_\infty} e_j \times h_k^* \cdot \hat{z} dA = \int_{A_\infty} e_k^* \times h_j \cdot \hat{z} dA = 0 \qquad\qquad j \neq k \qquad (1.7)$$

where A_∞ is the infinite cross section, * denotes the complex conjugate, and $\hat{z}$ is the unit vector parallel to the waveguide axis. In particular, each bound mode is orthogonal to all radiation modes, and therefore, to the total radiation field E_{rad} and H_{rad}. The mode normalization N_j for a nonabsorbing waveguide is defined by

$$N_j = \frac{1}{2}\left|\int_{A_-} \mathbf{e}_j \times \mathbf{h}_k^* \cdot \hat{z} dA\right| \tag{1.8}$$

The modulus ensures that N_j is positive for all modes. Combining the orthogonality conditions with normalization, then for two forward propagating modes, we obtain

$$\frac{1}{2}\int_{A_-} \mathbf{e}_j \times \mathbf{h}_k^* \cdot \hat{z} dA = N_j \delta_{jk} \tag{1.9}$$

When an optical waveguide is excited, each mode will, in general, carry power. The portion of source power exciting a particular mode depends on the nature of the source. For nonabsorbing waveguides, the total power in each mode is found by integrating the Poynting vector over the infinite cross section.

$$P_j = \frac{1}{2}|a_j|^2 \int_{A_-} \mathbf{e}_j \times \mathbf{h}_j^* \cdot \hat{z} dA \tag{1.10}$$

in terms of the mode normalization

$$P_j = |a_j|^2 N_j \tag{1.11}$$

1.1.2 Scalar Wave Equation

Generally, the solution of the Maxwell source-free equation, or, equivalently, the homogeneous vector wave equation is cumbersome. The waveguide used for long distance communication has a small core-cladding difference in refractive index profile, or, equivalently, $n_{co} \approx n_{cl}$, where n_{co} and n_{cl} are the refractive index of core and cladding,

respectively. This kind of waveguide is called a weakly guiding waveguide. For a weakly guiding waveguide, the modes are nearly transverse electromagnetic waves with $e_z \cong 0$, $h_z \cong 0$, and

$$\mathbf{h}_t = (\frac{\varepsilon_o}{\mu_o})^{1/2} n_{co} \hat{\mathbf{z}} \cdot \mathbf{e}_t \tag{1.12}$$

the polarization effects due to the waveguide structure are small, and these effects are contained in the $\nabla_t \ln n^2$ term of the vector wave Eq. (1.5). Hence, ignoring polarization effects altogether is equivalent to ignoring the $\nabla_t \ln n$ term in Eq. (1.5). Accordingly if we set

$$\mathbf{e}_t = e_x(x, y)\hat{\mathbf{x}} + e_y(x, y)\hat{\mathbf{y}} \tag{1.13}$$

where $\hat{\mathbf{x}}$ and $\hat{\mathbf{y}}$ are unit vectors parallel to the Cartesian axes. Let ψ denote e_x or e_y, this function ψ satisfies the scalar wave equation

$$\left[\nabla_t^2 + k^2 n^2(x, y) - \beta^2\right]\psi = 0 \tag{1.14}$$

This leads to an eigenvalue equation for the allowed values of β. So, we can resolve the scalar wave equation in the scalar function space and find the scalar modes of guide.

It is convenient to describe the orthogonality and normalization conditions of the scalar wave equation in terms of the vector expressions. Substituting Eq. (1.12) into Eq. (1.7) and letting ψ_j and ψ_k denote two distinct solutions of Eq. (1.14). ψ_j and ψ_k correspond to e_j and e_k respectively, leading to

$$\int_{A_-} \psi_j \psi_k dA = N_j \delta_{jk} \tag{1.15}$$

where

$$N_j = \frac{1}{2} n_{co} \left(\frac{\varepsilon_o}{\mu_o}\right)^{1/2} \int_{A_-} \psi_j^2 dA \tag{1.16}$$

and the power has the same formula form of (1.11).

1.2 Supermode Theory

The power exchange along a coupler is described either in terms of the coupling mode equations (CME) or in terms of the beating of supermodes. The coupled mode equations are a perturbation theory that considers the effect of the other fiber as a perturbation. However, when the two fibers are placed very close to each other, for example, in a coupler, the effect from the other fiber can no long be considered a perturbation, and the coupled mode equations lose their accuracy. The supermode theory considers the closely placed fibers as one composite waveguide and the light propagating in this composite waveguide still can be described by the Maxwell's equations and its solution or the eigenvalues represent the new modes, named supermodes. So far, there are no analytic methods to express the supermodes owing to the composite waveguides complicated structure. Several numerical methods have been used to calculate the supermodes of the composite structure [77-80]. Among them, the beam propagation method [81-83] provides the evolution of the field for a given excitation. Other methods, such as, the effective index, Fourier, finite-element, and variational method can provide the supermode propagation constants and the field shape, making them more adequate as design tools. For this thesis, the finite difference method and the fiber mode expansion method are used to calculate the supermode propagation constants and field distribution. The two methods are scalar but through polarization corrections [76], the scalar solutions are precise enough to describe the electromagnetic fields of the waveguides.

1.2.1 Transfer Matrix

It is well known that the closer the individual guides are, the less accurate the CME results are. In the case of fused fiber couplers, the supermode field is difficult to calculate

with CME, since individual waveguides lose their initial shapes and the fields fill the whole guides in the power exchange region. Then, the individual guides are well separated at the entrance and exit end where the set of individual modes is available. Meanwhile, each individual-mode coincides with a linear combination of corresponding to supermodes. If the coupler is considered as a "black box" and a linear system, the power exchange can be described by a transfer matrix [84]. At both ends of the coupler the actual field can be expanded with a set of individual modes.

$$z=0, \quad |\psi(0)\rangle = \sum_u \sum_{i=1}^{M} a_i(0) |lp_i^{(u)}(0)\rangle \tag{1.17}$$

$$z=L, \quad |\psi(L)\rangle = \sum_u \sum_{i=1}^{M} a_i(L) |lp_i^{(u)}(L)\rangle \tag{1.18}$$

$$u= I, II$$

where $|lp_i^{(u)}\rangle$ stands for the individual mode in Dirac notation, the superscript u distinguishes the fiber; M is the number of individual modes; a_i is the amplitude of individual mode. The transfer matrix T is defined as

$$\mathbf{a}(L) = \begin{bmatrix} a_1(L) \\ a_2(L) \\ \vdots \\ a_n(L) \end{bmatrix} = \begin{bmatrix} t_{11} & t_{12} & \cdots & t_{1n} \\ t_{21} & t_{22} & \cdots & t_{2n} \\ \cdots & \cdots & \cdots & \cdots \\ t_{n1} & t_{n2} & \cdots & t_{nn} \end{bmatrix} \begin{bmatrix} a_1(0) \\ a_2(0) \\ \vdots \\ a_n(0) \end{bmatrix} = \mathbf{T}\mathbf{a}(0) \tag{1.19}$$

Figure 1.1 The transmission function of a coupler.

Only the power of the individual fiber mode (or, in short, individual mode) is interesting. To be Practical, when measuring the power of an individual mode, we must consider the contribution from other modes in the same or other fibers, because it is impossible to distinguish the power if the fibers are very close. The contribution can be described with the integration of the overlap of their fields. So, the amplitude of the field in the jth mode in fiber (u) is given by

$$A_j^{(u)}(L) = \left\langle lp_j^{(u)}(L) \middle| \psi(L) \right\rangle = \sum_u \sum_{i=1}^M a_i(L) \left\langle lp_j^{(u)}(L) \middle| lp_i^{(v)}(L) \right\rangle = \sum_{i=1}^M a_i(L) N_{ij}(L) \delta_{ij}^{(uv)} \qquad (1.20)$$

where

$$\left\langle lp_i^{(u)} \middle| lp_j^{(v)} \right\rangle = N_{ij} \delta_{ij}^{(uv)} \qquad (1.21)$$

or in matrix form

$$\mathbf{A}(L) = \mathbf{N}(L)\mathbf{a}(L) \qquad (1.22)$$

If $u=v$, $\left\langle lp_i^{(u)} \middle| lp_j^{(v)} \right\rangle = \delta_{ij}$, the integral is for the same fiber and the individual modes are orthonormal. If $u \neq v$, $\left\langle lp_i^{(u)} \middle| lp_j^{(v)} \right\rangle \neq 0$, the integrals are not for the same fiber and the individual modes are non-orthogonal. $\mathbf{N}$ is the non-orthogonal coefficient matrix. Then, the power measured in jth mode in fiber (u) is given by

$$P_j^{(u)}(L) = A_j^{(u)*}(L) A_j^{(u)}(L) = \left| A_j^{(u)}(L) \right|^2 \qquad (1.23)$$

If the transfer matrix $\mathbf{T}$ and the launch field $a(0)$ are known, the output end field $a(L)$ or $A(L)$ are easily obtained. To get the transfer matrix $\mathbf{T}$, we consider the coupler as a composite structure and its field can also be expressed with a set of supermodes.

$$z=0, \quad |\psi(0)\rangle = \sum_{j=1}^G b_j(0) \left| SLP_j(0) \right\rangle \qquad (1.24)$$

where $|SLP_i\rangle$ represents the ith supermode with the orthogonality relations $\langle SLP_i|SLP_j\rangle = \delta_{ij}$. G is the number of the supermodes. It supposes that the deformations of the coupler are adiabatic along the longitudinal direction, the amplitudes of each supermode b_i preserving their initial values, i.e $b_i(0)=b_i(L)=b_i$. When the supermodes pass through the coupler, only the phase is accumulated and the lost power due to coupling to higher order modes is negligible. So, at the output end the total field is

$$z=L, \quad |\psi(L)\rangle = \sum_{j=1}^{G} b_j e^{i\alpha_j} |SLP_j(L)\rangle \tag{1.25}$$

where

$$\alpha_j = \int_0^L \beta_j dz \tag{1.26}$$

α_j is the supermode accumulated phase when it passes through the coupler. For the fusion and tapering coupler, it is not necessary to know all of the supermodes. The initial field is a linear combination of the individual fiber modes, similarly, the supermodes excited in the coupler are only those modes which coupling with the individual modes are not zero. In other words, because the separation distance between the fibers at the entrance and exit end is large, each fiber is quasi independent of the others. Thus, the individual modes can be well approximated as a combination of the corresponding supermodes. So at $z=0$ and $z=L$, there are

$$|lp_i^{(u)}\rangle = \sum_{j=1}^{G} |SLP_j\rangle\langle SLP_j|lp_i^{(u)}\rangle = \sum_{j=1}^{G} P_{ji}|SLP_j\rangle \tag{1.27}$$

where

$$P_{ji} = \langle SLP_j|lp_i^{(u)}\rangle \tag{1.28}$$

$\mathbf{P}$ is the passage matrix between the basis of individual modes and supermodes, $\mathbf{P^T}$ is the transposed of $\mathbf{P}$. The field at both ends can be expressed in terms of individual mode as well as supermodes.

$$|\psi(0)\rangle = \sum_i a_i(0)|lp_i^{(u)}(0)\rangle = \sum_j b_j|SLP_j(0)\rangle \tag{1.29}$$

and

$$b_j = \sum_{i=1}^{M} a_i(0)\langle SLP_j(0)|lp_i^{(u)}(0)\rangle = \sum_{i=1}^{M} p_{ji}(0)a_i(0) \tag{1.30}$$

Substituting the Eqs.(1.25) and (1.30) into the Eq.(1.20), we have

$$A_i^{(u)}(L) = \langle lp_i^{(u)}(L)|\psi(L)\rangle = \sum_{j=1}^{G} b_j e^{i\alpha_j}\langle lp_i^{(u)}(L)|SLP_j(L)\rangle$$

$$= \sum_{j=1}^{G}\sum_{i=1}^{M}\langle lp_i^{(u)}(L)|SLP_j(L)\rangle e^{i\alpha_j} p_{ji}(0)a(0) \tag{1.31}$$

that is

$$A(L) = P^T(L)SP(0)a(0) \tag{1.32}$$

where the S indicates the phase matrix $S_{ij} = e^{\alpha_i}\delta_{ij}$. From Eq. (1.22), the transfer matrix

is

$$T = N^{-1}P^T(L)SP(0) \tag{1.33}$$

For the fused fiber coupler situation, the separation distance between two fiber cores is large at entrance and exit region, the overlap integration between different fiber is very small, so the two fibers can be thought of as independent, i.e $N_{ij} = \langle lp_i^{(u)}|lp_j^{(v)}\rangle \ll 1$ (u$\neq$v), and N is a quasi unity matrix I. In addition, if the entrance and exit end fibers are identical, $P(L) = P(0)$. Thus, the transfer matrix is

$$T = P^T SP \tag{1.34}$$

After knowing the transfer matrix, the power transmission can be obtained by Eq. (1.23), but the important thing is to calculate the supermode propagation constant. That will be discussed in the numerical technique's section.

1.2.2 Two Mode Fiber Coupler

It is known that a two-mode fiber can support two LP_{01} and four degenerate LP_{11} modes for two polarization directions. At both ends of the coupler, the two cores are far from each other, so that the overlap integral of the fields of both fibers can be neglected. At the input end, the coupler is excited with a field distribution that resembles the modes of a fiber, referred to as individual modes. This initial field can be approximately expressed as the sum and difference of the corresponding two supermodes. The details are explained in Fig. 1.2. Here, The supermodes are identified by their correspondence to the individual waveguide modes of a cladding-air waveguide (vanishing core limit) and their field distributions are plotted in Fig. 1.3. Each initial individual mode is a combination of two supermodes that travel with slightly different propagation constants; these supermodes will change their relative phase difference as they travel along a coupler. When they are in-phase at the input end and out-of-phase at the output end of a coupler, it becomes apparent that the individual modes that initially started out on fiber I move over to fiber II at the output end of the coupler. This power transfer phenomenon can be described by a transfer matrix. Note that the complete exchange of light power is only possible between modes that have equal phase velocities or, equivalently, equal propagation constants. To be more precise, the propagation constants must be equal for each fiber in isolation. Equality of the propagation constants, also called phase synchronism, naturally occurs when the two fibers are identical. Here, the couplers are made from two identical two-mode fibers, so all the guided modes LP_{01}, $LP_{11}{}^e$, and $LP_{11}{}^o$, are in phase synchronism. That means all the power in LP_{01}, $LP_{11}{}^e$ and $LP_{11}{}^o$ modes of fiber I will completely transfer into the corresponding guided mode of fiber II respectively. The relationship between individual modes and supermodes in Eq. (1.27) at the entrance and exit ends of coupler can be written as

$$\begin{bmatrix} |lp_{01}\rangle^{(I)} \\ |lp_{11}^{o}\rangle^{(I)} \\ |lp_{11}^{e}\rangle^{(I)} \\ |lp_{01}\rangle^{(II)} \\ |lp_{11}^{o}\rangle^{(II)} \\ |lp_{11}^{e}\rangle^{(II)} \end{bmatrix} = \frac{1}{\sqrt{2}} \begin{bmatrix} 1 & 1 & 0 & 0 & 0 & 0 \\ 0 & 0 & 1 & 1 & 0 & 0 \\ 0 & 0 & 0 & 0 & 1 & 1 \\ 1 & -1 & 0 & 0 & 0 & 0 \\ 0 & 0 & 1 & -1 & 0 & 0 \\ 0 & 0 & 0 & 0 & 1 & -1 \end{bmatrix} \begin{bmatrix} |SLP_{01}\rangle \\ |SLP_{11}^{o}\rangle \\ |SLP_{02}\rangle \\ |SLP_{12}\rangle \\ |SLP_{11}^{e}\rangle \\ |SLP_{21}\rangle \end{bmatrix}$$

(1.35)

Here superscripts o and e stand for odd and even, the superscripts I, II indicate the left and right fiber in Fig. 1.2. $|SLP_{ij}\rangle$ represent supermodes, $|lp_{lm}\rangle$ represent individual modes. The transfer matrix is symmetric and can be obtained as

$$\mathbf{T} = \mathbf{P}^{T}\mathbf{S}\mathbf{P}$$

$$= \frac{1}{2} \begin{bmatrix} e^{i\alpha_{01}} + e^{i\alpha_{11}^{o}} & 0 & 0 & e^{i\alpha_{01}} - e^{i\alpha_{11}^{o}} & 0 & 0 \\ 0 & e^{i\alpha_{02}} + e^{i\alpha_{12}} & 0 & 0 & e^{i\alpha_{12}} - e^{i\alpha_{02}} & 0 \\ 0 & 0 & e^{i\alpha_{11}^{e}} + e^{i\alpha_{21}} & 0 & 0 & e^{i\alpha_{11}^{e}} - e^{i\alpha_{21}} \\ e^{i\alpha_{01}} - e^{i\alpha_{11}^{o}} & 0 & 0 & e^{i\alpha_{01}} + e^{i\alpha_{11}^{o}} & 0 & 0 \\ 0 & e^{i\alpha_{12}} - e^{i\alpha_{02}} & 0 & 0 & e^{i\alpha_{02}} + e^{i\alpha_{12}} & 0 \\ 0 & 0 & e^{i\alpha_{11}^{e}} - e^{i\alpha_{21}} & 0 & 0 & e^{i\alpha_{11}^{e}} + e^{i\alpha_{21}} \end{bmatrix}$$

(1.36)

To obtain the transmission, we suppose that LP_{01}, LP_{11}^{o}, and LP_{11}^{e} have amplitudes a_1, a_2 and a_3 and the coupler is excited from fiber I. Then the output amplitude of field by (1.31) is
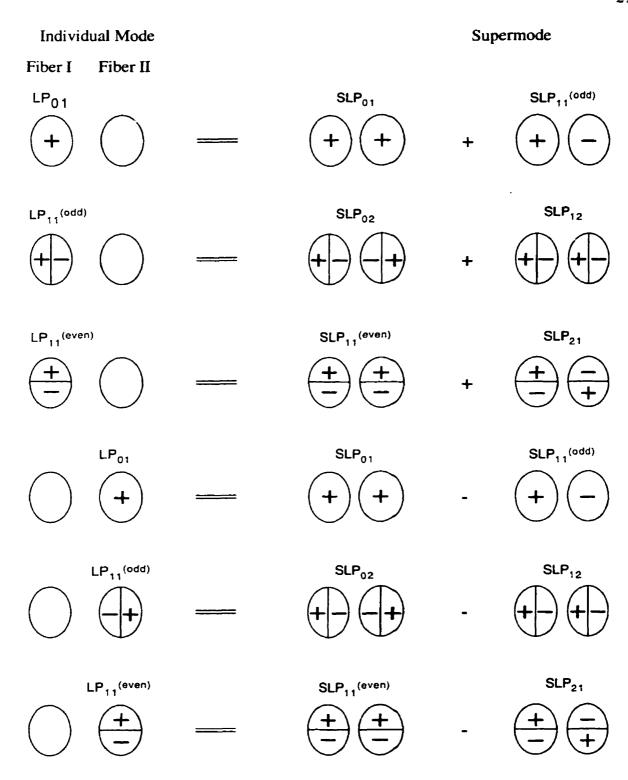
Figure 1.2 The relationship between the individual modes and supermodes.

SLP01

SLP11(odd)

SLP02

SLP12

SLP11(even)

SLP21
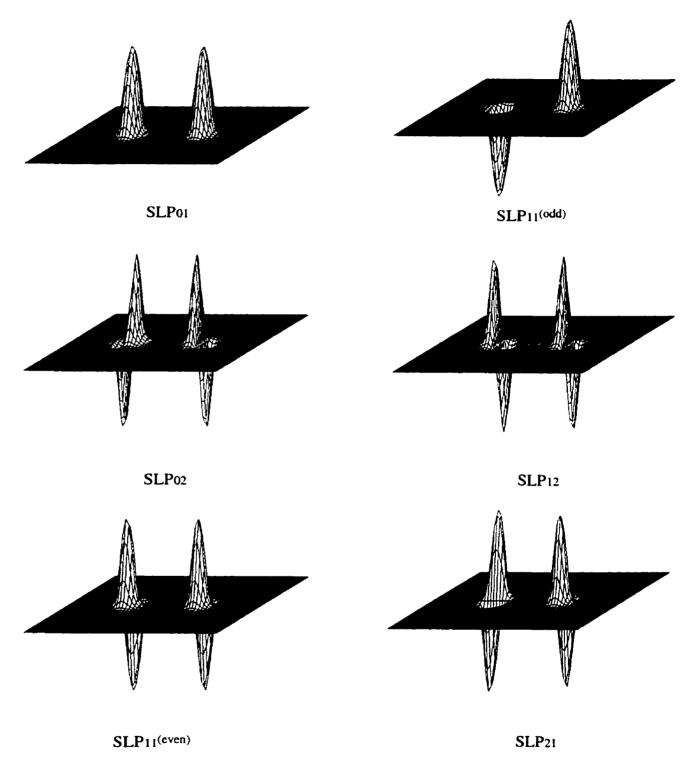
Figure 1.3 The supermode field distribution at the coupler end.

$$A(L) = T \begin{bmatrix} a_1 \\ a_2 \\ a_3 \\ 0 \\ 0 \\ 0 \end{bmatrix} = \begin{bmatrix} a_1 e^{\frac{i}{2}(\alpha_{01}+\alpha_{11}{}^o)} \cos\left(\frac{\alpha_{01} - \alpha_{11}{}^o}{2}\right) \\ a_2 e^{\frac{i}{2}(\alpha_{02}+\alpha_{12})} \cos\left(\frac{\alpha_{02} - \alpha_{12}}{2}\right) \\ a_3 e^{\frac{i}{2}(\alpha_{11}{}^e+\alpha_{121})} \cos\left(\frac{\alpha_{11}{}^e - \alpha_{21}}{2}\right) \\ i a_1 e^{\frac{i}{2}(\alpha_{01}+\alpha_{11}{}^o)} \sin\left(\frac{\alpha_{01} - \alpha_{11}{}^o}{2}\right) \\ i a_2 e^{\frac{i}{2}(\alpha_{02}+\alpha_{12})} \sin\left(\frac{\alpha_{02} - \alpha_{12}}{2}\right) \\ i a_3 e^{\frac{i}{2}(\alpha_{11}{}^e+\alpha_{121})} \sin\left(\frac{\alpha_{11}{}^e - \alpha_{21}}{2}\right) \end{bmatrix}$$

(1.37)

Accordingly, the transmission of each individual mode in one fiber is

$$P^{(I)}{}_{01} = a_1^2 \cos^2(\frac{\alpha_{01} - \alpha_{11}{}^o}{2})$$

$$P^{(I)}{}_{11}{}^o = a_2^2 \cos^2(\frac{\alpha_{02} - \alpha_{12}}{2})$$

$$P^{(I)}{}_{11}{}^e = a_3^2 \cos^2(\frac{\alpha_{11}{}^e - \alpha_{21}}{2})$$

(1.38)

and in other fiber is

$$P^{(II)}{}_{01} = a_1^2 \sin^2(\frac{\alpha_{01} - \alpha_{11}{}^o}{2})$$

$$P^{(II)}{}_{11}{}^o = a_2^2 \sin^2(\frac{\alpha_{02} - \alpha_{12}}{2})$$

$$P^{(II)}{}_{11}{}^e = a_3^2 \sin^2(\frac{\alpha_{11}{}^e - \alpha_{21}}{2})$$

(1.39)

Because we only consider the transmission of each individual-mode, we always assume that LP_{01}, $LP_{11}{}^o$ and $LP_{11}{}^e$ have equal components in the initial field and each mode has unit power, thus $a_1 = a_2 = a_3 = 1$. The above formulas only hold for the scalar approximation. Assuming that the light propagates with two perpendicular polarization directions in a nearly independent way, we can thus calculate the respective transmissions, then add them.

$$P^{(I)}_{01} = a_1^2 \left[\xi \cos^2(\frac{\alpha_{01}^x - \alpha_{11}^{o\,x}}{2}) + (1-\xi)\cos^2(\frac{\alpha_{01}^y - \alpha_{11}^{o\,y}}{2}) \right]$$

$$P^{(I)}_{11}{}^o = a_2^2 \left[\xi \cos^2(\frac{\alpha_{02}^x - \alpha_{12}^{o\,x}}{2}) + (1-\xi)\cos^2(\frac{\alpha_{02}^y - \alpha_{12}^{o\,y}}{2}) \right] \qquad (1.40)$$

$$P^{(I)}_{11}{}^e = a_3^2 \left[\xi \cos^2(\frac{\alpha_{11}^x - \alpha_{21}^{o\,x}}{2}) + (1-\xi)\cos^2(\frac{\alpha_{11}^y - \alpha_{21}^{o\,y}}{2}) \right]$$

ξ is the portion of power injected with an $\hat{x}$ direction polarization. In particular, if the light source is nonpolarized, $\xi = 1/2$. α_{ij}^x and α_{ij}^y are the accumulated phase in the $\hat{x}$ and $\hat{y}$ polarization directions, respectively, and depend on the shape of the coupler. The birefringence effect of the couplers on the total transmissions gives rise to a beat between the two different polarization directions.

1.2.3 Mode separating coupler

It is known that the power transfer in a coupler is a result of a beating of the supermodes. For example, LP_{01} can be expressed as the sum or difference of the supermode SLP_{01} and $SLP_{11}^{(odd)}$, each of them propagating with a slightly different propagation constant β_{01} and β_{11}^o. These superposed fields will change their relative phase as they travel along the coupler. If the fields are in-phase at z=0, and they will be the first time out-of-phase at $z=L$, the difference of phase must satisfy $\int_0^L (\beta_{01} - \beta_{11}^o)dz = \pi$. It is thus apparent that the light power that initially started out from fiber I moves to fiber II after traveling the distance L. The similar case occurs for LP_{11}^o, i.e., SLP_{02} and SLP_{12} beating with the propagation constants β_{02} and β_{12} respectively; and for LP_{11}^e, $SLP_{11}^{(even)}$ and SLP_{21} beating with the propagation constants β_{11}^e and β_{21} respectively. Using the transfer matrix, one can give the power transmission of the coupler measured at fiber I,

$$P^{(1)}{}_{01} = a_1^2 \cos^2[\frac{1}{2}\int_0^L (\beta_{01} - \beta_{11}{}^o)dz]$$ (1.41)

$$P^{(1)}{}_{11}{}^o = a_2^2 \cos^2[\frac{1}{2}\int_0^L (\beta_{02} - \beta_{12})dz]$$ (1.42)

$$P^{(1)}{}_{11}{}^e = a_3^2 \cos^2[\frac{1}{2}\int_0^L (\beta_{11}{}^e - \beta_{21})dz]$$ (1.43)

where a_1, a_2 and a_3 are the amplitudes of the LP_{01}, $LP_{11}{}^o$ and $LP_{11}{}^e$ mode components of the initial field, respectively. By a similar analysis of the polarizing beam splitter [5], if the length of coupler L simultaneously satisfies the following conditions:

$$\int_0^L (\beta_{01} - \beta_{11}{}^o)dz = 2m_1\pi$$ (1.44)

$$\int_0^L (\beta_{21} - \beta_{11}{}^e)dz = (2m_2 + 1)\pi$$ (1.45)

$$\int_0^L (\beta_{02} - \beta_{12})dz = (2m_3 + 1)\pi$$ (1.46)

where m_1, m_2 and m_3 are integers, the coupler will act as a mode separating coupler: if both LP_{01} and LP_{11} are excited at the input end through fiber I, after the coupler, LP_{01} will appear in fiber I and both orientation LP_{11} modes will appear in fiber II (see Fig. 1.4). Especially, when $m_1 = 0$, $m_2 \neq 0$ and $m_3 \neq 0$, SLP_{01} and $SLP_{11}{}^{(odd)}$ are still degenerate, the power of LP_{01} mode will stay in fiber I and the powers of both orientation LP_{11} modes transfer into fiber II. For this case, the taper ratio and elongation will be smaller than that of $m_1 \neq 0$ cases. To satisfy the Eqs (1.44)-(1.46), the longitudinal geometrical profile and index profile are very important.

Fiber I   Fiber I

$LP_{01}+LP_{11}$ LP_{01}

                                                                            LP_{11}

Fiber II   Fiber II
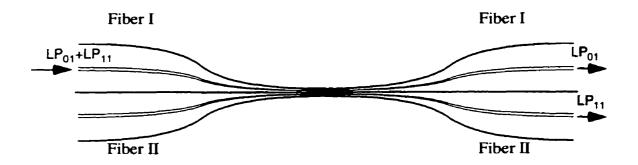
Figure 1.4   The mode separating coupler scheme.

1.3   Numerical Techniques

High speed and ease of reconfiguration are the foremost requirements of numerical techniques for design problems, where a system may have to be analyzed many times with different design parameters. Our two numerical draughthorses are the finite difference method and the fiber mode expansion method. The former is used to calculate the polished fiber coupler and the latter is an accurate and flexible way of calculating the fusion and tapering fiber coupler.

1.3.1   Finite Difference Method

The finite difference method is probably the best known numerical method for solving boundary value problems and has been applied to the optical waveguide problems for some years. This method demands the division of the waveguide cross section into small subregions, and therefore, is suitable for modeling inhomogeneous media and complicated boundaries. A direct way of applying the finite difference method is to replace

the differentiation in the wave equation by the differences of the fields evaluated at the nodes of a rectangular mesh that discrete the waveguide cross section. The existing methods almost exclusively use a five-point finite difference formula because of its simplicity.

Before employing a finite difference method to determine the modal effective index and field distribution of an optical waveguide, it is frequently convenient to represent the transverse index profile $n(x,y)$ by the rectangular cell array structure as illustrated in Fig. 1.5, with a grid point located at the center of each cell of constant refractive index and changes in refractive index being permitted only at boundary cell.
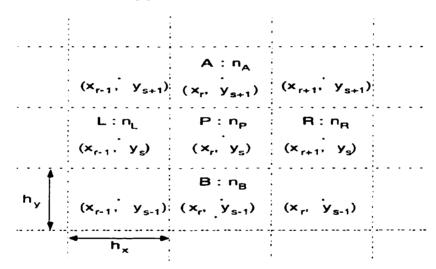
Figure 1.5 Cell structure of the finite difference grid.

Scalar modes are the eigensolutions of the equation

$$\nabla_t^2 \psi + k^2 n^2 \psi = \beta^2 \psi \tag{1.47}$$

where ψ is continuous throughout the solution domain. The usual five-point difference approximation for equation are established by defining the notation

$$n_{r,s} = n(x_r, y_s) \tag{1.48}$$

$$\psi_{r,s} = \psi(x_r, y_s) \tag{1.49}$$

and consider the Taylor series

$$\psi_{r+1,s} = \sum_{m=0}^{\infty} (\frac{h_x}{m!})^m (\frac{\partial^m \psi}{\partial x^m})_{r,s} \tag{1.50}$$

$$\psi_{r-1,s} = \sum_{m=0}^{\infty} (-1)^m (\frac{h_x}{m!})^m (\frac{\partial^m \psi}{\partial x^m})_{r,s} \tag{1.51}$$

which yield the approximation

$$(\frac{\partial \psi}{\partial x})_{r,s} = \frac{(\psi_{r+1,s} - \psi_{r-1,s})}{2h_x} + O(h_x^2) \tag{1.52}$$

$$(\frac{\partial^2 \psi}{\partial x^2})_{r,s} = \frac{(\psi_{r+1,s} - 2\psi_{r,s} + \psi_{r-1,s})}{h_x^2} + O(h_x^4) \tag{1.53}$$

A similar analysis leads to the results

$$(\frac{\partial \psi}{\partial y})_{r,s} = \frac{(\psi_{r,s+1} - \psi_{r,s-1})}{2h_y} + O(h_y^2) \tag{1.54}$$

$$(\frac{\partial^2 \psi}{\partial y^2})_{r,s} = \frac{(\psi_{r,s+1} - 2\psi_{r,s} + \psi_{r,s-1})}{h_y^2} + O(h_y^4) \tag{1.55}$$

The approximations (1.52) and (1.54) enable the scalar equation to be replaced by the five-point difference scheme

$$\frac{\psi_{r,s-1}}{h_y^2} + \frac{\psi_{r-1,s}}{h_x^2} + (kn_{r,s}^2 - \frac{2}{h_x^2} - \frac{2}{h_y^2})\psi_{r,s} + \frac{\psi_{r+1,s}}{h_x^2} + \frac{\psi_{r,s+1}}{h_y^2} = \beta^2 \psi_{r,s} \tag{1.56}$$

at the mesh point (x_r, y_s). By applying this approximation at each mesh point, with appropriate amendments when (x_r, y_s) is adjacent to the outer boundary of the solution domain, we obtain the algebraic eigenvalue problem.

$$H_f V_f = \beta^2 V_f \tag{1.57}$$

in which H_f is a band matrix, β is the scalar mode propagation constant, and V_f is the corresponding normalized eigenvectors representing the field profile.

1.3.2 Fiber Mode Expansion Method

To obtain the optical transmission of a longitudinally varying coupler, a numerical method is necessary because there is no accurate analytical solution. Several papers have given comparisons of different methods. Among them, some methods are very fast but not accurate, such as the effective-index method, some methods are relatively accurate but very slow, and others lack the flexibility to be practical for the calculation of the supermodes. Most numerical methods can calculate the propagation constant of a mode but do not give accurate values for the field at the interfaces. This is particularly difficult for fused fiber couplers because of the curvature at the interfaces: for all the methods describing the field with an array of points, the grid points are not on the interface. To improve the accuracy, the interpolation techniques and the increase of number of grid points can be used, but it is always limited by the computational power and the time available. The boundary conditions are also problematic because setting the boundary field to zero or defining an exponentially decreasing condition is not exact.

One useful method to overcome these problems and find various parameters of waveguides is the mode expansion method [85-87]. The central idea of the method is to expand the unknown modes of the waveguide on some known basis function, converting the actual differential eigen problem of scalar wave equation to a eigen value problem that can be solved with less effort. The method especially suitable for the coupler cases has been developed by Daxhelet *et. al* . [88]. For fused fiber couplers, the known waveguide is a two-layer optical fiber while its radius the same as that of the coupler cross section and its index equal to that of the fiber cladding. These two-layer fiber modes have

analytical expressions and thus can be computed with a very high accuracy. This method that has been referred to as the fiber mode expansion method (FMEM) is adequate for resolving scalar wave equations and the validity of its results can be furthermore increased by calculating polarization corrections to the modal propagation constants, using a perturbative approach.

For convenience, we use the Dirac symbol to represent the scalar field and rewrite the scalar wave equation as

$$\nabla^2|SLP\rangle + k^2 n^2(x,y)|SLP\rangle = \beta^2|SLP\rangle \tag{1.58}$$

where ∇^2 represents the transverse Laplacian operator, $|SLP\rangle$ is the supermode modal field of a coupler, β its propagation constant and $n(x,y)$ is the cross section index profile of the waveguide. One defines a reference fiber that has well-known modal eigenfunctions $|lp_i\rangle$ obeying the following scalar wave equation

$$\nabla^2|lp_i\rangle + k^2 n_f^2(x,y)|lp_i\rangle = \tilde{\beta}_i^2|lp_i\rangle \tag{1.59}$$

where $\tilde{\beta}_i$ is the propagation constant of mode $|lp_i\rangle$ and $n_f(x,y)$ is the cross section index profile of the reference fiber. It is well known that all the fiber modes including guided, evanescent and the radiation modes constitute a complete set of functions upon which any field can be expanded. However, in practical cases, the expansion will be limited to a finite number of guided modes. All the evanescent and radiation modes are neglected because of their very small contribution to the guided modes. So, the mode of the composite structure under study can be expanded in terms of the modes of the reference waveguide

$$|SLP\rangle = \sum_i c_i|lp_i\rangle \tag{1.60}$$

Substituting Eq. (1.59) and (1.60) into (1.58), we obtain

$$\sum_i c_i \bar{\beta}_i^2 |lp_i\rangle + \sum_i c_i k^2 \left[n^2(x,y) - n_f^2(x,y) \right] lp_i\rangle = \beta^2 \sum_i c_i |lp_i\rangle \tag{1.61}$$

If the vector $\langle lp_j |$ is applied to both sides of this equation, we obtain

$$\sum_i \left\{ \beta_i^2 \delta_{ij} + k^2 \langle lp_j | \left[n^2(x,y) - n_f^2(x,y) \right] lp_i\rangle \right\} c_i = \beta^2 c_j \tag{1.62}$$

Defining

$$C_{ij} = \langle lp_i | k^2 \left(n^2 - \bar{n}_f^2 \right) |\varphi_j\rangle = \int \varphi_i \left[k^2 \left(n^2 - \bar{n}_f^2 \right) \right] \varphi_j ds \tag{1.63}$$

$$H_{ij} = \delta_{ij} \bar{\beta}^2 + C_{ij} \tag{1.64}$$

The Eq. (1.61) can be rewritten as a matrix problem

$$HV = \beta^2 V \tag{1.65}$$

The problem is thus conversed to a matrix eigenvalue problem. To solve this equation, a shifted inverse power method can be used to iterate the eigenvectors. Note that the integrals in Eq. (1.63) are only computed in the regions where the index of the guide under study differs from that of the reference waveguide. When the waveguide cross section geometry presents the circular symmetry or slightly deviates from it, the reference waveguide is naturally chosen to be a two-layer (core/cladding) step-index fiber, which is still a well-know waveguide with analytical eigenfunctions. Since the index profile is two dimensional, the subscript i relative to the fiber modes actually represents a pair of subscripts (l, m). The solutions are the so-called LP_{lm} modes, which are combinations of Bessel and trigonometric functions [76]. Once the supermode fields are generated, we can do the polarization corrections. In the scalar approximation, each supermode is doubly degenerate. For each polarization direction, the propagation constants are given by [76]

$$\beta_x^2 = \beta^2 - \frac{\int_A \frac{\partial \psi(x,y)}{\partial x} \psi(x,y) \frac{\partial \ln n^2(x,y)}{\partial x} dA}{\int_A \psi^2(x,y) dA}$$

$$\beta_y^2 = \beta^2 - \frac{\int_A \frac{\partial \psi(x,y)}{\partial y} \psi(x,y) \frac{\partial \ln n^2(x,y)}{\partial y} dA}{\int_A \psi^2(x,y) dA}$$

(1.66)

where β is the scalar unperturbated propagation constant of any supermode of the considered 2×2 fused coupler.

1.3.3 Shifted Inverse Power Iteration Method

In the last two sections, light propagating in waveguide is finally converted into a eigenvalue problem. The direct method for solving the eigenvalue equation such as Gaussian elimination, pivoting strategies and LU decomposition may not be the best method to use for large sparse systems of equations. However, there is an alternative class of methods that can be used for this problem; namely, the iterative method starting from a first approximation that is successively improved until a sufficiently accurate solution is obtained. One of the most widely used method is the shifted inverse power iteration method.

For a eigenvalue problem

$$HV = \beta^2 V \tag{1.67}$$

It is assumed that a square matrix H of order Q has distinct eigenvalues β_i^2 ($i=$ 1,2,3,......,Q) together with Q corresponding eigenvectors u_i. It is also assumed that any initial non-null vector V can be expressed as a linear combination of these eigenvectors,

$$V_0 = \sum_{i=1}^{Q} \gamma_i u_i \tag{1.68}$$

in which at least one of the scalar coefficients γ_i is non-zero. The shifted inverse power eigenvalue equation can be written as

$$(\mathbf{H} - \tau^2 \mathbf{I})^{-1} \mathbf{V}_m = (\beta^2 - \tau^2)^{-1} \mathbf{V}_m \qquad (1.69)$$

where $\mathbf{I}$ is the identity matrix and τ is an initial estimate to the required eigenvalue β^2 and its iteration form is

$$\mathbf{V}_{m+1} = (\mathbf{H} - \tau^2 \mathbf{I})^{-1} \mathbf{V}_m = (\mathbf{H} - \tau^2 \mathbf{I})^{-(m+1)} \mathbf{V}_0 \qquad (1.70)$$

where m $(=1,2,3,...)$ is the iteration counter. It is next assumed that the eigenvalues are so ordered that

$$\left| \beta_i^2 - \tau^2 \right| \langle \left| \beta_{i+1}^2 - \tau^2 \right| \qquad (i=1, 2, 3,..., Q-1) \qquad (1.71)$$

which enables (1.70) to be rewritten in the form

$$\mathbf{V}_{m+1} = (\beta_1^2 - \tau^2)^{-(m+1)} \left(\gamma_1 \mathbf{u}_1 + (\beta_1^2 - \tau^2)^{(m+1)} \sum_{i=2}^{Q} \frac{\gamma_i \mathbf{u}_i}{(\beta_i^2 - \tau^2)^{m+1}} \right) \qquad (1.72)$$

For sufficiently large m, this becomes

$$\mathbf{V}_{m+1} = (\beta_1^2 - \tau^2)^{-(m+1)} \left(\gamma_1 \mathbf{u}_1 + \delta \right) \qquad (1.73)$$

in which the components of δ tend to zero, hence

$$\mathbf{V}_{m+1} \propto \frac{\gamma_1 \mathbf{u}_1}{(\beta_1^2 - \tau^2)^{(m+1)}} \qquad (1.74)$$

This shows that after m time iterations the current improved eigenvector is proportional to the true eigenvectors. If one normalizes the guess eigenvectors in each iteration step, it will ensure that the components of $\mathbf{V}_{m+1}$ converge to constant finite values as m is sufficiently large. If we set

$$V_m \bullet V_m = \chi_m^{\ 2} \tag{1.75}$$

replacing the vector by its normalized vector, the iteration process in (1.70) become

$$V_{m+1} = (H - \tau^2 I)V_m / \chi_m = (\beta^2 - \tau^2)^{-1} V_m / \chi_m \tag{1.76}$$

when m is sufficiently large, $V_{m+1} \approx V_m$, so that the eigenvalue could be obtained from (1.76) as

$$\beta_1^2 = \tau^2 + \frac{1}{\chi_m} \tag{1.77}$$

The corresponding eigenvectors will converge into

$$u_1 \approx \frac{V_m}{\chi_m} \tag{1.78}$$

where β^2 is the eigenvalue of H that is closer to the initial estimate τ^2 than the other (Q-1) eigenvalues β_i^2 (i=1, 2, 3, ..., Q). During each inverse power iteration m, it requires the solution of a system of linear equations of the form

$$(H - \tau^2 I)V = \bar{H}V = b \tag{1.79}$$

where H is independent of m. There are two ways of solving these problems. One is the completely LU decomposition method which factories H into triangular product. This method can determine any desired eigenmode of a waveguide, but it does not preserve their sparse diagonal structure due to considerable non-zero fill-in of the band. Thus it needs a large computer memory to store the whole band. The other is the Rayleigh quotient method that does not require the storage of matrix H. However, this method can only find the fundamental symmetric and leading anti-symmetric polarized modes of waveguide structure that possess left-right symmetry. Higher order modes can be found only if an accurate initial approximation to that mode's field profile is available. Stern et al

[89] applied BI-CGSTAB [90] with incomplete LU to the inverse power iteration method overcoming the limitation of both above methods. By their method, the bandwidth and the sparse pattern of the matrix can be preserved. Thus their iterative solver is faster when execute times are large and the relative memory requirement is reduced. In this thesis, their method was used to resolve the linear equation at each iteration step.

Chapter 2

Polishing Method

2.1 Introduction

The unique kind of mode separating coupler was fabricated by Thornburg *et al.* using a polishing method [91]. They polished a two-mode fiber and brought in contact with a prism in such a manner as to only allow the LP_{11} mode to couple into the prism. The LP_{11} mode was received through another two-mode fiber that was stacked on the other side of the prism. However, this device is not an all-fiber mode separating coupler. Sorin *et al.* [70] polished two different fibers; one a single mode fiber and the other a two-mode fiber, and stacked them together. Their coupler's function is to convert the LP_{01} mode into the LP_{11} mode in the other branch. Barcelos *et al.* [73] and Pechstedt *et al.* [74] constructed couplers in which the function is selective LP_{11} mode coupling from the fiber into waveguides, or the reverse. In this chapter we will study the possibility of fabricating a mode separating coupler by polishing two identical fibers.

2.2 Polishing Method

The methods of fabricating a polished fiber can be divided into two groups. One is Nicholls' method [31], where a bare fiber is cemented into a slot in a prepared quartz

Polished region

Fiber

Fused silica block

(a)

Polished   Fiber

(b)

Polished   Coupler

(c)
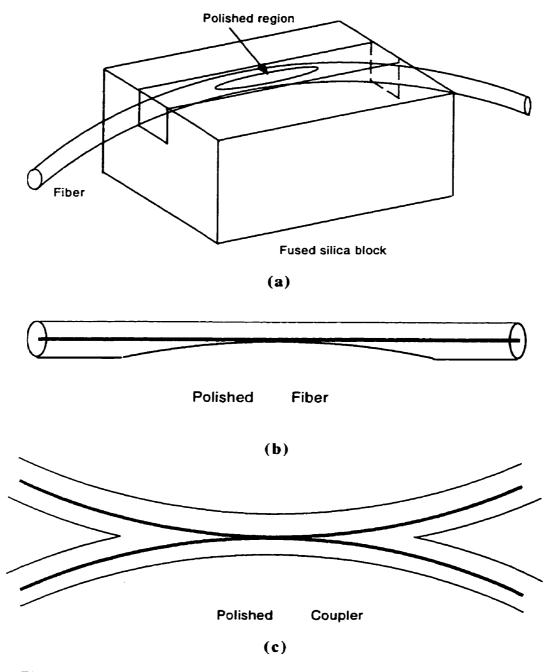
Figure 2.1 Schematic diagram of (a) set up. (b) polished fiber. (c) polished coupler used in by Nicholls *et al.*

block and both the block and the fiber are ground until the outer polished surface of the cladding just becomes grazed. Fig. 2.1(a) shows the schematic diagram of the fiber polishing setup by Nicholls' method. The polished fiber is shown in Fig. 2.1(b), and the polished coupler is shown in Fig. 2.1(c).

The other polishing method is attributed to Hussey *et al.* [92]. A bare fiber is suspended under slight tension over a small diameter diamond grit polishing wheel. The polished length can be altered by changing the contact angle of the fiber on the wheel or diameter of the polishing wheel. The polished amount is controlled by dynamically monitoring the transmission loss with a detector [33]. The schematic diagram of Hussey's set up is shown in Fig. 2.2.

Polishing Wheel

Laser

Fiber

Detector

(a)

Polished   Fiber

(b)
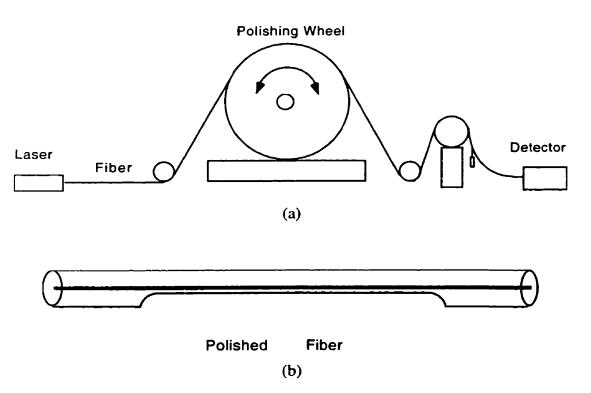
Figure 2.2 Schematic diagram of (a) polishing setup and (b) polished fiber used by Hussey *et. al.*

2.3 Numerical Analysis

From the viewpoint of coupling mechanism, polished couplers can be divided into two groups: weak coupling and strong coupling devices. The first group is characterized by the fact that the modes become coupled through their evanescent fields. A typical example of such couplers is made by Digonnet and Shaw [26]: their fiber cores were not polished. The mechanism of weakly coupled devices can be analyzed by using coupled mode theory [78, 79], or a perturbation theory [71]. A sufficient power transfer cannot be obtained if the distance between the cores is too large. However, when this distance is too small or two cores are touching, the aforementioned theory can be inaccurate [93].

Lately, fiber specialists have been paying more attention to the second group, which is characterized by the fact that the coupling region is regarded as a new single waveguide, in which the beat phenomenon between supermodes of this composite structure results in the exchange of power. Here, an entire coupler with strong coupling made by the polishing technique is considered. Such a coupler consists of two identical fibers with their cores nearly touching each other (Fig. 2.1 (c)). Since the core of the coupling region still plays most the important role in guidance of the light wave, it cannot be neglected anymore. We will use the supermode theory to analyze this kind of coupler and find the proper conditions to realize mode separation.

2.3.1 Effective Index

By the supermode theory, the fiber contact region can be regarded as a new waveguide and the optical modes are not the simple combination of the individual fiber modes. The supermodes of the new waveguide need to be calculated. For the polished coupler, the fiber modes expansion method is not suitable because the optical wave of polished couplers is distributed in the small core region, so it would need too many fiber modes to

be computed. Alternatively, we use the finite difference method to calculate the scalar modes.

For scalar modes, the electromagnetic fields and their gradients are assumed to be completely continuous throughout the modeled waveguide structure, so that such modes are the eigensolutions of a single scalar Helmoltz equation.

$$\nabla_t^2 \psi + k^2 n^2 \psi = \beta^2 \psi \tag{2.1}$$

where ψ, $\dfrac{\partial \psi}{\partial x}$ and $\dfrac{\partial \psi}{\partial y}$ are continuous throughout the solution domain, k is the wave number in vacuum, n is the refractive index and β is modal propagation constant. This equation can be replaced at each internal grid point by the usual five-point difference approximation.

$$\frac{\psi_{r,s-1}}{h_y^2} + \frac{\psi_{r-1,s}}{h_x^2} + (kn_{r,s}^2 - \frac{2}{h_x^2} - \frac{2}{h_y^2})\psi_{r,s} + \frac{\psi_{r+1,s}}{h_x^2} + \frac{\psi_{r,s+1}}{h_y^2} = \beta^2 \psi_{r,s} \tag{2.2}$$

where h_x and h_y are the steps in $\hat{x}$ and $\hat{y}$ direction respectively. Thanks to the symmetry of the coupler structure, the calculation is required for one quadrant only and the mesh covering this area is shown in Fig. 2.3.

The refractive index changes only in the cells that covers the interface between core and cladding, cladding and air. The refractive indices in such cells are taken to be their average values.

$$\bar{n}^2_{r,s} = \frac{1}{h_x h_y} \iint_{h_x h_y} n^2(x, y) dx dy \tag{2.3}$$

The finite difference grid is enclosed by an outer rectangular box boundary, along which is imposed a closed boundary condition with zero values for the field profile at all points in boundary AB and BC. For the grid points on the boundary x and y axes, the field profile values depend on the supermode to be calculated.

If the supermode is symmetrical with respect to the y axis, that is the field value is equivalent at both sides of y axis, the supermode is named an even mode; if the supermode is anti-symmetrical to the y axis, that is the absolute field value is equivalent at both sides of y axis but the left side field is negative, the supermode is an odd mode. If the supermode is symmetrical with respect to the x axis, the field value is equivalent on both sides of x axis; while the supermode is anti-symmetrical to the x axes, the absolute field value is equivalent at both sides of x axis but the below side field is negative. These boundary conditions are summarized as follows when the coupler is enclosed by a grid with $L \times L$ points.
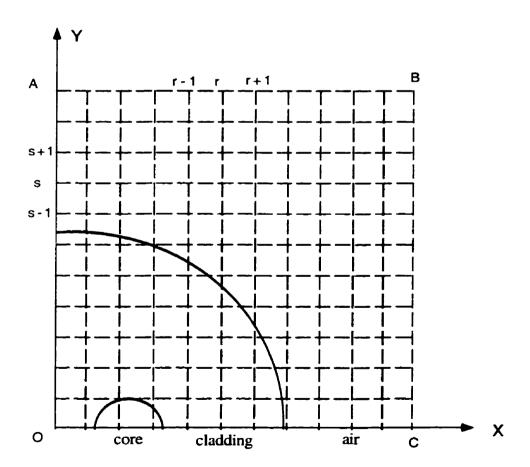
Figure 2.3 The grid points and calculation area.

$$\psi_{r,L+1} = 0$$

$$\psi_{L+1,s} = 0 \qquad (r, \; s=1...L) \qquad\qquad (2.4)$$

$$\psi_{0,s} = \psi_{2,s} \qquad \text{(y symmetric modes)}$$

$$-\psi_{0,s} = \psi_{2,s} \qquad \text{(y anti-symmetric modes)}$$

$$\psi_{r,0} = \psi_{r,2} \qquad \text{(x symmetric modes)}$$

$$-\psi_{r,0} = \psi_{r,2} \qquad \text{(x anti-symmetric modes)}$$

By applying the discretisation equation (2.2) at each internal grid point, with boundary conditions when grid point is on a boundary of the solution domain, we obtain a set of equations. If we rewrite the field profile subscript as

$$\psi_m = \psi_{r,s} \qquad \text{with } m = r+L(s-1), \qquad (r, \; s=1...L) \qquad\qquad (2.5)$$

the set of equations can be represented in a matrices form

$$\mathbf{H}\psi = \beta^2 \psi \qquad\qquad (2.6)$$

So, the finite difference scheme converts Eq. (2.2) into a matrix eigenvalue problem. Where $\mathbf{H}$ is a real band matrix and β is the modal propagation eigenvalue and ψ is the eigenvector corresponding the appropriate modal field profile.

The matrix eigenvalue problem can be solved by means of the shifted inverse power iteration method that is presented in Chapter 1. The effective index of a supermode depends upon the depth of the polished part of a fiber. For clarity, we give the definition of the polishing degree

$$p = \frac{d_{cl}}{\rho_{cl}} \qquad 0<p<1 \qquad\qquad (2.7)$$

where d_{cl} is the depth of polished part of fiber and ρ_{cl} is the cladding radius of the fiber as shown in Fig. 2.4. p is independent of the fiber core radius.
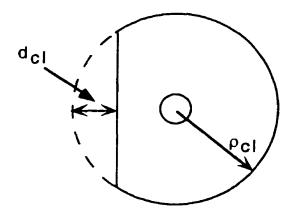
Figure 2.4 Cross section of polished fiber.

For the polished coupler the two cores of fibers exist, so the supermodes are still guided in the core area. Although the supermodes are not simply linear combinations of the individual fiber modes, they are still determined by the individual fiber modes. In the weakly guiding approximation, the two-mode fiber can support the six modes, two LP_{01} modes and four degenerates LP_{11} modes in two polarization directions. Since the two polarization signals do not interfere with each other, we can only consider the propagation for one polarization and add the two polarization transmissions at the output end of coupler. In one polarization direction, the two-mode fiber has one LP_{01} mode and two LP_{11} modes with two orientation lobes, consequently, six supermodes are supported in composite structure. These supermodes are identified by the same way as fusion couplers in the vanishing core limit. Thus, the six supermodes are SLP_{01}, $SLP_{11}^{(odd)}$, SLP_{02}, SLP_{12}, $SLP_{11}^{(even)}$, SLP_{21}. Their effective indices as functions of the polishing degree are calculated and plotted in Fig. 2.5. The fiber used in calculation is SMF28™ and its parameters are listed in Table. 2.1. This kind of fiber becomes a two-mode fiber when it is operated at 0.9754 μm light source. From Fig. 2.5 we can see that: (i) When the polishing degree is less than 0.85, the supermodes effective indices are degenerate; the effective indices are the same as those of the individual fiber modes. (ii) When the

polishing degree is equal 1, half part of the fiber is polished and the coupler seems like a single fiber, for this case only three supermodes are in the core and the other modes become the cladding modes, which coincides with the individual two-mode fiber situation. (iii) When the polishing degree is 0.928, which corresponds to the two cores touching for SMF28™ fiber, the six supermodes are still in the core area. For a polishing degree of 0.948, the supermode SLP_{12} becomes a cladding mode, so it is not necessary to worry about the power loss if the polishing degree is less than 0.948. The cladding refractive index is 1.451129 for 0.9754 μm indicated in Fig. 2.5 by the heavy dash-dot line.

ρ_{co}	ρ_{cl}	Δn	n_{cl}	λ
4.5 μm	62.5 μm	0.045	1.451129	0.9754 μm

Table 2.1 The parameters of SMF28™ fiber used for simulation.
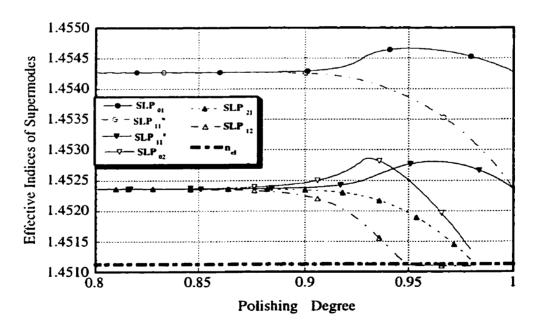
Figure 2.5 Effective index of supermodes versus polishing degree for SMF28™ operating at 0.9754 μm.

In the supermode formalism, the power exchanges are caused by the beat phenomenon between supermodes, which can be described by a beat length, which is the distance along the coupler for which there is total transfer of power from one fiber to the other and back again. When the phase difference between supermodes changes by π, the power transfers into the other fiber and when it changes 2π the power comes back to the entrance fiber. The beat length between the supermodes i and j is defined by

$$Z_{b_{ij}} = \frac{2\pi}{\beta_i - \beta_j}$$

(2.8)

where β_i and β_j are the supermode propagation constants. Fig. 2.6 shows the beat length corresponding to the effective indices of the supermodes in Fig. 2.5. The beat between SLP_{01} and $SLP_{11}^{(odd)}$, SLP_{02} and SLP_{12}, and $SLP_{11}^{(even)}$ and SLP_{21}, correspond to the coupling lengths of LP_{01}, LP_{11}^{o}, and LP_{11} respectively. It is worth noting that the beat lengths of both orientation LP_{11} modes are very different. The value of the odd LP_{11} mode beat length is much smaller than that of even LP_{11} mode; that means the interaction between SLP_{02} and SLP_{12} is much stronger than that between $SLP_{11}^{(even)}$ and SLP_{21}. This can be explained intuitively by physical mechanisms, since the field distribution of $SLP_{11}^{(even)}$ has a zero zone in the core center and oriental to the supermodes SLP_{21}, the integration of field overlaps between these two supermodes is smaller than that between SLP_{02} and SLP_{12}. The other thing that needs to be mentioned is that there are two crossing points A and B between beat length curve of LP_{01} and even LP_{11} mode in Fig. 2.6 corresponding to the polishing degree 0.9065 and 0.9510, respectively. That means the LP_{01} and even LP_{11} mode will oscillate synchronously at the crossing point, and the two modes can not be separated.

The mode separating couplers made from the polishing method can be divided into two groups. If the polishing degree is less than 0.9, the beat lengths are long and the

interaction between supermodes is weak. However, because a practical polished coupler can not be very long due to the difficulty of the fiber alignment, the polishing degree is usually larger than 0.86. So, a coupler in which the polishing degree is less than 0.9 is named as weakly coupling coupler. If the polishing degree is between 0.9 and 0.948, the beat lengths are short and the interactions between supermodes are stronger, and a coupler functioning as a mode separating coupler may be fabricated with short longitudinal size. If the polishing degree is more than 0.948, some supermodes will become cladding modes and much power loss will occur. So, the polishing degrees recommended for mode separating couplers range from 0.86 to 0.9 and from 0.91 to 0.948 for the polished coupler made of SMF28™ fiber.
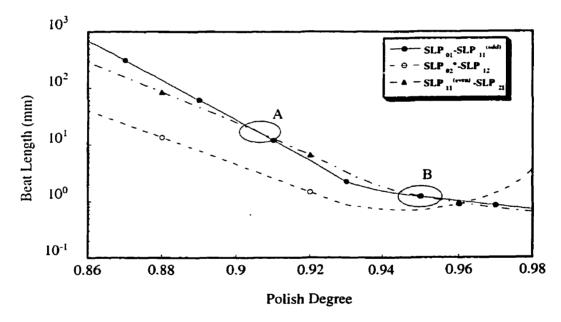
Figure 2.6 Beat lengths versus polishing degree for SMF28™ fiber. The parameters are the same as those in Fig. 2.5.

2.3.2 Uniform Coupler

If the fiber is polished by Hussey's method, the polished flat region is uniform except for the short transitions at each end of the polished region. A reasonably simplified model of

the coupler assumes that the two cores are almost parallel [92], so that the effective indices of the supermodes are the constant along the coupler longitudinal direction. Thus, the transmission of the coupler can be calculated by the transfer matrix method presented in Chapter 1. Since the transmission is measured in individual fibers, and the two branch fibers are well separated, the non-orthogonal coefficient is very small and can be neglected. So we have the transmission

$$P^x{}_{01} = a_1{}^2 \cos^2\left(\frac{\Delta\alpha_{01}}{2}\right)$$

$$P^x{}_{11(odd)} = a_2{}^2 \cos^2\left(\frac{\Delta\alpha^o{}_{11}}{2}\right) \qquad (2.9)$$

$$P^x{}_{11(even)} = a_3{}^2 \cos^2\left(\frac{\Delta\alpha^e{}_{11}}{2}\right)$$

where

$$\Delta\alpha_{01} = (\beta_{01} - \beta_{11}^o)z$$

$$\Delta\alpha_{11}^o = (\beta_{02} - \beta_{12})z \qquad (2.10)$$

$$\Delta\alpha_{11}^c = (\beta_{11}^c - \beta_{21})z$$

The total transmission is the summation of the two polarization direction components.

$$P'_j = \xi P_j{}^x + (1 - \xi)P_j{}^y \qquad (2.11)$$

where ξ is the polarization ratio of light source. If the source light is not polarized, the value of ξ can be taken as 0.5. The transmission of the uniformly polished coupler against the coupler length is plotted in Fig. 2.7 for SMF28™ with a polishing degree of 0.8832, and a distance between the two core centers of 14.6 μm. We can see that if the coupler length is 106.0 mm, the transmissions of LP_{01}, $LP_{11}{}^o$ and $LP_{11}{}^e$ modes in one branch of the coupler are 99.4%, 0.4% and 0.2%, respectively. That means that if the LP_{01} and LP_{11} modes are injected into the input end of the coupler, the LP_{01} mode will still stay in branch 1 while both orientation LP_{11} modes will transfer into branch 2 after the light

propagates through the uniformly polished coupler. Thus, the coupler works as a mode separation device. However, we find that the oscillation of LP_{11}^o mode is much more rapid than that of the LP_{11}^e mode because its beat length is shorter than that of the LP_{11}^e mode. This rapid oscillation leads to a very narrow peak width, which imposes a strict requirement for the coupler length. Fig. 2.8 shows a strong coupling coupler situation where the parameters used in calculation are a polishing degree of 0.9264 or a distance between the two core centers of 9.2 μm. When the coupler length is 10.35 mm, the transmissions of LP_{01}, LP_{11}^o and LP_{11}^e modes are 99.8%, 0.12%, 0.17% respectively, and the coupler also functions as a mode separation device. The advantage of this kind of coupler is to reduce the length of coupler, thus reducing the difficulty of aligning the polished fibers parallel. Its length is only about one tenth of the coupler with the weak coupling condition. Nevertheless, it requires high precision polishing degree.
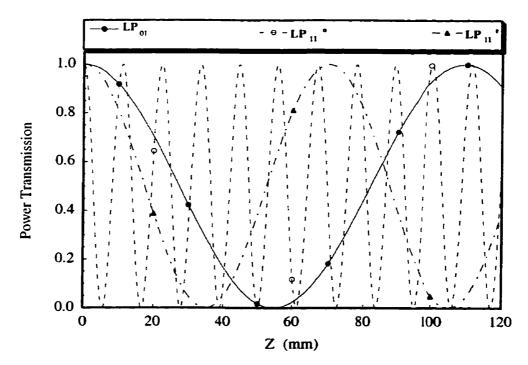
Figure 2.7 The transmission versus coupler length when the polishing degree is 0.8832 or the distance between two core centers is 14.6 μm.
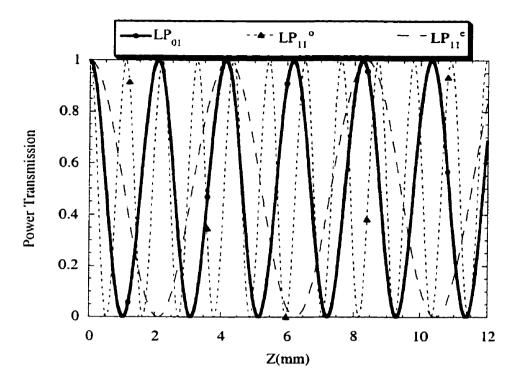
Figure 2.8   The transmission versus coupler length when the polishing degree is 0.9264 or the distance between two core centers is 9.2 μm.

2.3.3   Non-Uniform Coupler

If the fiber is polished by Nicholls' method, the polished region is no longer uniform. In order to calculate the transmission, the longitudinal profile of the coupler must be known. The longitudinal profile of a polished coupler is shown in Fig. 2.9. Where $d(z)$ is the distance between the two cores, d_0 is the minimum distance in the coupler waist, R is the curvature radius of the coupler and h is the half distance difference between $d(z)$ and d_0. The distance between the two core centers is

$$d(z) = d_0 + 2h \tag{2.12}$$

and

$$h = R - \sqrt{R^2 - z^2} \tag{2.13}$$
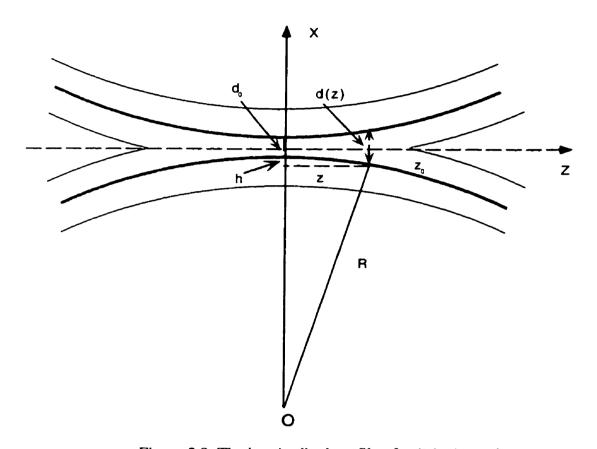
Figure 2.9 The longitudinal profile of polished coupler.

so

$$d(z) = d_0 + 2(R - \sqrt{R^2 - z^2})$$ (2.14)

The polishing degree p varies along the longitudinal direction z. At the waist of the coupler the polishing degree is maximum and at the end of the coupler z_0 the polishing degree is zero. The distance $d(z)$ can be also expressed in terms of the polishing degree by

$$d(z) = 2[1 - p(z)]\rho_{cl}$$ (2.15)

Substituting Eq. (2.15) into (2.14), the relationship between the polishing degree and longitudinal coordinate z is obtained.

$$p(z) = 1 - \frac{1}{\rho_{cl}}\left[\frac{d_0}{2} + (R - \sqrt{R^2 - z^2})\right]$$ (2.16)

Usually, we prefer to express the longitudinal profile starting from the end of the coupler. Thus, we rewrite the expression as

$$p(z) = 1 - \frac{1}{\rho_{cl}}\left[\frac{d_0}{2} + (R - \sqrt{R^2 - (z+z_0)^2})\right]$$ (2.17)

where z_0 is half the length of the coupler; its value can be measured or calculated by setting $d(z)$ as $2\rho_{cl}$ in Eq. (2.14). So we have

$$z_0 = \pm\left[R^2 - (R - \rho_{cl} + \frac{d_0}{2})^2\right]^{\frac{1}{2}}$$ (2.18)

From Eq. (2.18), if the curvature radius of coupler R and the distance d_0 between the core centers in the waist of coupler are given, length of the coupler can be calculated. The longitudinal profile of the polishing degree and the distance between the core centers can be obtained from Eqs. (2.14) and (2.17) respectively. Fig. 2.10 shows the distance between core centers as function of longitudinal coordinate z when d_0 is 0.909 μm and the radius of curvature is 16.68 m. Fig. 2.11 shows the polishing degree as a function of the longitudinal coordinate z when the maximum polishing degree is 0.9273 and the radius of curvature is 16.68 m. Both calculations are for the fiber SMF28™. We can see that the longitudinal profile of polishing degree and the distance between the core centers are parabolic functions. So, this non-uniform coupler has the parabolic structure.

The transmission of this kind of coupler can also be calculated by the formula (2.9) and (2.11), but the accumulated supermode phase differences need to be calculated by integration along whole length of the coupler L_c.
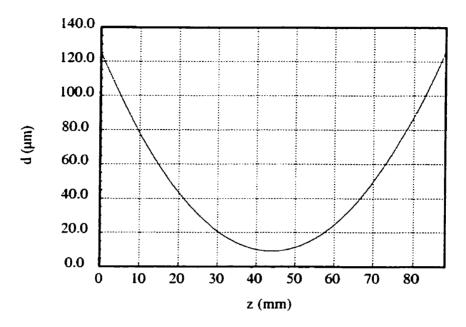
Figure 2.10 Distance between the fiber core centers as a function of longitudinal coordinate for $d_o = 0.909$ μm and $R = 16.68$ m.
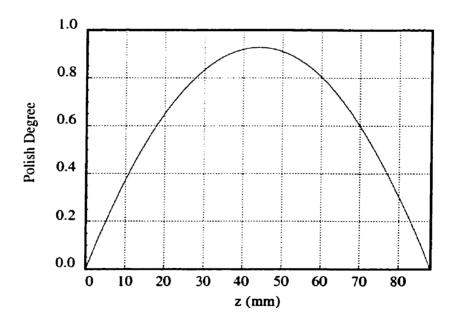
Figure 2.11 Polishing degree profile along the coupler longitudinal direction for $d_o = 9.09$ and $R = 16.68$ m.

$$\Delta\alpha_{01} = \int_{L_c} (\beta_{01} - \beta^o{}_{11})dz$$

$$\Delta\alpha^o{}_{11} = \int_{L_c} (\beta_{02} - \beta_{12})dz \qquad (2.19)$$

$$\Delta\alpha^e{}_{11} = \int_{L_c} (\beta^e{}_{11} - \beta_{21})dz$$

This kind of coupler can also be divided two groups: one corresponds to a situation where the fiber cores are nearly touching in the waist of coupler. Since the longitudinal profile of the distance between two core centers is a parabolic function, the interactions between supermodes are only strong in the waist region. In order to work as a mode separating device, this kind of coupler length needs to be long. Fig. 2.12 shows the transmission as the function of the curvature radius for SMF28™ fiber when d_0 is 9.09 μm or the maximum polishing degree is 0.9273. We find that when the curvature radius is 16.68 m corresponding to the coupler length of 87.94 mm, the transmissions of LP_{01}, $LP_{11}{}^o$ and $LP_{11}{}^e$ are 99.96%, 0.02% and 0.03% respectively. Under these conditions, this coupler acts as a mode separating coupler. The other group is comprised couplers made of fibers that have had part of core removed during the polishing process. Fig. 2.13 shows the transmission against the curvature radius for SMF28™ fiber when d_0 is 8.47 μm or the maximum polishing degree is 0.9323 (when polishing degree is 0.928, the two cores touch each other). We can see that when the curvature radius is 3.18 m, corresponding to the coupler length of 38.50 mm, the transmissions of LP_{01}, $LP_{11}{}^o$, and $LP_{11}{}^e$ are 99.94%, 0.01% and 0.01% respectively. Thus, this coupler acts as a mode separating coupler too. The latter coupler length and the curvature radius are shorter than that of the previous couplers because the interactions between supermodes are very strong when part of the fiber core has been removed. From the point of the fabrication view, the short length couplers are easier to make, and the remove of the little part of the fiber core will not results in much excess loss. Cryan et al. [94] reported that they fabricated five polished
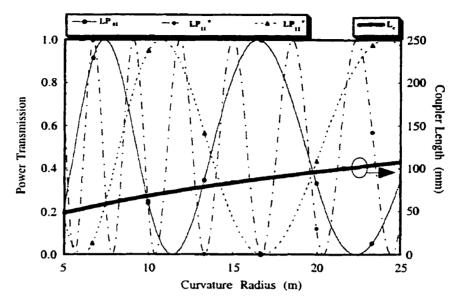
Figure 2.12 Transmission and coupler length versus the curvature radius for the cores are nearly touching coupler. When the coupler has the maximum polishing degree of 0.9273 or d_0 of 9.09 μm at its waist.
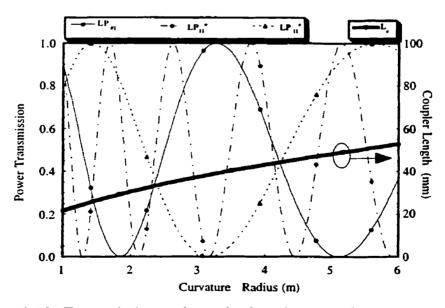
Figure 2.13 Transmission and coupler length versus the curvature radius for part of core removed coupler. When the coupler has the maximum polishing degree of 0.9323 or d_0 of 8.47 μm at its waist.

couplers with 1 μm part of fiber core removed . All of them have an excess loss of about 0.35 dB. So, the core-polished coupler is possible.

2.3.4 Elliptical Core Fiber Couplers

The elliptical core fiber is often used for preserving polarization, but it also has advantages for the fabrication of couplers because both orientation LP_{11} modes have relatively large different propagation constants. To compare with the circular core fibers, we use the SMF28™ fiber parameters except for the ellipticity, but keep the core area and the index difference as constant. The core shape is characterized by the variation of its eccentricity which is defined as

$$e = \frac{\sqrt{b^2 - a^2}}{b} \tag{2.20}$$
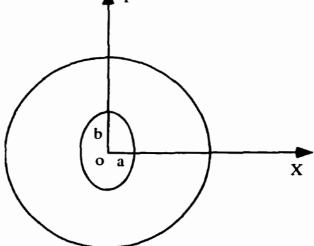
Figure 2.14 The elliptical core fiber with Cartesian coordinates.

When a is equal to b, e becomes zero, the core is circular. The maximum value of e is 1 corresponding to a is equal to zero, and the core is shaped like a line. For the circular fiber, a dimensionless parameter V is applied to fibers and referred to the fiber parameter.

$$V = k\rho_{co}\sqrt{n_{co}^2 - n_{cl}^2} = k\sqrt{ab}\sqrt{n_{co}^2 - n_{cl}^2} \qquad (2.21)$$

where ρ_{co} is the circular core radius. To study the elliptical core fiber, we first calculate the scalar effective indices of the fiber mode. The results plotted in Fig 2.15 shows the effective indices of the fiber modes as functions of the eccentricity. All the fiber modes are named after their equivalent in the circular core approximation. From Fig. 2.15(a) we can see that when the eccentricity is small the both orientation LP_{11} modes are degenerated and that they gradually separate with the increasing eccentricity. When the eccentricity is 0.80, the LP_{02} mode converts into a core mode, and when the eccentricity is 0.93, the LP_{11}^o mode is cut off. So, there are always more than three core modes in the fiber core for $e > 0.8$. However, when the fiber parameter V is reduced, both LP_{11}^o and LP_{02} modes are cut off. Fig. 2.15(b) and (c) show the effective indices of the fiber mode as the function of eccentricity when $V = 2.6$. The V reduction can be realized by decreasing the index difference from 0.0045 to 0.0028 keeping the other parameters identical to those of Fig. 2.15(a). From Fig. 2.15(b) we can see that the LP_{02} mode is always a cladding mode and the LP_{11}^o mode is cut off at the eccentricity of 0.69 point. The V reduction can also be done by reducing the circular core radius from 4.5 µm to 3.55 µm, keeping the other parameters identical to those of Fig. 2.15(a). From Fig. 2.15(c) we can also see that the LP_{02} mode is always a cladding mode and the LP_{11}^o mode is cut off at the eccentricity 0.72 point. Consequently, for the elliptical core fiber, when V is about 2.6 and the eccentricity is larger than 0.72, only the LP_{01} and LP_{11}^e modes are guided in fiber core while the LP_{11}^o mode is cutoff.
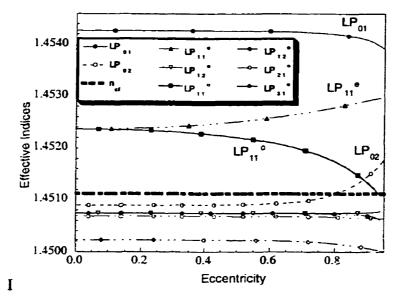
Figure 2.15(a)   Effective indices of fiber modes as functions of the fiber core eccentricity. When the Δn is $0.0045, \rho_{co}$ is 4.5 μm, and V is 3.3, the LP_{02} mode converts into core mode at eccentricity of 0.80 and the $LP_{11}{}^o$ mode cuts off at e of 0.93.
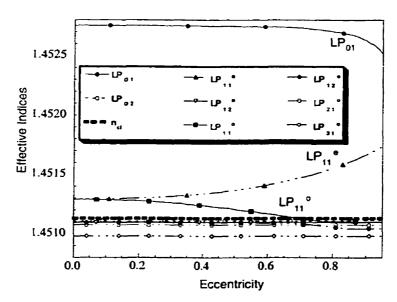
Figure 2.15(b)   Effective indices of fiber mode as functions as fiber core eccentricity. When Δn is $0.0028, \rho_{co}$ is 4.5 μm, and V is 2.6, the LP_{02} mode stays in cladding and the $LP_{11}{}^o$ mode cuts off at e of 0.69.
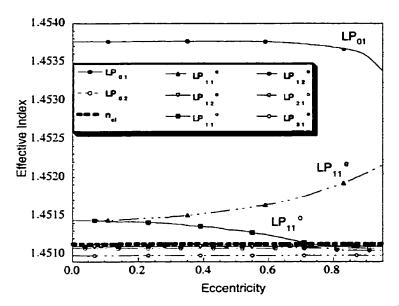
Figure 2.15(c)   Effective indices of mode as functions as fiber core eccentricity. When Δn is $0.0045, \rho_{co}$ is 3.55 μm, and$V$ is 2.6, the LP_{02} mode stays in cladding and the $LP_{11}{}^o$ mode cuts off at e of 0.72.
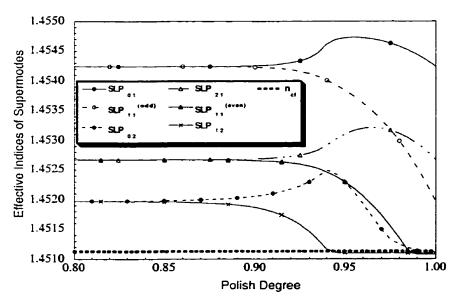
Figure 2.16   Effective indices of supermodes versus the polishing degree. The single fiber has Δn of 0.0045, e of 0.7 and the two fiber cores touch at polishing degree of 0.939.

If we select the fiber of Fig. 2.15(a) with the eccentricity 0.7 and place the fibers parallel to their long axes to make a coupler, there will be six supermodes propagating in the coupler. The effective indices of supermodes versus polishing degree are calculated in Fig. 2.16. For the eccentricity 0.7, the long and short semi-axes are $b=5.33$ and $a=3.80$ µm respectively, and the two fiber cores touch at polishing degree 0.939. Knowing the effective indices of the supermodes, the beat lengths can be easily obtained by Eq. (2.8) and their values are plotted in Fig. 2.17. From it we can see that the coupler made of this kind of fiber will be very similar to that made of circular core fibers. That is why we do not repeat the analysis and transmission calculation again.
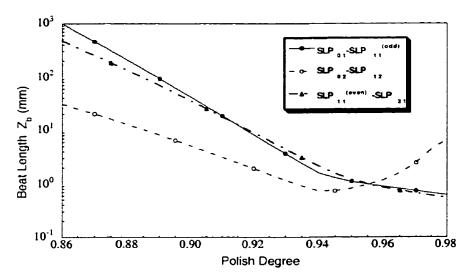
Figure 2.17 The beat lengths between supermodes versus the polishing degree. The single fiber has Δn of 0.0045, e of 0.7 and the two fiber cores touch at polishing degree of 0.939.

Couplers made of the fiber shown in Fig. 2.15(b) and (c) are more of interest because they only have four supermodes if the eccentricity is larger than 0.72. Thus, there are two beat length curves and the mode separating conditions become much more simple. As an example, we calculate the coupler transmission consisting of Fig. 2.15(b) fibers with an eccentricity of 0.8. The results plotted in Fig. 2.18 are the effective indices of supermodes

as a function of the polishing degree. For the elliptical core of eccentricity 0.8, the long and short semi-axes are $b=5.81$ and $a=3.49$ μm respectively. If the fiber is polished along the short semi-axis direction, the two fiber cores will touch at polishing degree 0.944. Fig 2.19 shows the beat lengths between these supermodes as a function of polishing degree. From it we can see that the two curves cross at a polishing degree 0.925 where we can not separate the two modes. Except for this intersection point, we can properly design the coupler structure and have it satisfy the mode separation conditions.

Knowing the effective indices of supermodes, we can calculate the transmission of the coupler that depends on its structure. For convenience comparison with the circular core fiber case, we only calculate the weak coupling situation. For the "uniform coupler", the transmission versus the coupler length is plotted in Fig. 2.20 with a polishing degree of 0.881 or a distance between two core centers of 14.9 μm. We can see that when the coupler length is 28.4 or 87.0 mm, the transmission of LP_{01} and LP_{11}^e are 0.01% and 99.98% respectively. The coupler works to separate the LP_{01} and LP_{11}^e modes. For the "parabolic coupler", the transmission and coupler length versus the curvature radius is depicted in Fig. 2.21 with d_o of 9.6 μm or the maximum polishing degree 0.923 at the waist. When the curvature radius is 14.85 m, the transmission of LP_{01} and LP_{11}^e are 99.97% and 0.01% respectively, and the corresponding coupler length is 82.79 mm.
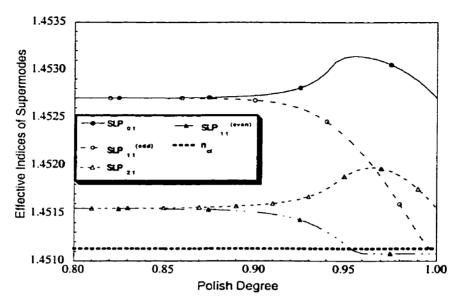
Figure 2.18 Effective indices of supermodes vs the polishing degree. The single fiber has Δn of 0.0028, e of 0.8 and the two fiber cores touch at polishing degree of 0.944.
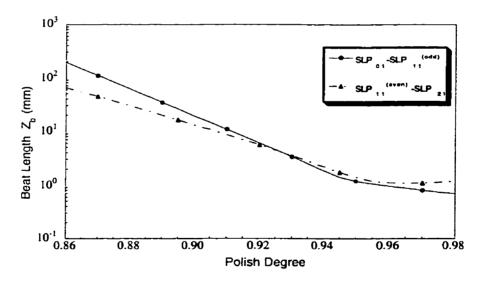
Figure 2.19 The beat lengths between supermodes vs the polishing degree. The single fiber has Δn of 0.0028, e of 0.8 and the two fiber cores touch at polishing degree of 0.944.
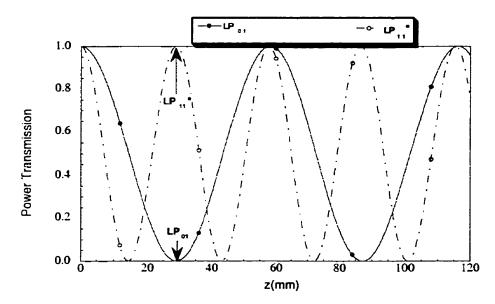
Figure 2.20 The "uniform coupler" transmission versus its length when the polishing degree is 0.881 or the distance between two fiber core centers is 14.9 μm.
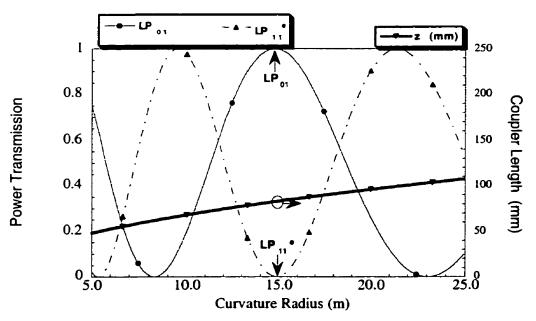
Figure 2.21 The "parabolic coupler" transmission and coupler length vs the curvature radius when the d_o of 9.6 μm or the maximum polishing degree of 0.923 in waist. The coupler works as a mode separation device when the R is 14.85 m.

2.4   Discussion

We have studied the possibility and feasibility of fabricating mode separating couplers by the polishing method. The simulation results show that mode separating couplers can be made by the polished method with both uniform and parabolic longitudinal profile structures. For the uniform coupler, the coupler length can be made short if the two fiber cores are nearly touching. While for the parabolic coupler, the coupler length is still long even if the two fiber cores are nearly touching at the coupler waist. To reduce the length of parabolic couplers, they should consist of fibers in which a small part of the core has been removed.

To compare the two coupler structures, Fig. 2.8 and Fig. 2.13 are re-plotted in Fig. 2.22 and Fig. 2.23 respectively. If we set the transmission tolerance of the mode separating coupler for LP_{01} to more than 98%, and the LP_{11} mode to less than 1%, a uniform coupler with polishing degree of 0.9264, will have a length ranging from 10.32 to 10.38 mm. That means the precision requirement for the uniform coupler length is 10.35 ± 0.03 mm. However, for a parabolic coupler of d_0 of 8.468 μm, its curvature radius could be from 3.14 to 3.22 m. So, the precision requirement for the curvature radius is 3.18 ± 0.04 m and the corresponding coupler length is 38.50 ± 0.25 mm. We can see that the tolerance of the parabolic coupler is larger than that of the uniform couplers. Furthermore, a computer controlled technique for cutting curved grooves in the polished fiber optic substrates was developed [95] which made the curvature radius of groove and other parameters easily changed in software to facilitate cutting the groove and then produce the optically contacted bonded coupler with parabolic longitudinal profile. Using a highly elliptical core fiber can largely increase the tolerances. For the uniform coupler, the precision requirement is 28.4 ± 1.8 mm under the same tolerance mentioned above. For the parabolic

coupler, the precision requirement is 15.05±0.80 m for the curvature radius and 82.79±1.12 mm for length. So, the advantage of using the elliptical core fiber is obvious.

In conclusion, the mode separating coupler may be made by the polishing method with both uniform and parabolic structures. Among them, the parabolic coupler is easier to fabricate and has larger tolerances. However, the requirements of fabricating mode separating couplers with the polishing method are very strict. One solution is to use the highly elliptical core fibers that only support LP_{01}, LP_{11}^e modes while the LP_{11}^o mode is cutoff. For this case, the mode separating conditions become simple and the mode separating coupler may be easier to construct. Andrew, Corp. has announced that they successfully manufactured D-shaped and highly elliptical core fibers. Using these kinds of fibers, it is not necessary to polish the fibers. The mode separating couplers may be realized just by sticking or fusing two fibers together, then adjusting the coupling region length. The other solution is to use the fusion and tapering method that will be discussed in the next chapter.
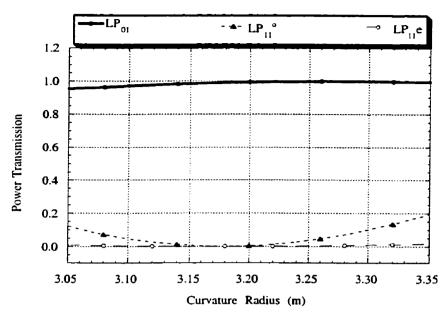
Figure 2.22 The transmission versus coupler length when the polishing degree is 0.9264 or the distance between two cores is 9.2 μm.
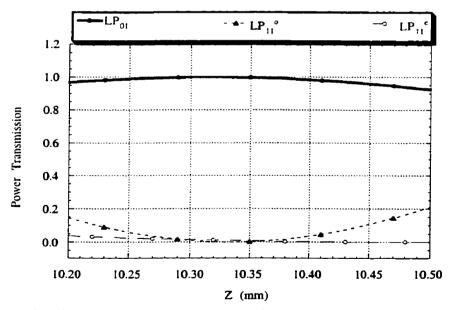
Figure 2.23 Transmission as a function of the curvature radius when d_o is 8.468 μm.

Chapter 3

Fusion and Tapering Method

3.1 Introduction

In this chapter, we investigate the mode separating coupler achieved by a fused two-mode fiber coupler. As opposed to a polished coupler, fused couplers are easy to fabricate and do not require any measurement of phase velocity. In Reference [71], it is mentioned that mode filters consisting of elliptical core fibers are preferable to those of circular core fibers. We will show in later section that the fused couplers made of both elliptical and circular core fibers are acceptable for separating the modes. We start in Section 3.2 by describing the structure of a fused coupler. The transverse and longitudinal profiles are modeled and the effect on the longitudinal profiles by the flame width and sweep distances are studied. In Section 3.3, the effective indices of supermodes of couplers are calculated by the fiber mode expansion method. In Section 3.4, the transmission of the coupler made of two-mode fibers is described by the beating between supermodes. The numerical analysis and calculation results show that it is possible to transfer the power of LP_{11} modes in any orientationin into the other branch simultaneously by choosing appropriate sweeping lengths and elongation for both cases. The characteristics of two mode couplers such as the beat length, birefringence and adiabatic criteria are quantitatively studied in section 3.5~7.

3.2 Structure

The first physical explanation of the behavior of the fused coupler was done by Bures *et al.* [42]. For a fused coupler, the individual guides are well separated in the entrance and exit ends, whereas the fiber cores are reduced significantly and can not confine the light in the cores in the waist region. The light guided in the waist region of the fused coupler is confined by the boundary between the fiber cladding and the external medium, which is air unless some other material is used. Field distribution depends on the spatial beating of the supermodes along the coupler. Besides, a simple model explaining the 'coupling-beating-coupling' resulting from a tapered structure created by the tapering process has been developed [84, 96]. The propagation of light through a taper depends on both the refractive index profiles in cross section and longitudinal profile. The structure of the coupler is schematized in Fig. 3.1(a) and (b). It consists of two identical completely fused two-mode fibers.
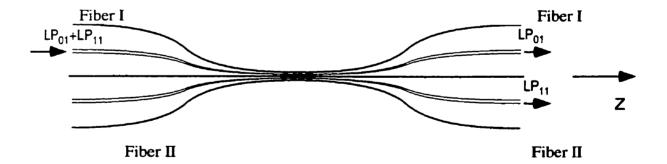
Figure 3.1(a) Schematic longitudinal profile of a fusion and tapering coupler.
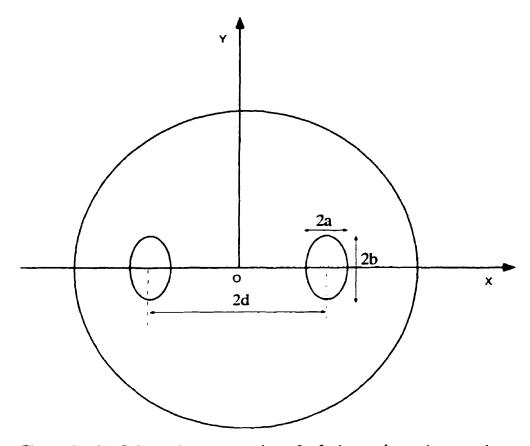
Figure 3.1(b) Schematic cross section of a fusion and tapering coupler.

It is known that a two-mode fiber can support two LP_{01} and four degenerate LP_{11} modes for two polarization directions. At the two ends of the coupler, the two cores are far from each other, so that the overlap integral of the fields of both fibers can be neglected. At the input end, the coupler is launched with a field distribution that resembles the modes of a fiber, referred to as individual modes. This initial field can be approximately expressed as the sum and difference of the corresponding two supermodes. Here, the supermodes are identified by the mode when the coupler is approximated by a two-layers structure of cladding and air. Each initial individual mode is a combination of two supermodes that travel with slightly different propagation constants; these supermodes will change their relative phase as they travel along a coupler. When they are in-phase at the input end and

out-of-phase at the output end of a coupler, it becomes apparent that the individual modes that initially started out on fiber I move over to fiber II at the output end of the coupler. If the coupler is designed appropriately to ensure that the supermodes corresponding to LP_{01} are in-phase and the others corresponding to LP_{11} are out-of-phase, the coupler will work as a mode separating coupler.

3.2.1 Transverse Profile

The fusion couplers consist of two laterally adjacent fused fibers with transverse profiles represented in Fig. 3.2 (a), (b) and (c). The two parallel fibers are heated and the adjacent cladding materials melt, the cross section forms of the coupler evolve gradually from two circles to dumb-bell form, and finally become a large circle if the fusion time is enough long. In the latter case, we say that the coupler has been completely fused because its cross section form will not be changed even if it is fused more. To describe the fusion phenomena, a definition of the fusion degree f is introduced. Couplers without fusion are described by two adjacent circular fibers: their fusion degree is defined as $f=0$; The cross section of completely fused couplers is a large circle: their fusion degree is defined as $f=1$. The fusion degree is defined as

$$f = \frac{l_0 - l_t}{l_0 - l_{min}}$$

(3.1)

where l_0 is the lateral dimension of the coupler before fusion, l_{min} is the minimum lateral dimension of the coupler after fusion or the lateral dimension of a completely fused coupler and l_t is the real lateral dimension of the coupler after fusion. f is a non-dimension quantity that describes the relative lateral shrink of the coupler after fusion.
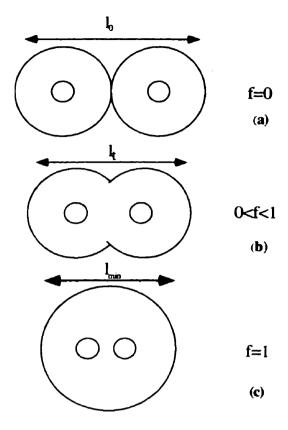
Figure 3.2 The cross section and fusion degree of a coupler

Let ρ_{cl} indicate the radius of fiber cladding, R_c the radius of the completely fused coupler, and $2d$ the distance between the two fiber cores. During the fusion process, the cross section area stays unchanged. For the completely fusion situation

$$2\pi\rho_{cl}^2 = \pi R_c^2 \tag{3.2}$$

so that,

$$R_c = \sqrt{2}\rho_{cl} \tag{3.3}$$

$$d = R_c - \rho_{cl} = (\sqrt{2} - 1)\rho_{cl} \tag{3.4}$$

The coupler lateral dimension before and after fusion, is $l_o=4\rho_{cl}$ and $l_{min}=2R_c$, respectively, so the fusion degree can be defined as

$$f = \frac{4\rho_{cl}-l}{4\rho_{cl}-2R_c} = \frac{4\rho_{cl}-l}{2\rho_{cl}(2-\sqrt{2})} \tag{3.5}$$

In practice, the coupler dimensions are measured by a microscope, so it is convenient to use l_o and l_t to express this formula

$$f = \frac{l_o-l_t}{\frac{l_o}{2}(2-\sqrt{2})} = \frac{1-\frac{l_t}{l_o}}{1-\frac{1}{\sqrt{2}}} \tag{3.6}$$

where l_o and l_t are the lateral dimensions of coupler before and after fusion that can be measured by a microscope.

3.2.2 Longitudinal Profile

The longitudinal profile of a coupler is determined by the flame temperature distribution and flame position. The existing models are parabolic [42, 81, 97], and exponential [59, 82, 83, 98]. These taper shapes have been deduced by approximating the measured shapes of real tapers, and not by analysis of the processes by which the taper profile is formed. The problem of finding what particular taper profile results from stretching a fiber in a particular heat source with its own temperature distribution is more or less complicated. Eisenmann and Birks [59] described a simple tapering model in which a fixed length cylindrical section of fiber is heated to a uniform temperature and stretched. In addition, Birks et al. [98] modified their original model to consider a variation of the heat region. Gonthier [99] developed a more general model in which the flame width and position can be changed and the distribution of the temperature along the fiber is

approximated by a Gaussian function. The analysis is extended here to include the case where the flame is allowed to sweep along the fiber. This yields a general recipe for the fabrication of any reasonably shaped taper.

During the stretching process, the volume is conserved. A section of the coupler profile has a length l and a radius ρ around longitudinal coordinate z. When this section is to be stretched, volume conservation gives the relation

$$l\pi\rho^2 = W \tag{3.7}$$

so, it has

$$\frac{d\rho}{\rho} = -\frac{1}{2}\frac{dl}{l} \tag{3.8}$$

where W is a constant. We assume that when the couplers are heated and stretched, the radius reduction of the coupler $d\rho$ in an infinite small section is proportional to the heat source temperature $T(z)$ and inversely proportional to its radius $\rho(z)$, i.e.,

$$d\rho \propto \frac{T(z)}{\rho} \tag{3.9}$$

so, the relative elongation is

$$\delta l = \frac{dl}{l} \propto \frac{T(z)}{\rho^2} \tag{3.10}$$

The relative temperature distribution of a flame F is approximated by a Gaussian function [99]

$$F(z) = \exp\left[-\left(\frac{z-z_f}{\sigma}\right)^2\right] \tag{3.11}$$

where z_f is the central position of the flame and σ depends on the flame width l_f by

$$l_f = 2\sqrt{\ln 2}\,\sigma \qquad (3.12)$$

During the tapering process, the elongation speed (about 0.1 mm/s) is slower than the flame sweep speed (about 3 mm/s). So, if the flame is swept with moving distance z_s around the central position z_f, the temperature distribution of the flame can be considered as the normalized integration of Gaussian function which can be written as

$$F'(z) = \frac{erf\left(\dfrac{z-z_f+z_s}{\sigma}\right) - erf\left(\dfrac{z-z_f-z_s}{\sigma}\right)}{erf\left(\dfrac{z_s/2}{\sigma}\right) - erf\left(-\dfrac{z_s/2}{\sigma}\right)} \qquad (3.13)$$

The total elongation of a coupler can be written as

$$\delta L = K \int_{z_f^-}^{z_f^+} \frac{G(z)}{\rho^2(z)} dz \qquad (3.14)$$

In this formula, the temperature is replaced by its relative distribution and the real temperature values are included in the proportionality constant K. z_{f+} and z_{f-} are the flame limits with values that are determined arbitrarily by $G(z_f)=10^{-4}$. $G(z)$ is the temperature distribution of a flame, which is $F(z)$ without sweeping and $F'(z)$ with sweeping. The longitudinal profile is dependent on the flame width and the flame sweeping length. To describe the longitudinal profile an inverse taper ratio (ITR) and a normalized slope Ω_s is defined as

$$ITR = \frac{\rho(z)}{\rho_o} \qquad (3.15)$$

$$\Omega_s = \frac{1}{\rho(z)}\frac{d\rho}{dz} = \frac{1}{ITR}\frac{d(ITR)}{dz} \qquad (3.16)$$

ρ_o is the original radius of couplers before tapering and $\rho(z)$ is the longitudinal profile after tapering.

Fig. 3.3 and Fig. 3.4 show the simulated longitudinal profile and the corresponding taper slopes of four couplers formed under various conditions. All the couplers are stretched 30 mm and with a flame width of 4 mm without sweeping (Fig. 3.3(a)), a flame width of 2 mm without sweeping (Fig. 3.3(b)), a flame width of 4 mm and flame sweep distance of 10 mm (Fig. 3.4 (a)), and a flame width of 2 mm and flame sweep distance of 10 mm (Fig. 3.4 (b)). Comparing Fig. 3.3 (a) with (b), it is found that for the flame without sweeping case the longitudinal profile with a 4 mm wide flame has a larger waist radius, longer length and smaller slope than that with a 2 mm wide flame. It means that the longitudinal profile is very sensitive to the flame width when flame is not swept and the large flame width is good at reducing the tapering slope. However, comparing Fig. 3.4 (a) with (b), it is found that for the flame sweeping case the longitudinal profile with a 4 mm wide flame has nearly the same waist radius, and the same maximum slope value as that with a 2 mm wide flame, but a longer length than that with a 2 mm wide fame. It means that the longitudinal profile is not very sensitive to the flame width when flame is swept and the narrow flame is good at reducing the coupler length and creating a uniform waist of the coupler. Furthermore, comparing Fig. 3.3(a) with Fig. 3.4 (a), and Fig. 3.3 (b) with Fig. 3.4 (b), it is found that under the same conditions, the longitudinal profiles with flame sweeping have much larger waist radius, longer length and much smaller taper slope than that of the nonsweeping flame case. In reality, in order to keep the taper adiabatic, it is always desirable to have a small taper slope. Thus, it is better to let the flame sweep during the tapering process. When the flame is stationary, the wide flame is to be considered. Sometimes, we want the total coupler length short or the coupler waist uniform; for those cases it is better to use the narrow flame and sweep it along the fibers. Longitudinal profiles, like the transverse profile, will directly affect the transmission characteristics of the coupler. So, carefully controlling the coupler structure leads to the

realization of various kinds of devices. Mode separating couplers are realized by adjusting

the transverse and longitudinal profile.
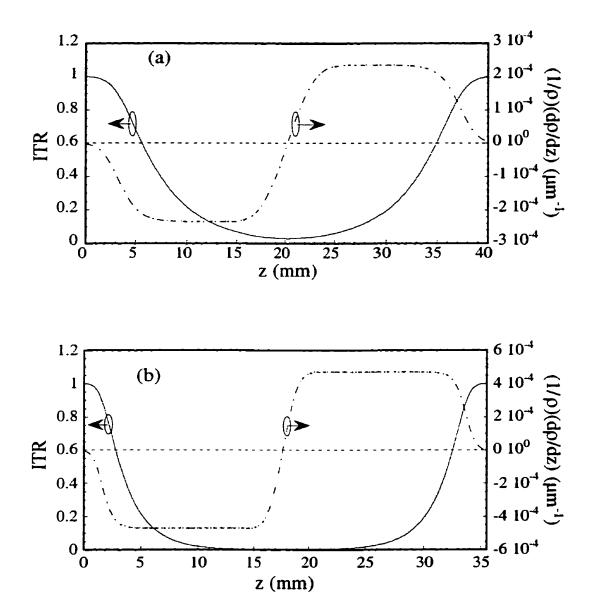
Figure 3.3 The longitudinal profile of a coupler after stretching 30 mm without

sweeping and a flame width of (a) 4 mm, (b) 2 mm.
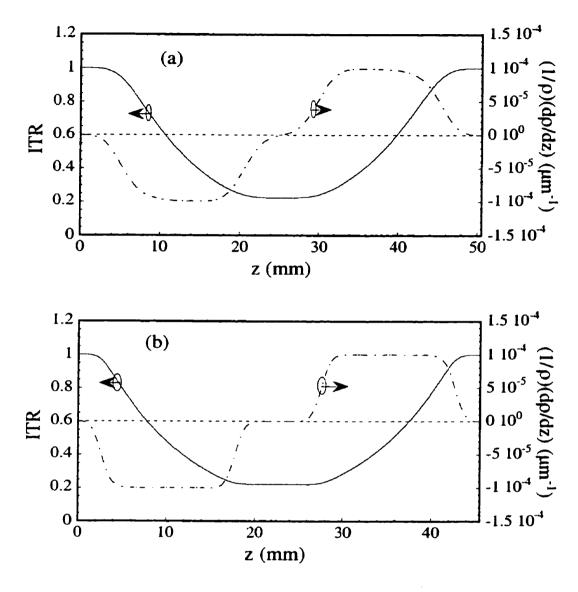
Figure 3.4 The longitudinal profile of couplers after stretching 30 mm with sweep distance of 10 mm and a flame width of (a) 4 mm, (b) 2 mm.

The other thing that needs to be mentioned is that except for the variation of the coupler transverse and longitudinal dimensions, the distribution of the refractive index of the coupler also changes during the fusion and tapering process. Usually, the core dopant diffuses when the temperature is high (about 1100 °C), and the relative index difference

decreases as the heating time increases [100-104]. During the fabrication of the coupler, the waist is always heated for a longer duration than the sides, so that the index step is smaller at the waist than that at the sides. For simplicity, the variation of index step is assumed to decrease as a linear function from the entrance end to the middle point in the simulation procedure.

3.3 Propagation Constants in the Scalar Approximation

To obtain the optical transmission of a longitudinally varying coupler, a numerical method is necessary because there is no analytical solution. A number of numerical techniques have been proposed so far for the analysis of waveguides, as reviewed by Saad [77], Marcuse [78], Vassallo [79] and Chiang [80]. Most of the numerical methods can calculate the propagation constant of a mode in the scalar approximation but do not give accurate values for the field at the interfaces that are necessary to calculate the polarization corrections. To overcome this problem, a method based on an expansion on the modes of a known waveguide has been developed [88], which has been presented in Chapter 1. For fused couplers, the known waveguide is a two-layer optical fiber because its modes have analytical expressions and thus can be computed with a very high accuracy. This method solves scalar wave equations and the validity of its results can be furthermore increased by calculating polarization corrections to the modal propagation constants, using a perturbative approach. This method is especially convenient for the multimode situation. The accuracy of this method has been proven by comparison of its results with analytical results in the case of a single fiber, and with results of the field correction method in the case of a coupler [105].

Now we consider a coupler made of two identical circular core fibers. To minimize the polarization effect, it is supposed that this coupler has been completely fused and its cross section is like a large radius fiber with two cores. Its structure is drawn in Fig. 3.5. The reference waveguide is selected as a two-layer fiber with a radius that is the same as the coupler radius and its index is the same as the coupler cladding index. For this kind of reference fiber, its optical modes are well known and can be written as the products of Bessel and trigonometric functions.
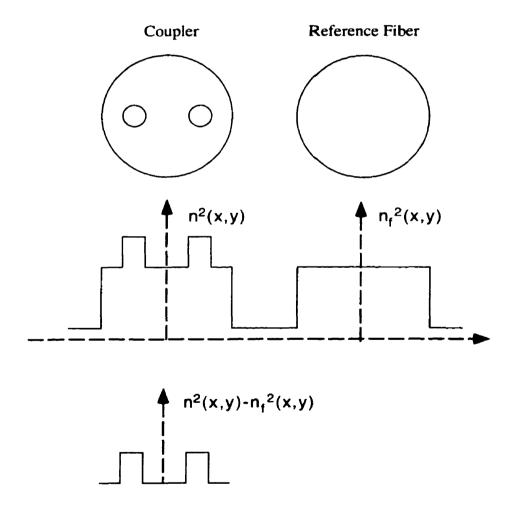
Figure 3.5 The scheme of the fiber mode expansion method.
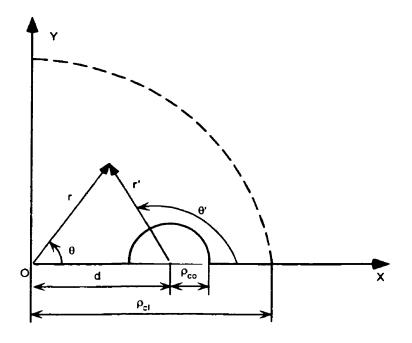
Figure 3.6 Transverse profile of the coupler.

The guided modal fields $\left| l p_{l_m}^f \right\rangle$ of the reference fiber have analytical expressions [76]

$$\left| l p_{lm}^f \right\rangle = \begin{cases} A_{lm} \dfrac{J_l(U_m R)}{J_l(U_m)} \begin{cases} \cos(l\theta) \\ \sin(l\theta) \end{cases} & \text{if} \quad R \leq 1 \\[4mm] A_{lm} \dfrac{K_l(W_m R)}{K_l(W_m)} \begin{cases} \cos(l\theta) \\ \sin(l\theta) \end{cases} & \text{if} \quad R > 1 \end{cases}$$ (3.17)

where A_{lm} is the normalization constant

$$A_l = \left(\frac{\mu_0}{\varepsilon_0}\right)^{\frac{1}{4}} \left(\sqrt{\frac{2}{\pi n_{co}}}\right) \frac{U K_l(W_m)}{\rho V \sqrt{K_{l-1}(W_m) K_{l+1}(W_m)}} \qquad l \neq 0$$

$$A_0 = \left(\frac{\mu_0}{\varepsilon_0}\right)^{\frac{1}{4}} \left(\frac{1}{\sqrt{\pi n_{co}}}\right) \frac{U K_0(W_m)}{\rho V K_l(W_m)} \qquad l = 0$$ (3.18)

and

$$R = \frac{r}{\rho_{cl}} \ , \qquad U = \frac{2\pi}{\lambda} \rho_{cl} \sqrt{n_{cl}^2 - n_{eff}^2} \ \text{ and } \ W = \frac{2\pi}{\lambda} \rho_{cl} \sqrt{n_{eff}^2 - n_{cx}^2} \tag{3.19}$$

where ρ_{cl} is the cladding radius of the coupler or the reference fiber. J_l and K_l are Bessel functions. The supermodes of the coupler can be expanded by the reference fiber modes

$$|SLP_i\rangle = \sum_{j=}^{N} c_j |lp_j^f\rangle \tag{3.20}$$

Substituting (3.20) into the scalar wave equation and considering the orthogonality of the reference fiber modes, one obtains Eq. (1.62)

$$\sum_i \left\{ \bar{\beta}_i^2 \delta_{ij} + k^2 \left\langle lp_j^f \left| \left[n^2(x,y) - n_f^2(x,y) \right] \right| lp_i^f \right\rangle \right\} c_i = \beta^2 c_j \tag{3.21}$$

or $\mathbf{Hv} = \beta^2 \mathbf{v}$

where $\bar{\beta}$ is the propagation constant of the reference fiber modes and their values can be obtained by resolving the fiber mode eigenfunction. $n^2(x, y)$ is the index profile of the coupler and $n_f^2(x, y)$ is the index profile of the reference fiber. Their difference is restricted in the coupler core region and zero in the other region (see Fig. 3.5 and Fig 3.6). $\mathbf{H}$ is a Hermitian matrix with a dimension that depends on the numbers of the reference fiber modes to be used in the calculation. By the symmetrical property, the even supermodes are expanded in terms of the even reference fiber modes, the odd supermodes are expanded in terms of the odd reference fiber modes. To obtain the element of the eigen matrix, the important thing is to calculate the integration in the core area.

$$\left\langle lp_i^f \left| (n^2(x,y) - n_f^2(x,y)) \right| lp_j^f \right\rangle = \iint_{core} \varphi_i(r,\theta) \left[n^2(r,\theta) - n_f^2(r,\theta) \right] \varphi_j(r,\theta) ds \tag{3.22}$$

The eigenfunction can be solved by the inverse power iteration method (see Chapter 1, section 1.3.3). For each eigenvalue β, there is a set of eigenvectors that is corresponding to the expansion coefficients, so one can obtain the supermode field. The accuracy of the

fiber mode expansion method depends on the number of reference fiber modes that are used in the expansion. Fig. 3.7 shows the effective index of the six supermodes where we used $l=30$ and $m=40$ in the reference fiber modes to expand the supermode field, so that, the order of **H** is 1200×1200.

FMEM is still a scalar method, so its results represent scalar mode properties. If we are to account for the coupler polarization properties in the propagation constant, we must add a correction to the scalar propagation constants. To determine the correction we would have to solve the vector wave equation. However, the $\ln n^2$ term on the right of Eq.(1.5) is small for weakly guiding waveguides, so that the polarization correction can be obtained by perturbation method [76] and expressed in Eq. (1.65).

The square of the index profile of a completely fused coupler made of two identical circular core fibers can be written from inspection of Fig. 3.6 as

$$n^2(x,y) = n_{cl}^2 \left\{ 1 + 2\Delta \left(1 - H\left(\sqrt{(x-a)^2 + y^2} - \rho_{co} \right) \right) \right.$$
$$\left. + 2\Delta \left(1 - H\left(\sqrt{(x+a)^2 + y^2} - \rho_{co} \right) \right) - 2\Delta' H\left(\sqrt{x^2 + y^2} - R_c \right) \right\}$$

(3.23)

where

$$\Delta = \frac{n_{co}^2 - n_{cl}^2}{2n_{cl}^2} \ , \quad \Delta' = \frac{n_{cl}^2 - n_{ex}^2}{2n_{cl}^2}$$

(3.24)

The square of the index profile of a completely fused coupler made of two identical elliptical core fibers can be written by Fig. 3.1 as

$$n^2(x,y) = n_{cl}^2 \left\{ 1 + 2\Delta H\left(1 - \frac{(x-d)^2}{a_e^2} - \frac{y^2}{b_e^2} \right) \right.$$
$$\left. + 2\Delta H\left(1 - \frac{(x+d)^2}{a_e^2} - \frac{y^2}{b_e^2} \right) - 2\Delta' H\left(\sqrt{x^2 + y^2} - R_c \right) \right\}$$

(3.25)

Where $H(x)$ is the Heaviside function and its derivative is the Dirac delta function.

$$\frac{dH(x)}{dx} = \delta(x)$$ (3.26)

So, the integration of Eq. (3.20) is only non-zero at the interfaces between core and cladding, the cladding and air. All the parameters used for calculation are shown in Table. 3.1. In general, the fiber cores are deformed after fusion, which can be seen in the cross section measurement of couplers presented in Chapter 5 and in the photographs of coupler cross sections from the work of others [54, 84]. The mode separating couplers may be constructed directly with elliptical core fiber. If the coupler is made of elliptical core fiber, the above method should be suitable too. To confirm this, we use the FMEM to calculate the elliptical fiber case. The modes of elliptical core fibers characterized by Mathieu's equations have been discussed in several papers [14, 106-109]. The complete analysis in the weakly guiding elliptical core case is that of Show et.al. [109]. The cutoff values of a fiber mode are defined by the normalized frequency of the minor axis $V_a = ka\sqrt{n^2_{co} - n^2_{cl}}$, and these values vary for different ellipticities a/b. We calculated the third order core mode cutoff value of a fiber to be 3.46 when $a/b = 0.75$ with the FMEM method, which is similar to Show's result ($V = 3.5$).

After fusion, the relative index difference between the core and cladding is reduced and the core area expanded. So, the typical index differences and radii of cores of both the circular and elliptical core fibers are chosen and listed in Table. 3.1. Where n_{co}, n_{cl} and n_{ext} stand respectively for the refractive index of the core, cladding and external medium. The values a_e and b_e indicate the minor and major axes of the fiber core and R_c represents the radius of the coupler. The effective index versus the inverse taper ratio (ITR) of the six supermodes for the circular core fiber case is shown in Fig. 3.7(a), and effective index of the elliptical core case ($a/b = 0.75$) is given in Fig. 3.7(b). The circular and elliptical core
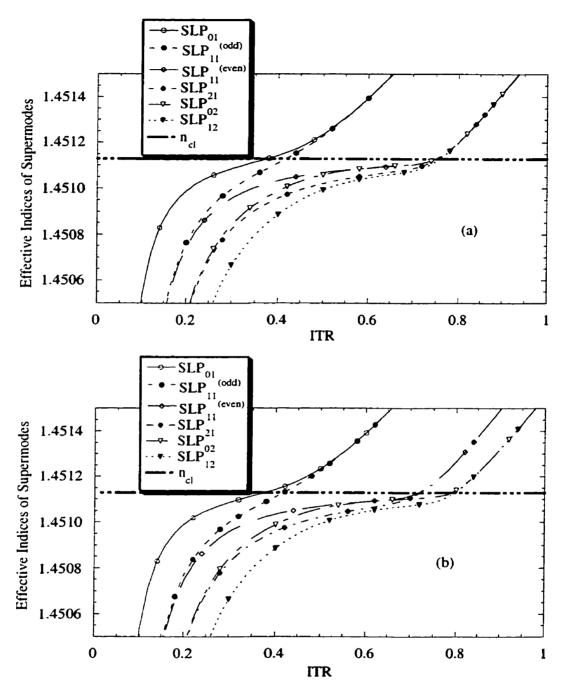
Figure 3.7 Effective indices of supermodes versus ITR (a) the coupler with two circular core fibers. (b) the coupler with two elliptical core fibers ($a/b = 0.75$). The parameters used in calculation are in Table 3.1.

fibers have the same index step and the same core area, i.e., $V^2_{core} = V_a V_b$. It is noticeable that the effective indices of four supermodes $SLP_{11}^{(even)}$, SLP_{21}, SLP_{12} and SLP_{02} are degenerate at the entrance end of the coupler and almost separated simultaneously around ITR=0.75 for the circular core fiber situation. For the elliptical core situation, the effective indices become twofold degenerate at the entrance end and the SLP_{11}, SLP_{21} and SLP_{02}, SLP_{12} separate at ITR 0.71 and 0.80 respectively.

	nco	ncl	next	a(μm)	b(μm)	Va	λ(μm)
E-core	1.4525	1.4511	1.000	7.8	10.4	3.20	0.9754
C-core	1.4525	1.4511	1.000	9.0	9.0	3.69	0.9754

Table 3.1 Parameters of both elliptical and circular core fibers.

3.4 Transmission

After knowing the propagation constants and the longitudinal profile, one can obtain the transmissions of the coupler from Eq. (1.39). As shown in Fig. 3.8, the coupler longitudinal profile is expected to vary with the sweep distance. Fig. 3.9 depicts the transmission versus the elongation when the flame width is 4 mm and the sweep distance is 10 mm. Fig. 3.10 depicts the transmission versus the elongation when the flame width is 4 mm and the sweep distance is 66.5 mm for circular core fibers and 37.75 mm for elliptical core fibers. To obtain the maximum LP_{11} mode transfer efficiency, the two LP_{11} peaks should coincide at a same elongation. Figs. 3.9(a) and (b) show that when the sweep distance is short, it is impossible that the power in the two orientation LP_{11} modes completely transfer into the other branch at a certain elongation. For the circular core case (Fig. 3.10(a)) the two peaks of LP_{11} overlap completely when sweep length is 66.5 mm and elongation is 50.6 mm; while for the elliptical core case (Fig. 3.10(b)) the two peaks
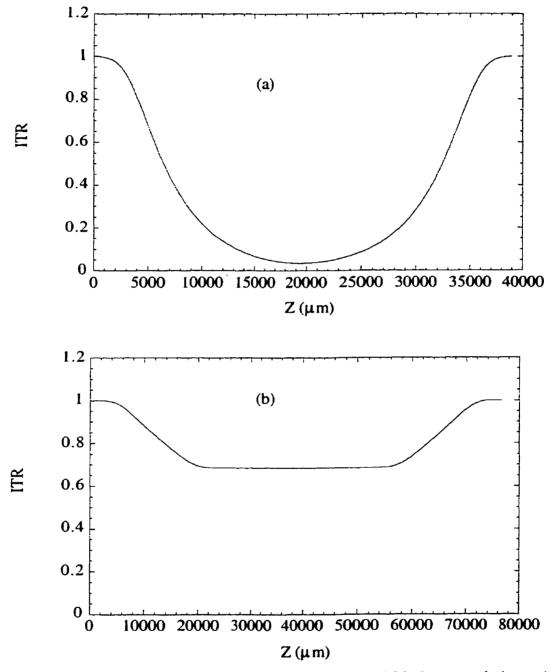
Figure 3.8 Longitudinal profile of coupler for flame width 4 mm and elongation 28.4 mm. (a) ITR versus longitudinal coordinate without flame sweeping. (b) ITR versus longitudinal coordinate with a sweep distance $Z_s = 37.75$ mm.
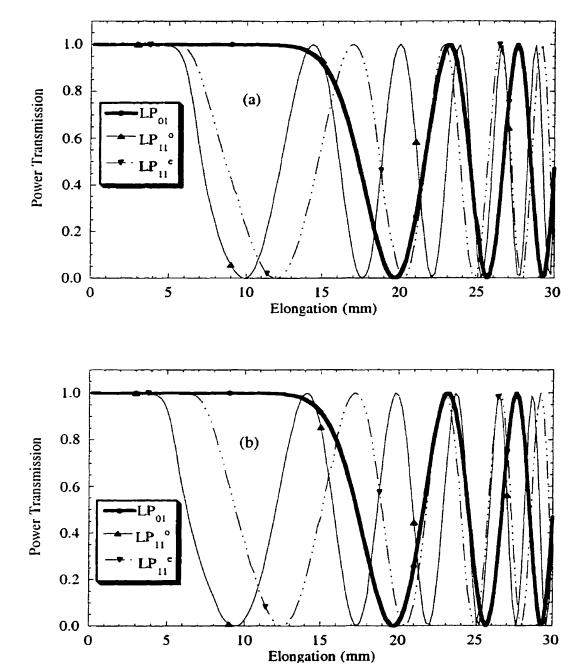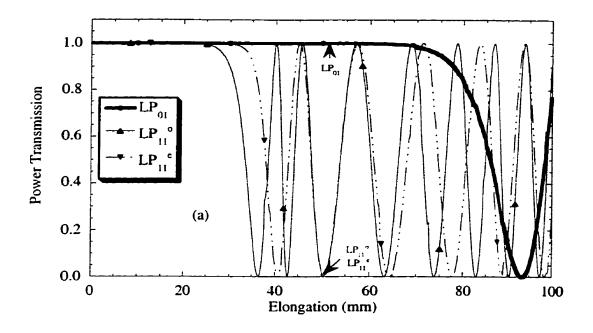
Figure 3.9 Transmissions in one branch of coupler versus elongation for the sweep length 10 mm and flame width 4 mm. (a) the coupler consists of circular core fibers (b) the coupler consists of elliptical core fibers.
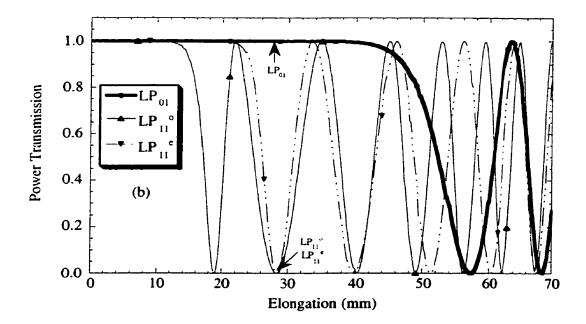
Figure 3.10 Transmissions in one branch of the coupler versus elongation for flame width 4 mm (a) the coupler consists of circular core fibers with sweep length 66.5 mm. (b) the coupler consists of elliptical core fibers with sweep distance 37.75 mm.

superpose when sweep length is 37.75 and elongation is 28.4 mm. From Fig. 3.10(a) we find that if we stop the elongation at about 50.6 mm, that the total power of the LP_{01} mode is in the original fiber while the power of both LP_{11} modes completely transferred into the other fiber, thus, the coupler acts as a mode separating device. From Fig. 3.10(b) of the elliptical core coupler, when the elongation is 28.4 mm, the coupler will work as a mode separation device too. It is noted that to realize the mode separation conditions a longer sweep distance is needed in the circular fiber core case than that in the elliptical fiber core case. From the fabrication point of view, when the flame width and flame sweep distance are fixed, one prefers the coupler with short elongation for its smaller birefringence. One also prefers couplers with a relatively short flame sweep distance because it is easier to align the flame translation parallel to the fibers. So, using the elliptical core fiber to fabricate the mode separating coupler may have certain advantages when compared to the circular core fiber.

3.5 Beat Length

The beat length is another important parameter of couplers because the power exchanges are described by the beating between supermodes. The two supermodes in-phase at input end $z=0$ will change their relative phase as they are propagating in the coupler due to their slightly different propagation constants. As the light travels the distance Z_b along the coupler, the relative phase between two supermodes goes from in-phase to out-of-phase and back; correspondingly, the power transfers from the original branch into the other branch and back the original branch again. The distance between each power transfer is called as the beat length. For a uniform coupler, the beat length is constant, but in the case of a fused coupler the beat lengths varies along the longitudinal direction. For our case, there are three beat lengths for each polarization direction defined as

$$Z_{b_{ij}} = \frac{2\pi}{\beta_i - \beta_j} = \frac{\lambda}{n_{eff_i} - n_{eff_j}} \qquad (3.27)$$

where β_i, β_j are supermode propagation constants and n_{eff_i}, n_{eff_j} are supermode effective indices. The numerical results are shown in Fig. 3.11(a) and (b) for both the circular and elliptical core fiber cases respectively. They show that all the beat lengths are small when ITR is small due to the fiber cores losing their guiding function and all the supermodes propagating in the cladding. The beat lengths of SLP_{01} and SLP_{11}, which is corresponding to the power oscillation of individual LP_{01} mode measured in one branch at output of the coupler, is much longer than other beat lengths when ITR is in the range about from 0.4 to 0.8. This is because in this situation the SLP_{01} and SLP_{11} are still guided in the fiber cores and their propagation constant difference is small, while the other higher order supermodes propagate in the cladding where they have relatively large propagation constant difference (see Fig. 3.7). This is a favorable result for fabricating a mode separating coupler because the mode separation conditions (1.44)-(1.46) for $m_I = 0$ may be satisfied. For example, in Fig. 3.11, if the ITR value at the coupler waist is more than 0.7, the beat length corresponding to LP_{01} mode is longer than about 100 m. It means that there is no power transfer from the LP_{01} mode within the length of the coupler. While the beat lengths corresponding to both LP_{11} modes are about 100 mm, which is a reasonable length for a coupler size. In Fig. 3.10(a) and (b), the ITR values at the waist of circular core and elliptical core coupler are 0.68 and 0.69 when the elongation is 50.6 mm and 28.4 mm respectively where the couplers function as mode separating couplers, which agree well with the above analysis. Meanwhile, with increasing ITR, for the circular core fiber case, the beat length difference between Z_{b11-21} and Z_{b02-12} remains
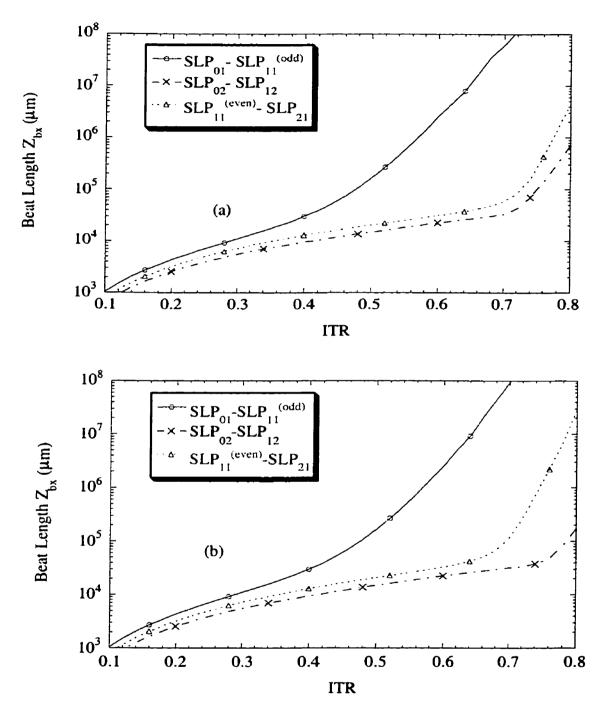
Figure 3.11 Beat lengths of supermodes as a function of ITR. (a) for a circular core fiber coupler, (b) for an elliptical core fiber coupler. The parameters used for calculation are listed in Table 3.1.

small while for the elliptical core fiber case it becomes large. These coincide with the transmission curves of two LP$_{11}$ modes for the circular core coupler diverge more slowly than those of the elliptical core coupler case, as shown in Fig. 3.11(a) and (b). When the ITR is more than 0.8, all the beat lengths are very large, thus there is no any power transfer.

3.6 Birefringence

The geometrical forms of the coupler introduce the form birefringence, which is important in experiments because the measurement is generally affected by the state of polarization at the entrance end of coupler. The propagation constants calculated by the fiber mode expansion method need further the polarization correction with a perturbation method (see Eq. (1.66)). So, the scalar propagation constants split into two values that are along the x and y polarization directions respectively at every longitudinal point. During the simulation, it is assumed that there is no coupling between the two polarization states of the mode due to the fact that the birefringence axes do not change and the supermodes of the coupler are linearly polarized along this axis. Taking into account the effect of polarization, the transmission has been expressed in Eq. (1.40). For the particular value $\xi=1/2$, this equation can be rewritten as

$$P_i = \frac{a_i^2}{2}\left[1 + \cos\frac{(\overline{\alpha}_i^x - \overline{\alpha}_i^y)}{2}\cos\frac{(\overline{\alpha}_i^x + \overline{\alpha}_i^y)}{2}\right]$$

(3.28)

If $\overline{\alpha}_i^x$ and $\overline{\alpha}_i^y$ are different, one can observe that the transmission is modulated by beating between the two different polarization direction signals. The transmission oscillation frequency versus elongation is characterized by $(\overline{\alpha}_i^x + \overline{\alpha}_i^y)/2$, and the envelope of the

oscillation amplitude is modulated by a frequency $(\overline{\alpha}_i^x - \overline{\alpha}_i^y)/2$, where $\overline{\alpha}_i^x$ and $\overline{\alpha}_i^y$ are defined as

$$\overline{\alpha}_1^x = \int_0^L (\beta_{01}^x - \beta_{11}^x)dz$$

$$\overline{\alpha}_1^y = \int_0^L (\beta_{01}^y - \beta_{11}^y)dz \tag{3.29}$$

By the beat length definition, the accumulated phase difference can also be rewritten as

$$\overline{\alpha}_1^x = \int_0^L \frac{2\pi}{Z_{b1}^x(z)}dz \tag{3.30}$$

If the beat length $Z_b(z)$ is replaced by an equivalent beat length $\overline{Z}_b$, which corresponds to a uniform structure. Then,

$$\overline{\alpha}_1 = \frac{2\pi L}{\overline{Z}_b^x} \tag{3.30}$$

After an increase Δl_e of elongation, the envelope varies one cycle, so that

$$2\pi = \frac{(\overline{\alpha}_1^x - \overline{\alpha}_1^y)}{2}\Delta l_e \tag{3.31}$$

and after the transmission oscillates one cycle, an increase Δl_a of elongation is given by

$$2\pi = \frac{(\overline{\alpha}_1^x + \overline{\alpha}_1^y)}{2}\Delta l_s \tag{3.32}$$

The number of transmission oscillations during one envelope cycle is then

$$\Pi = \frac{\Delta l_e}{\Delta l_s} = \frac{(\overline{\alpha}_1^x + \overline{\alpha}_1^y)}{(\overline{\alpha}_1^x - \overline{\alpha}_1^y)} \tag{3.33}$$

Substituting Eq. (3.30) into the above formula

$$\Pi = \frac{\overline{Z}_{b1}^x + \overline{Z}_{b2}^y}{\overline{Z}_{b1}^x - \overline{Z}_{b2}^y} \tag{3.34}$$

If there is no birefringence, $\overline{\alpha}_1^x = \overline{\alpha}_1^y$, or $\overline{Z}_{b1}^x = \overline{Z}_{b2}^y$, Π is infinite, which means that the nodes of the envelope never appear, and the oscillation amplitude is constant. In order to avoid a zero denominator, the Q_z is introduced to describe the birefringence that is defined as the inverse of Π

$$Q_z = \frac{\overline{Z}_{b1}^y - \overline{Z}_{b1}^x}{\overline{Z}_{b1}^y + \overline{Z}_{b1}^x} \tag{3.35}$$

The magnitude of Q_z represents the equivalent beating length difference of two polarization directions in function of ITR. The smaller Q_z is, the less polarization dependent of the coupler is. Numerical results are shown in Fig. 3.12(a) and (b) for the circular and elliptical core fiber couplers for the complete fusion case. Fig. 3.12 shows that Q_z is small for medium *ITR* and becomes large for small *ITR*. The latter can be explained by the fact that the coupler has become a two-layer waveguide when *ITR* is small and the index difference between cladding and the external medium is large, so the polarization correction is large. For the complete fusion case, the Q_z of an elliptical core fiber coupler is still small if the *ITR* is not too small. For the mode separating coupler, to obtain the maximum power transfer efficiency of LP_{11} modes, a small birefringence is desirable. Since the ITR values of most mode separating couplers are larger than 0.5, the birefringence is not a big issue in their fabrication process.
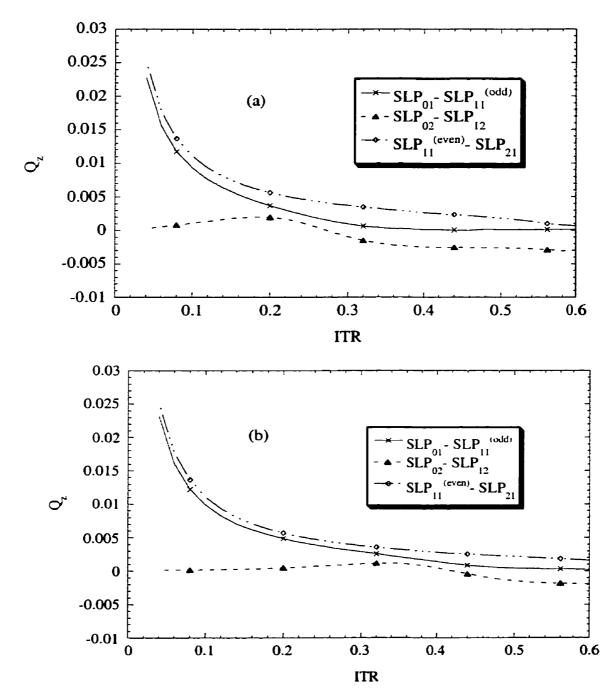
Figure 3.12 Birefringence of couplers as a function of ITR. (a) for circular core fibers. (b) for elliptical core fibers. The parameters used in the calculation are listed in Table 3.1.

3.7 Adiabatic Criterion

Tapering of an optical fiber leads to a loss of power from the core modes because of the departure from the transitional invariance of the uniform fiber. However, in principle, the loss can be kept arbitrarily small by using a sufficiently small taper angle. Two types of curves for delineating between adiabatic propagation and appreciable local mode coupling have been described [110, 111].

A taper is approximately adiabatic if the taper angle is small enough everywhere to ensure that there is negligible loss of power from the bound mode as it propagates along the length of the coupler. The loss can be quantified by local mode coupled equations.

If the backward light in the taper is neglected, the expansion of the exact field is described by

$$\Psi(x,y,z) = \sum_{j}^{m} b_j(z)\hat{\psi}_j(x,y,\beta(z))\exp\left[i\int_0^z \beta(z')dz'\right] \qquad (3.36)$$

where

$$\hat{\psi}_i = \frac{\psi_i}{\sqrt{\int_{A_-} \psi_i^2 dA}} \qquad (3.37)$$

where $\hat{\psi}_j$ denotes the scalar orthonormal local supermode field; the $b_j(z)$ and $\beta(z')$ are, respectively, the modal amplitude and propagation constant that are z-dependent. The integral within the exponent is the accumulated phase change along the taper. The sum implicitly includes the complete set of bound and radiation modes, then the scalar wave equation can be reformulated as a set of coupled local mode equations [76].

$$\frac{db_j}{dz} - i\beta_j b_j = \sum_j C_{jk} b_k \qquad (3.38)$$

where C_{jk} is the coupling coefficient between supermode j and k. It is defined by

$$C_{jk} = \frac{k}{2\sqrt{\beta_j \beta_k}} \frac{1}{n_{eff_j} - n_{eff_k}} \int_{A_-} \hat{\psi}_j \hat{\psi}_k \frac{\partial n^2}{\partial z} dA \qquad (3.39)$$

The coupled local mode equation can be solved approximately when only a small fraction of the total power is transferred between modes. For convenience, we assume that only the jth forward propagation local supermode is excited at $z=0$, the coupling effect is predominant to the supermode having its propagation constant close to the jth mode. The amplitude of these two modes are well approximated by

$$b_j(z) = b_j(0) \exp\left\{ i \int_0^z \beta(z')dz' \right\} \qquad (3.40)$$

$$b_{j+1}(z) = b_j(0) \exp\left\{ i \int_0^z \beta(z')dz' \right\} \int_0^z C(z') \exp\left\{ i \int_0^{z'} (\beta_j(z'') - \beta_{j+1}(z''))dz'' \right\} dz' \qquad (3.41)$$

where $b_j(0)$ is the amplitude of the jth local supermode at the beginning of the coupler. If we assume that the jth local supermode alone is initially excited with unit power, i.e. $b_j(0)=1$, then the fraction of power excited in the $(j+1)$th forward propagation supermode is

$$P_{j+1} = \left| \int_0^z C(z') \exp\left\{ i \int_0^{z'} (\beta_j(z'') - \beta_{j+1}(z''))dz'' \right\} dz' \right|^2 \qquad (3.42)$$

Since the coupler is slowly varying, $C(z)$ and $(\beta_j - \beta_k)$ are also slowly varying, and the exponential term in (3.42) causes the integral to oscillate very rapidly. The maximum power transfer occurs after half a beat length, the coupling coefficient and the propagation difference are approximately constant over this distance, i.e.,

$$C(z) \approx C$$

$$\beta_j(z'') - \beta_{j+1}(z'') \approx \frac{\pi}{z_b} \qquad (3.43)$$

Substituting (3.43) into (3.42), and considering the coupler is adiabatic, it should be $P_{j+1}<<1$. So, we have

$$P_{max} \approx \left|\frac{CZ_b}{\pi}\right|^2 <<1 \tag{3.44}$$

If we set

$$CZ_b = 1 \tag{3.45}$$

then

$$P_{max} \approx \frac{1}{\pi^2} \approx 10\% \tag{3.46}$$

and the loss is approximately 10% per half beat length. When the index profile has a step variation, the coupling coefficient is proportional to the relative taper slope $(1/\rho)d\rho/dz$, therefore, Eq. (3.39) can be rewritten as

$$C_{jk} = \frac{1}{\rho}\frac{\partial\rho}{\partial z}\overline{C}_{jk} \tag{3.47}$$

where $\overline{C}_{jk}$ are the normalized coupling coefficients that are independent of the longitudinal structure of the coupler. The adiabatic criterion is defined by using the normalized taper slope.

$$\Omega_W = \left|\frac{1}{\rho}\frac{d\rho}{dz}\right| \tag{3.48}$$

Eq. (3.45) is the weak power transfer criterion that provides a delineation between weak and strong coupling that occurs between two local modes. It compares the local coupling length to the beat length. As for a fused coupler, its slopes must be small enough to prevent undesired coupling to higher-order modes that would not be recovered into the

cores. Substituting Eq.(3.45) and (3.47) into (3.48), the adiabatic criteria can be rewritten as

$$\Omega_w = \left| \frac{\delta n_{eff}}{\lambda} \frac{1}{C} \right| \tag{3.49}$$

In the coupling region, defined as the region between the entrance or exit end and waist of the coupler, the higher order supermodes with same symmetry as the core modes will be excited if the longitudinal slopes vary abruptly. In two-mode fiber couplers, the supermodes can be divided into four groups depending on their symmetry. If we only consider the first higher order cladding modes, the details are given in Table 3.2.

core modes	cladding modes	coupling coefficients
$SLP_{01}^{(even)}$, $SLP_{02}^{(even)}$	$SLP_{21}^{(even)}$	$C_{01-02}^{(even)}$, $C_{01-21}^{(even)}$ $C_{02-21}^{(even)}$
$SLP_{11}^{(odd)}$, $SLP_{12}^{(odd)}$	$SLP_{31}^{(odd)}$	$C_{11-12}^{(odd)}$, $C_{11-31}^{(odd)}$, $C_{12-31}^{(odd)}$
$SLP_{21}^{(odd)}$	$SLP_{22}^{(odd)}$	$C_{21-22}^{(odd)}$
$SLP_{11}^{(even)}$	$SLP_{12}^{(even)}$	$C_{11-12}^{(even)}$

Table 3.2 Guided core and cladding modes and their coupling in coupler

The normalized coupling coefficients for an elliptical core case are shown in Fig. 3.13. The power transfer criterion is usually described by a delineation curve as a function of ITR. The lowest curve is the limitation of the relative slope $(1/\rho)d\rho/dz$. If the coupler slope is smaller than the limits given by the delineation curve for each ITR point, then the coupler is said to be adiabatic. Fig 3.14 shows the delineation curves for the circular core
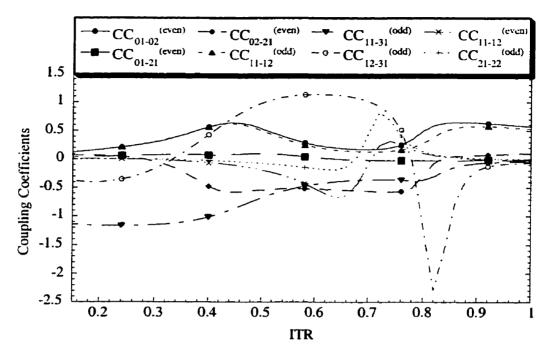
Figure 3.13 Coupling coefficients of an elliptical core coupler as a function of ITR.
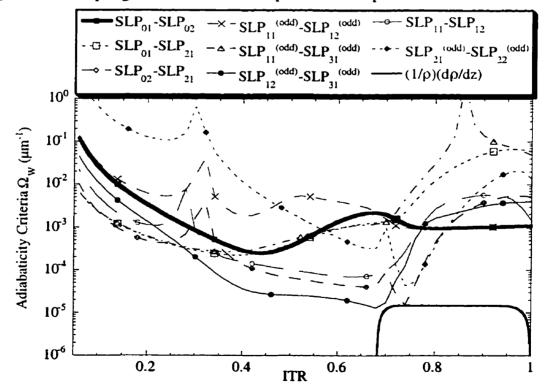
Figure 3.14 Delineation curves of adiabaticity criteria of the circular core coupler. The normalized slope curve is for 50.6 mm elongation and 66.50 mm sweep length.
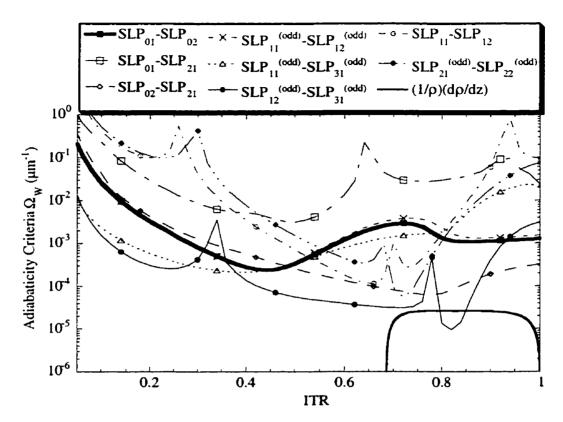
Figure 3.15 Delineation curves of adiabaticity criteria of the elliptical core coupler. The normalized slope curve is for 28.4 mm elongation and 37.75 mm sweep length.

fiber coupler. For a single mode circular core fiber coupler [88], since only SLP_{01} and SLP_{11} are excited at the coupler entrance, only the curves involving one of these two modes are to be considered. Here, since there are six supermodes and the field values of the supermodes corresponding to individual LP_{11} modes are large at the interface between the cladding and core, these lead to easy coupling into higher order cladding modes. So, the delineating curves are lower than the SLP_{01-02} curve. Fig. 3.15 gives the delineation curves for an elliptical core fiber with $a = 7.8$ μm, $b = 10.4$ μm and cladding radius 62.5 μm. Among them, the SLP_{12-31} curve is the lowest, and it limits the acceptable slope of

an adiabatic coupler. Under mode separation conditions, the coupler made of identical circular core fibers is an adiabatic, while the coupler made of identical elliptical core fiber is a non-adiabatic. However, there are several methods such as using prepolishing, pre-etching and thermally expanded fibers that can reduce the distance between two fiber cores and further reduce the elongation so that the adiabatic conditions may be satisfied. These methods will be discussed in the next chapter.

3.8   Discussion

The characteristics of fused couplers consisting of two identical elliptical and circular core fibers have been studied in detail using supermode analysis. The transmissions of the elliptical core fibers and the circular core fibers have been compared. It is observed that to obtain high power transfer efficiency for the LP_{11} mode, both the elliptical and circular core fibers are acceptable, whereas from the point of view of fabrication the choice of elliptical core fibers is preferable due to the shorter flame sweep distance and elongation. The calculation shows that to reach a complete transfer of the LP_{11} mode one should adjust the sweep length to ensure that both LP_{11} modes transfer at the same elongation. On the other hand, to reduce the power loss and keep the coupler adiabatic, the circular core fiber is better than that of elliptical core fibers. However, there are several improvement methods that can make the elliptical core fiber couplers satisfy the adiabatic criteria. There will be presented in the next chapter.

Chapter 4

Improvement Methods

4.1 Introduction

In the previous chapter, we showed that the adiabatic conditions of the elliptical core fiber couplers with standard profile are not completely satisfied. To resolve the problem, the distance between two fiber cores must be small to reduce elongation. To reach this aim, some preparation work on the fibers is necessary, such as the pre-etching, prepolishing and thermal expanded methods. Besides, these methods can also reduce the beat lengths of supermodes, so the couplers could be made shorter. For clarity, the couplers made by these methods are called "improved couplers" and the previous couplers are called "normal couplers". At the mode separation elongation point, ITR values in the "improved coupler" waist will be larger than that of "normal couplers", thus the birefringence of "improved couplers" will not be large. Other improvement methods are to use highly elliptical core fibers or thermally expanded core fibers. Especially, highly elliptical core fibers only support LP_{01} and even LP_{11} modes while the odd LP_{11} is cutoff, then the mode separation conditions become simpler. In this chapter, we will discuss each method and give the typical simulation results to confirm the above ideals.

4.2 Pre-etched Fiber Couplers

The etch method was first used to fabricate a power splitter [21]. When the two parallel and contacted fibers are immersed into the etching liquid and the cladding of fiber is removed by etching, the evanescent field in one fiber will penetrate into the other fiber and tend to excite a light wave in it. By a similar process, Sheem et. al. [19] inserted a pair of twisted fibers through a plastic container that contained an etching solution composed of HF and NH_4F. The etched fiber diameter is a linear function of etching time with the correct mixture ratio of HF and NH_4F. Lamont et. al. [112] demonstrated that controlled removal by etching of the outer cladding of a depressed-cladding-index fiber permits the fabrication of low-loss fusion and tapered couplers. Here, the fabrication process of couplers would be the same as Lamont's. We assume that the cladding radius of fibers has been etched first, then the fibers are completely fused and tapered. The simulation processes are the same as those described in the previous chapter except for the reduction of the cladding radius. Effective indices of the supermodes, transmission, longitudinal profile, birefringence, and adiabatic criteria of the couplers made of pre-etching fibers will be calculated.

4.2.1 The Limitation of Cladding Radius

Before doing the pre-etching, it is necessary to estimate how much of cladding can be removed without affecting the guiding properties of the fiber. The field distribution of fiber modes can be analytically expressed by Bessel functions. For a fiber having a relative index difference of 0.0014 and a core radius of 9.0 μm, its normalized field distribution of LP_{01} and LP_{11} modes are plotted in Fig. 4.1. From this distribution we see that when the cladding radius is 40.5 μm, the relative value of the field at the cladding interface is only 0.01% of the maximum field value and can be neglected. For the pre-

etching method, if the minimum cladding radius is larger than 40.5 μm, the light wave will be well confined inside the fiber core. In the following discussion, the etched fiber radius is assumed to be 42.5 μm, corresponding to a relative value of the field at its surface of 0.005%.
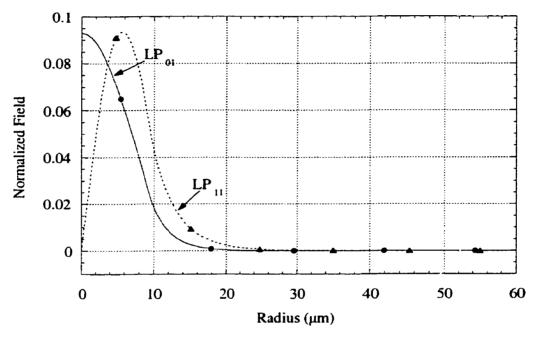
Figure 4.1 Normalized radial field distribution. The fiber has a relative index difference of 0.0014 and a core radius of 9.0 μm.

4.2.2 Transmission

For the pre-etched fusion and tapering coupler, the effective indices of the supermodes are conveniently calculated by the FMEM. The numerical results for a fiber with a cladding radius of 42.5 μm are plotted in Fig. 4.2 for the circular core fiber case and Fig. 4.3 for the elliptical core fiber case, with parameters are identical to those in Table. 3.1 except for the cladding radius. Because the precision of calculation is 10^{-7}, we can give a separation criterion: when the effective index difference of degenerated supermodes is more than 5×10^{-6}, the two supermodes start to separate. For the circular core without etching case,

shown in Fig. 3.7(a), the separation points locate at ITR of 0.5 for SLP_{01} and $SLP_{11}^{(odd)}$, ITR of 0.76 for SLP_{02} and SLP_{12}, and ITR of 0.74 for $SLP_{11}^{(even)}$ and SLP_{21}. While for the circular core and etched case, ITR's are 0.6, 0.84, and 0.80, respectively for the separation points. For the elliptical core without etching case, shown in Fig. 3.7(b), the values of ITR are 0.52, 0.80 and 0.72 respectively for the separation between SLP_{01} and $SLP_{11}^{(odd)}$, SLP_{02} and SLP_{12}, and $SLP_{11}^{(even)}$ and SLP_{21}. While for elliptical core and etched case shown in Fig. 4.3, ITR's are 0.6, 0.86, and 0.74, respectively for the separation points. We see that all the ITR values in the etched cases are larger than the corresponding values without etching. For clarity, the results are summarized in Table. 4.1. This is because the distance between two fiber cores with etching is shorter than that of without etching. The coupler without etching needs a smaller diameter and the ITR will be smaller. Consequently, to reach the mode separation point, the required elongation for the etched coupler is shorter than that of normal couplers under the same conditions. Fig. 4.4 shows the transmission of an etched coupler for the circular core case. When the flame width is 4 mm, flame sweep distance is 59 mm and the elongation is 32.4 mm, the coupler works as a mode separating coupler. While from Fig. 3.10(a) the coupler without etching operates as a mode separating coupler under the conditions of 4 mm flame width, 66.5 mm sweep distance and 50.6 mm elongation. Fig. 4.5 shows the transmission of an etched coupler with an elliptical core. When the flame length is 4 mm, flame sweep distance is 15 mm and the elongation is 12.4 mm, the coupler functions as a mode separating coupler. While from Fig. 3.10(b) the coupler without etching functions as a mode separating coupler under the conditions of 4 mm flame width, 37.75 mm sweep distance and 28.4 mm elongation. To compare the parameters for etched and normal couplers, the conditions for the couplers functioning as mode separating couplers are summarized in Table. 4.2. We can see that all the values of sweep distance and elongation

for both circular and elliptical core cases become smaller when using the pre-etching method. This leads to the relaxation of requirements for fabricating the mode separating coupler.
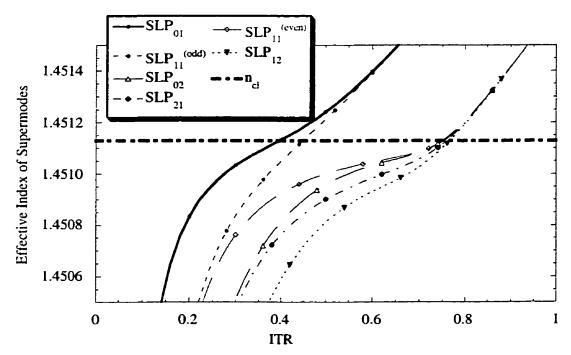
Figure 4.2 The effective indices of supermodes against the ITR for the coupler made of two identical circular core fibers with cladding radius etched to 42.5 μm. The other parameters are the same as that in Fig. 3.6(a).

Separation	SLP_{01} & SLP_{11}	SLP_{02} & SLP_{12}	$SLP_{11}^{(even)}$ & SLP_2
C-core	0.50	0.76	0.74
C-core (etched)	0.60	0.84	0.80
E-core	0.52	0.80	0.72
E-core (etched)	0.6	0.86	0.74

Table 4.1 The values of ITR corresponding to the separation points between supermodes.
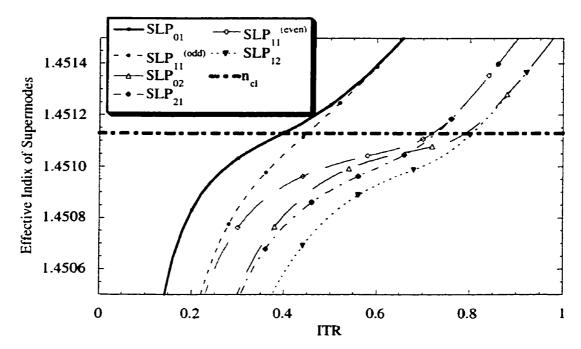
Figure 4.3 The effective indices of supermodes against the ITR for a coupler made of two identical elliptical core fibers with cladding radius etched to 42.5 μm. The other parameters are the same as that in Fig. 3.6(b).

	Flame width (mm)	Sweep distance (mm)	Mode separating coupler elongation (mm)
C-core	4.0	66.5	50.60±0.40
C-core (etched)	4.0	59.0	32.40±0.40
E-core	4.0	37.75	28.40±0.40
E-core (etched)	4.0	15.0	12.40±0.40

Table 4.2 The parameters of the couplers functioned as mode separating couplers.
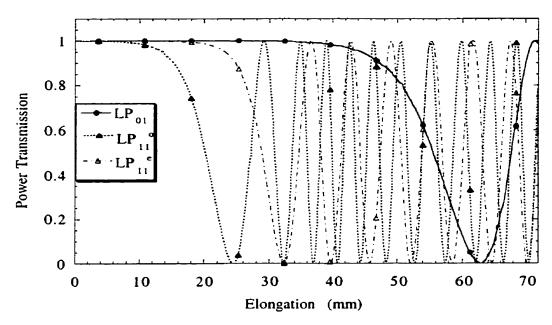
Figure 4.4 The transmission versus elongation for etched and circular core
fiber couplers. The parameters are listed in Table. 4.2.
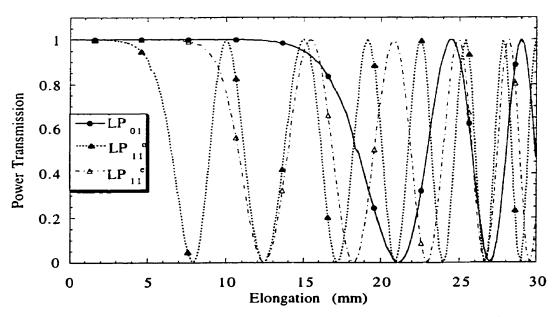
Figure 4.5 The transmission versus elongation for etched and elliptical core
fiber couplers. The parameters are listed in Table. 4.2.

The longitudinal profiles for the etched couplers functioning as mode separating couplers are plotted in Fig. 4.6 and Fig. 4.7 for both circular and elliptical core cases respectively. The value of ITR at the waist of each coupler is 0.76 and 0.66 for the circular and elliptical core coupler respectively. While for the coupler without etching, the ITR at the waist is 0.68 and 0.69 for circular and elliptical core cases respectively. In general, under the same conditions, the ITR decreases when the sweep length decrease or the elongation increase. For the circular core fiber coupler, the sweep distance changes from 66.5 mm to 59.0 mm but the elongation reduces to 12.2 mm after etching the fiber, so the ITR at the waist becomes larger. For the elliptical and etched coupler, however, when the sweep distance reduces to 22.75 mm and the elongation reduces to 16 mm, the ITR value at the waist of the coupler becomes smaller. Comparing the etched coupler length with that of normal couplers, we can see that the coupler length reduces from 128 mm to 102 mm for circular core couplers and from 77 mm to 38 mm for elliptical core couplers respectively. This is one of the advantages of employing the pre-etching method.
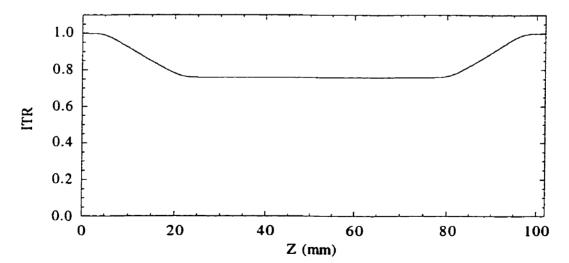
Figure 4.6 Simulation longitudinal profile of the etched circular core coupler for 4.0 mm flame width, 59 mm sweep distance and 32.4 mm elongation.
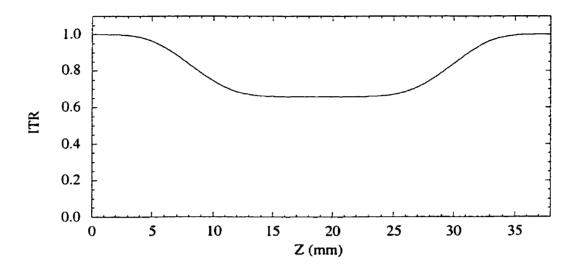
Figure 4.7 Simulation longitudinal profile of the etched and elliptical core coupler for 4.0 mm flame width, 15 mm sweep distance and 12.4 mm elongation.

4.2.3 Beat Length

The beat lengths of etched couplers were calculated and are plotted in Fig 4.8(a) and (b) for the circular and elliptical core coupler respectively. We can see that all the beat lengths become shorter than the corresponding values of normal couplers. It may be explained in as follows: when the distance between two fiber core centers becomes shorter due to pre-etching of the fibers, the beating supermodes will have a slightly larger difference of propagation constants than that of normal couplers under the same ITR values; and by the definition of the beat length, its value is inversely proportional to the difference of propagation constants. The relative shorter beat length for the LP_{11} mode is good for the mode separating coupler because the coupler length can be made shorter.
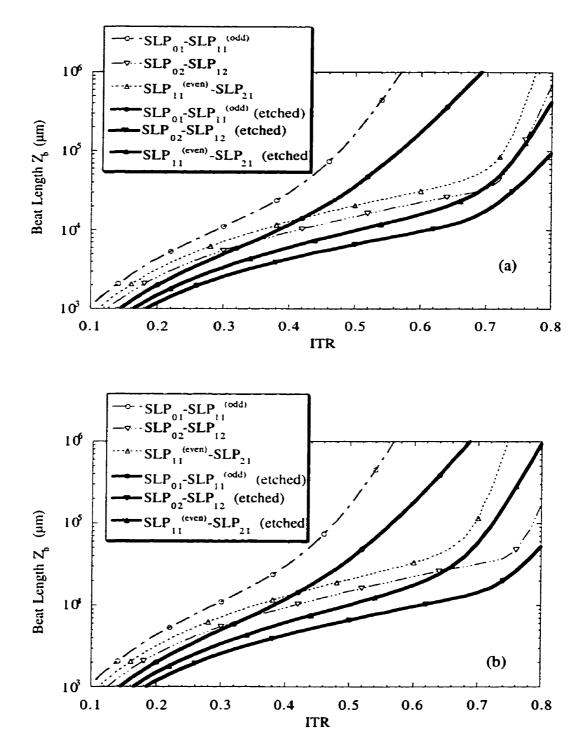
Figure 4.8 The beat length versus ITR for (a) a circular (b) an elliptical core fiber coupler. The solid and dashed lines stand for the etched and normal couplers respectively.

4.2.4 Birefringence

The birefringence of the etched couplers is calculated and plotted in Fig 4.9 and Fig. 4.10 for the circular and elliptical core fiber coupler respectively. One can see that the birefringence is larger than the corresponding values of a normal coupler. It is because the radius of the cladding becomes smaller after fiber pre-etching, giving the supermodes a slightly larger difference of modal fields on the interface between the cladding and air than they would without etching. So, the propagation constant corrections for x and y direction have a slightly larger value. However, the birefringence decreases with the increase of ITR. When ITR is larger than 0.55, all the birefringence values for both etched and non-etched couplers are less than 0.005. For the etched coupler the ITR at the waist is always larger than 0.66, so the pre-etched method will not induce additional birefringence.
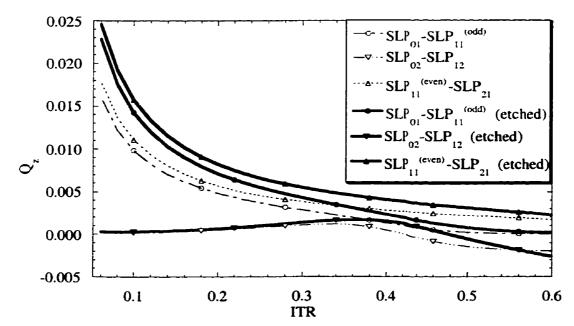
Figure 4.9 Birefringence versus ITR for a circular core fiber coupler. The solid and dash lines stand for the etched and non-etched fiber couplers respectively.
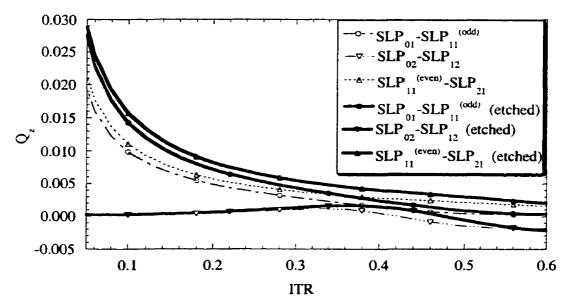
Figure 4.10 The birefringence versus ITR for a circular core fiber coupler. The solid and dash lines stand for the etched and non-etched fiber couplers respectively.

4.2.5 Adiabatic Criteria

The adiabatic criterion delineation and the slope curves are calculated for the pre-etched coupler. The results shown in Fig. 4.11 and Fig. 4.12 illustrate the couplers are adiabatic for both circular and elliptical core couplers. Actually, the pre-etching method is aimed at reducing the distance between the two fiber cores, in turn reducing the elongation, and better realizing the adiabatic coupler. Comparing the numerical results in Fig. 4.12 with those in Fig. 3.15 reveals that the nonadiabatic "normal coupler" becomes an adiabatic coupler after pre-etching the fibers. So, the pre-etching could be used as an improvement method to reduce the power loss and realize the adiabatic coupler.
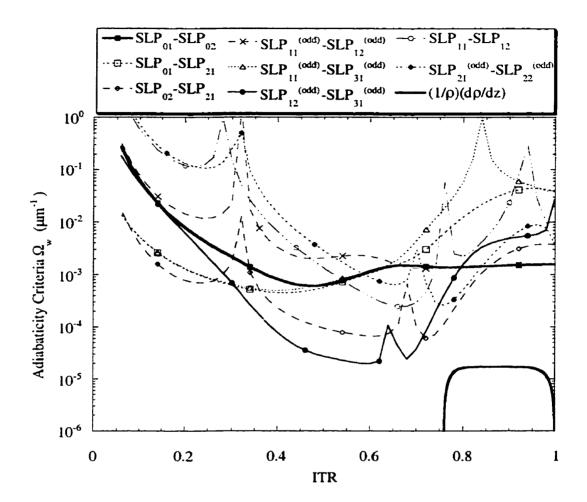
Figure 4.11 The adiabatic criterion's delineation and slope curve versus ITR for etched and circular core fiber coupler. The slope curve is lower than all the delineation curves, showing that the coupler is adiabatic.
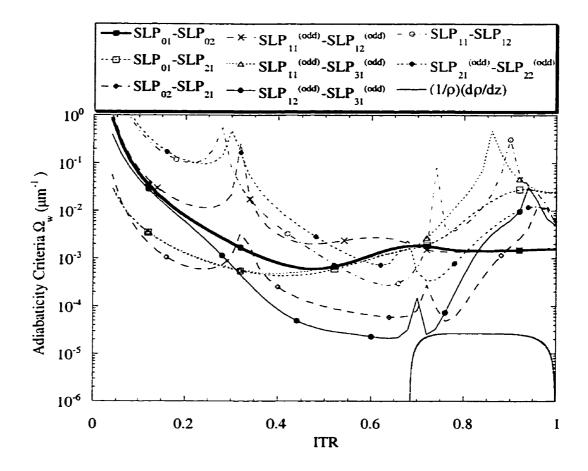
Figure 4.12 The adiabatic criteria delineation and slope curve versus ITR for etched and elliptical core fibre coupler. The slope curve is lower than all the delineation curves, showing that the coupler is adiabatic.

4.3   Prepolished Fiber Couplers

For the construction of wavelength flat couplers, the prepolishing [92, 113, 114] and pre-etching [112] methods were used to introduce the asymmetry between two identical fibers. The further development of the prepolishing method is described by O'Sullivan [115]. Although the method has already been shown to be suitable for asymmetric

couplers in general, it can also be used for identical fiber couplers to reduce the distance between the two fiber cores and realize adiabatic couplers.

In principle, both prepolishing and pre-etching methods are equivalent, because it is the distance between the two fiber cores rather than the cross section shape that determines the properties of the coupler. Especially when the two parallel fibers are completely fused, and all the cross sections are circles for both prepolishing and pre-etching cases.

4.3.1 Comparison between Prepolishing and Pre-etching

The coupler optical properties mainly depend on the distance between the two fiber cores. If we assume that the coupler is completely fused, its cross section is a circle after fusing. For the pre-etching case, the total cross sectional area is conserved before and after fusion. Thus, we have

$$2\pi\rho_e^2 = \pi R_e^2 \tag{4.1}$$

Then

$$R_e = \sqrt{2}\rho_e \tag{4.2}$$

and

$$d_e = 2(R_e - \rho_e) = 2(\sqrt{2} - 1)\rho_e \tag{4.3}$$
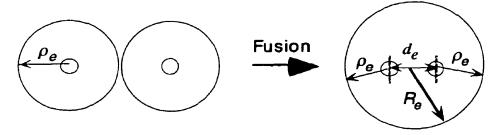
Figure 4.13 The cross section of the etched fiber coupler before and after fusion.

where ρ_e is the cladding radius of etching fiber, R_e and d_e are the radius and the distance between the cores of the completely fused coupler as defined in Fig. 4.13.

For a prepolished fiber, its cross sectional area is the difference between a circle and a crescent area. The crescent area is

$$S_a = \frac{1}{2}\rho_{cl}^{~2}(\alpha - \sin\alpha) \tag{4.4}$$

where α, ρ_{cl} are defined in Fig. 4.14. So, we have

$$2\left[\pi\rho_{cl}^{~2} - \frac{1}{2}\rho_{cl}^{~2}(\alpha - \sin\alpha)\right] = \pi R_p^{~2} \tag{4.5}$$
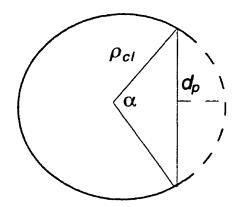
Figure 4.14 The cross section of the polished fiber.
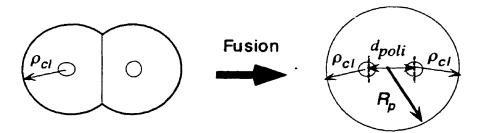
Figure 4.15 The cross section of the prepolished fiber coupler before and after fusion.

Thus

$$R_p = \rho_{cl} \sqrt{2 - \frac{\alpha - \sin \alpha}{\pi}}$$ (4.6)

and

$$d_{poli} = 2\rho_{cl} \left(\sqrt{2 - \frac{\alpha - \sin \alpha}{\pi}} - 1 \right)$$ (4.7)

where R_p and d_{poli} are the radius and the distance between two fiber cores for the prepolished and completely fused couplers as defined in Fig. 4.15. Let the distances between the two fiber cores be equal to that of pre-etching cases, then we have

$$\rho_e = \frac{\rho_{cl}}{\sqrt{2} - 1} \left(\sqrt{2 - \frac{\alpha - \sin \alpha}{\pi}} - 1 \right)$$ (4.8)

where

$$\alpha = 2 \cos^{-1} (1 - p)$$ (4.9)

where p is the polishing degree and α is the angle shown in Fig. 4.14. Because of the limitation of the radius in the pre-etching method discussed in section 4.2.1, Eq. (4.8) only holds for an etched radius of more than 40.5 μm. From Fig. 4.16 we see that for an etched fiber radius of 42.5 μm, the corresponding polish degree is 0.469. So, we choose the prepolish degree 0.469 in the following calculation.

4.3.2 Numerical Results

To study the effect of prepolishing fiber couplers, a numerical calculation was done by the FMEM. The fiber had the same parameters as listed before in Table. 3.1 and was prepolished. The polishing degree was 0.469 to obtain the equivalent distance between two cores as in the pre-etching case. To avoid the unnecessary repetition, only the elliptical core coupler case was calculated.
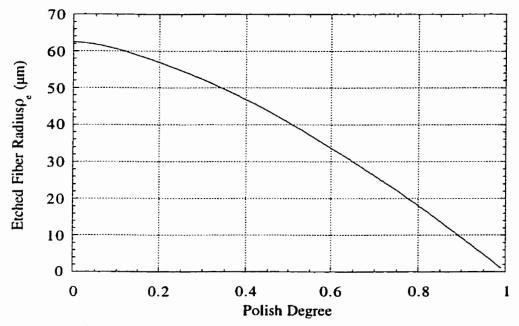
Figure 4.16 The etched fiber radius versus the polishing degree when the distance between the two fiber cores in the completely fused coupler is equivalent.
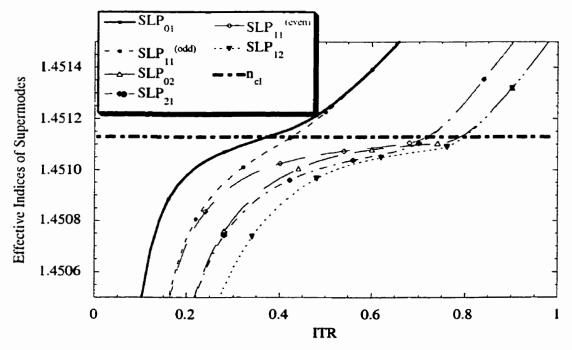
Figure 4.17 The effective indices of supermodes for a prepolished elliptical core fiber coupler.
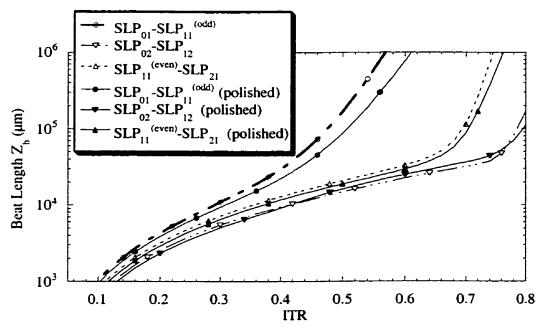
Figure 4.18   The beat lengths versus ITR for a prepolished and an unpolished fiber coupler. The solid and dashed lines represent the prepolished and unpolished fiber cases respectively.

The calculated effective indices of the supermodes are plotted in Fig. 4.17. The calculated beat lengths of the prepolished couplers are compared with those of the normal coupler in Fig. 4.18. From those curves we can see that the beat lengths between SLP_{01} and $SLP_{11}^{(odd)}$, and $SLP_{11}^{(even)}$ and SLP_{21} become smaller in the prepolished fiber case, while the beat length between SLP_{02} and SLP_{12} becomes larger than the corresponding values in the normal coupler case in the range from 0.425 to 0.785 of ITR.

The birefringence of the prepolishing and normal couplers are plotted in Fig. 4.19 for comparison. We can see that the birefringence of prepolished couplers increases a small amount under the same ITR except for the mode formed by the beating between SLP_{02} and SLP_{12}, while the maximum value of Q_z is -0.004 when ITR is 0.6. Therefore the

birefringence of a pre-polished coupler is still very small. Fig. 4.20 compares the birefringence of the prepolished coupler with that of pre-etched fiber couplers. We can see that the birefringence of the prepolished coupler is smaller than the corresponding values of the pre-etched fiber couplers. For the mode separating couplers, the values of ITR at the coupler waist are always relatively large. This is because the beat length difference between the two orientation LP_{11} modes is large when ITR is more than 0.5. This demonstrates that the birefringence is a minor concern in the fabrication of mode separating couplers.

The transmission of a prepolished elliptical core fiber coupler is shown in Fig. 4.21. From those curves we can see that the coupler functions as a mode separating coupler when the elongation is 32.4 mm. The other parameters used for the calculation are 4 mm flame width and a 46.0 mm sweep distance. Comparing the value in Fig. 4.21 with the transmission of a normal coupler in Fig. 3.10(b), it is found that the elongation and sweep distance of prepolished fiber couplers are longer than that of normal couplers. The reasons are that the beat length differences of the supermodes corresponding to the two orientation LP_{11} mode become smaller for prepolishing couplers. However, the adiabatic criteria delineation curves plotted in Fig. 4.22 show that the prepolished fiber coupler is adiabatic when the elongation is 32.4 mm and the sweep distance is 46.0 mm. Consequently, the prepolishing method is able to realize an adiabatic coupler that functions as a mode separating device, although its elongation and sweep distance may be longer than that of unpolished normal couplers.
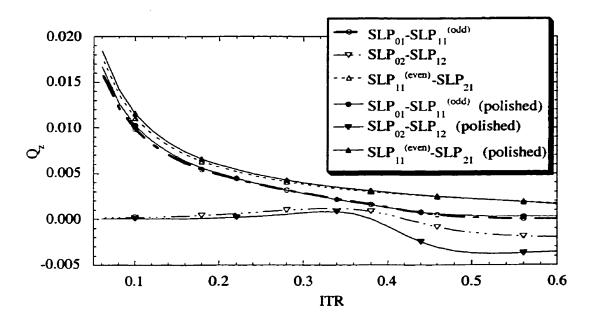
Figure 4.19 The birefringence versus ITR for a prepolished and an unpolished fiber coupler. The solid and dashed lines represent the prepolished and unpolished fiber cases respectively.
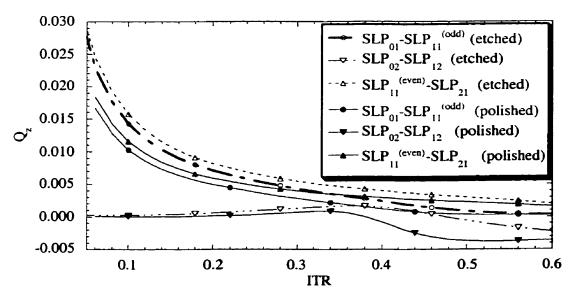
Figure 4.20 The birefringence versus ITR for a prepolished and a pre-etched fiber coupler. The solid and dashed lines represent the prepolished and pre-etched fiber cases respectively.
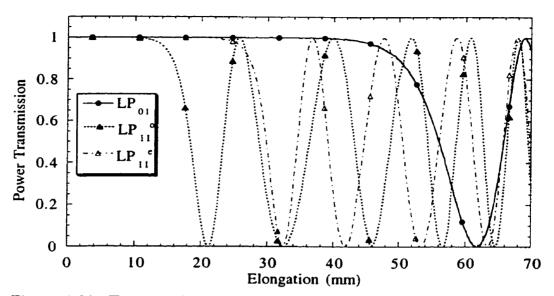
Figure 4.21 Transmission as a function of elongation for prepolished elliptical core couplers with 4 mm flame width and 46 mm sweep distance.
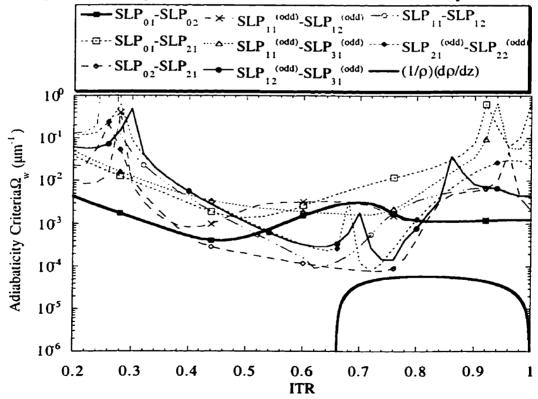
Figure 4.22 The adiabatic criteria delineation and coupler slope versus ITR for a prepolished elliptical core fiber coupler. The slope is lower than all the delineation curves showing that the coupler is adiabatic.

4.4 Highly Elliptical Core Fiber Couplers

In the previous chapter, mode separating couplers made of circular and elliptical core fibers were studied and the results showed that elliptical core fibers are better for the fabrication of mode separating couplers as they permit one to use shorter flame sweep distance and a shorter elongation. In an extreme case, if the fiber core eccentricity is very high and the fiber parameter is relatively small, the fiber will possibly only support the LP_{01} mode and the even LP_{11} mode, the odd LP_{11} mode being cutoff [4, 71]. Correspondingly, there are only four core supermodes propagating in the coupler. Thus, the mode separation conditions become simpler and easier to satisfy.

Consider two identical elliptical core fibers interacting along their minor x axes, and their two major y axes are parallel. The refractive index difference between the core and the cladding is 0.0014, and the semi-major and semi-minor axes a and b are 5.0 and 16.2 μm respectively. The index difference and core areas are identical to that of Chapter 3. So, the LP_{01} and even LP_{11} modes are guided in the two mode fibers and the odd LP_{11} is cutoff. Therefore, the four supermodes such as SLP_{01}, $SLP_{11}^{(odd)}$, $SLP_{11}^{(even)}$, and SLP_{21} are guided in the coupler. Effective indices of the supermodes were calculated by FMEM and the results are shown in Fig. 4.23. If the couplers are adiabatic, the four supermodes will not couple into higher order modes. Accordingly, it is only necessary to consider two different beat lengths formed by the four supermodes. These are plotted in Fig. 4.24. Consequently, the mode separation conditions will be easily realized. In Fig. 4.25(a), (b), and (c) the transmissions are plotted for flame sweep distances of 10 mm, 20 m, and 30 mm respectively when the flame width is fixed at 4 mm. From Fig. 4.25 it can be seen that the flame sweep distances determine the transmission and furthermore determine the mode separation conditions. In Fig. 4.25(a), when the power in the LP_{11} mode

completely transfers from original branch into the other branch at 12.5 mm of elongation, only 88.7% of the power in the LP_{01} mode stays in the original branch, meaning that 11.3% of the power in LP_{01} mode transfers into the other branch also. For this case the coupler can not separate the LP_{01} and LP_{11} modes. In Fig. 4.25(b), when the elongation is 17.6 mm, the power in the LP_{11} mode completely transfers into the other branch and 99.2% of the power in LP_{01} mode is still in the original branch. For this case, the LP_{01} and LP_{11} modes are almost separated. When the flame sweep distance is 30 mm in Fig. 4.25(c), the LP_{01} and LP_{11} modes can be completely separated at the elongation of 22.8 mm point. In Fig. 4.26, the adiabatic criteria for a coupler made with an elongation of 17.6 mm, flame width of 4 mm and sweep distance of 20 mm is plotted. It can be seen that the coupler corresponds to the Fig. 4.25(b) adiabatic case.

Thanks to simulation one can know that there are some advantages in using the highly elliptical core fibers to fabricate mode separating couplers. In particular, because only the even LP_{11} mode exists in this kind of fiber, the mode separation conditions become simple and easier to realize. Furthermore, this kind coupler may be very stable because the elliptical fibers are polarization maintaining fibers. However, aligning the two semi-major axes of elliptical core fibers parallel may be very difficult.

4.5 Thermally Expanded Core Fiber Couplers

Distance reduction between the two fiber cores could decrease the excess loss of the couplers thanks to a small taper slope. To realize this, the prepolishing and pre-etching method have been proposed, but another kind of method, using thermally expanded core (TEC) fibers, could also achieve the goal. It has been reported that phosphorus and
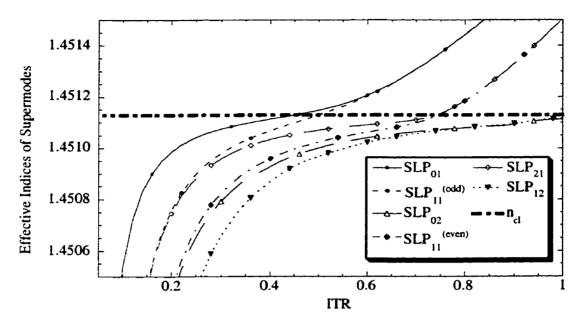
Figure 4.23 The effective indices of supermodes for highly elliptical core fibers as a function of ITR. There are only four supermodes in the core at the entrance region of coupler.
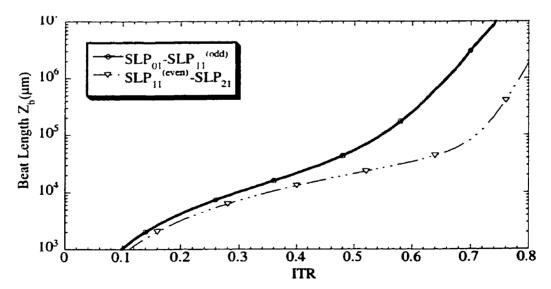
Figure 4.24 The beat lengths between supermodes for a highly elliptical core fiber as a function of ITR.
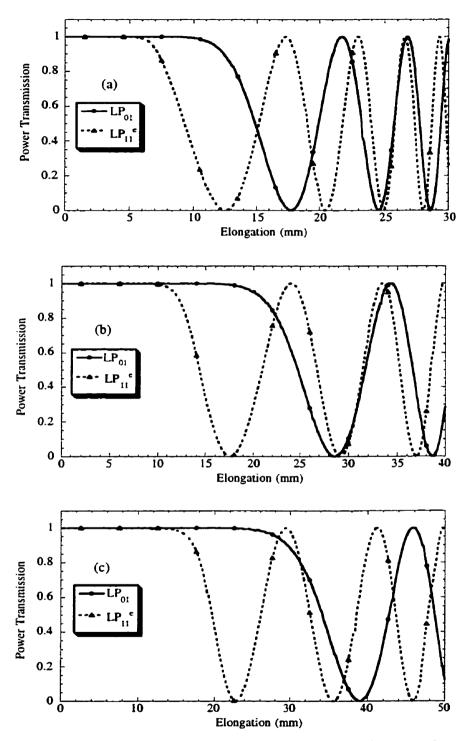
Figure 4.25 Transmission for a highly elliptical core fiber coupler as a function of ITR for the flame sweep distance (a) 10 mm, (b) 20 mm, and (c) 30 mm. The LP_{11}^o mode is cutoff.
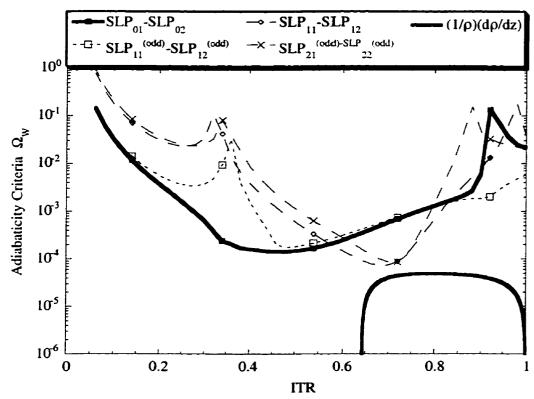
Figure 4.26 The adiabatic criteria delineation and slope curves versus ITR for the couplers made of the highly elliptical core fibers. The slope curve is lower than all the delineation curves showing that the coupler is adiabatic

fluorine [100, 103, 116, 117] in silica fiber diffuse due to heat treatment. It also has been shown that germanium can also diffuse [102, 103], so one gets a large core. Some fabrication methods and experimentally obtained characteristics of thermally diffused or expanded core fibers have been reported [57, 118, 119], and the phenomenon is expected to be useful to realize the mode separating couplers. In the following, we simulate a mode separating coupler made by the thermally expanded core fibers.

As in all previous simulations, the thermally expanded effects were considered in the fusion process as core shape changes and refractive index difference reductions. Here, the fiber is first placed in an oven under high temperature (1300–1700 °C) and for long time

pre-diffusion [103], then, they are used in standard coupler fabrication processes. The fiber core shape is still a circular but its radius will expand and the relative index difference will reduce. It is assumed the fiber conserves an equivalent step-index profile and the normalized frequency does not change [104] during the heating process. If the fiber in use is SMF28™ and is heated for a long time, which we consider an extreme case, the fiber core radius becomes 15 μm and the relative index difference 0.0005. This fiber is still two-mode fiber and couplers made of this kind of fiber will have six supermodes in one polarization direction. Fig. 4.27 shows the supermode effective indices. Fig. 4.28 plots the beat length between the supermodes. For convenient comparison, the beat lengths of normal couplers also plotted in Fig. 4.28. From this figure we can see that the beat length between SLP_{01} and $SLP_{11}^{(odd)}$ become shorter due to the thermally expanded core, but the beat lengths between SLP_{02} and SLP_{12}, $SLP_{11}^{(even)}$ and SLP_{21} change significantly only for an ITR larger than about 0.74. It is obvious that the decrease of the relative index difference reduces the light guidance function of the core. So, it only needs slight tapering and the power transfer will occur. Accordingly, couplers made of TEC fibers have relatively larger ITR values at their waist. However, to realize the mode separation, the accumulated phase difference must satisfy certain conditions, which lead to a long sweep distance. Fig. 4.29 shows the transmission of a coupler made of TEC fibers as a function of elongation. The parameters used in the calculation are 4 mm flame width and 110 mm flame sweep distance. The LP_{01} and LP_{11} modes separate for an elongation of 59.6 mm. The elongation range that keeps the two orientation LP_{11} mode power at less than 1% in the other branch is from 59.2 to 60 mm, which means the fabrication tolerance is 59.6±0.4 mm. The adiabatic criterion is given in Fig. 4.30, from which it could be seen that the coupler fabricated with flame width of 4
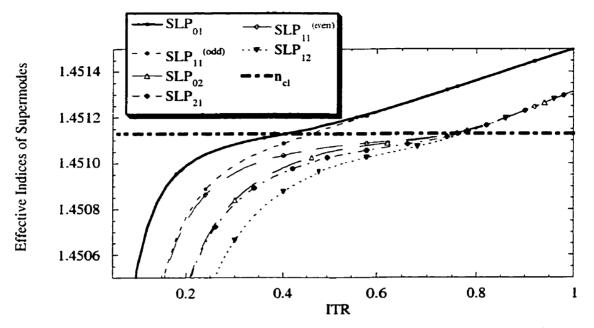
Figure 4.27 The effective indices of supermodes versus ITR for couplers made of the thermally expanded core fibers.
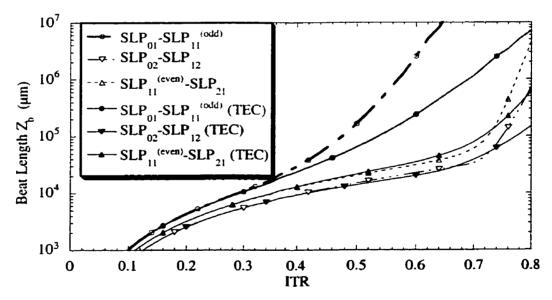
Figure 4.28 The beat lengths versus ITR for circular core coupler. The solid and dashed lines stand for the thermally expanded core fiber and standard normal couplers respectively.
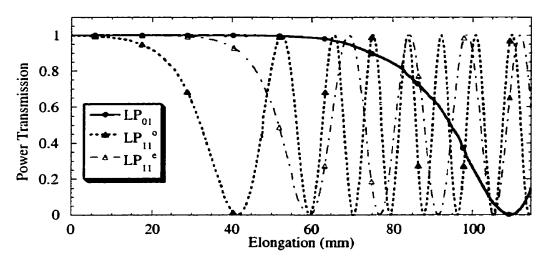
Figure 4.29 Transmission as a function of elongation. The calculated parameters are flame width of 4 mm and flame sweep distance of 110 mm. The modes are separated at an elongation of 59.6 mm.
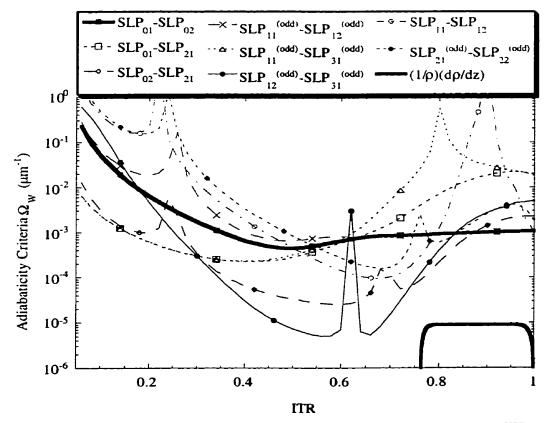
Figure 4.30 The adiabatic criteria delineation and slope curve versus ITR for couplers made of the TEC fibers.
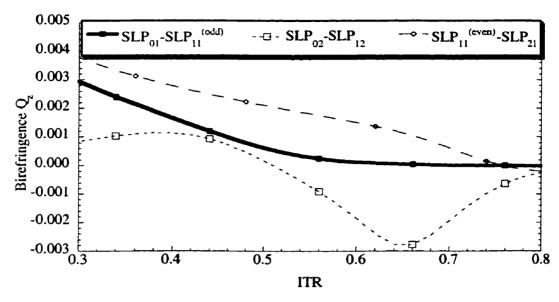
Figure 4.31 The birefringence parameters of a coupler consisting of TEC fiber versus ITR.

mm, sweep distance of 110 mm and elongation of 59.6 mm is adiabatic since the normalized slope is lower than all the criteria delineation curves. Fig. 4.30 also shows the minimum ITR value in the coupler waist is 0.767. Fig. 4.31 shows the birefringence parameters of the couplers versus ITR. When the ITR is 0.767, the maximum Q_z is 0.0005, which means the birefringence is very small. As a consequence, light of different polarization states will have nearly the same propagating properties in the couplers.

The main advantages of couplers consisting of TEC fiber are their small birefringence and their easy realization of adiabaticity due to the large inverse tapering ratio. Another advantage is its large fabrication tolerance. From Fig. 4.29 we see that the tolerance on elongation is 0.8 mm. Usually the elongation is controlled by a motor with precision of 0.005 mm, so there are no problems in controlling the elongation. However, this kind of coupler fabrication process requires a very long flame sweep distance, and for such a long

distance it is difficult to have the stable flame. A new heating technique developed recently with a microheater is suitable for long sweep distance [55-58]. It is worth noting that if the cores have been diffused too much, the beat length difference between the LP_{01} and LP_{11} modes will become very small; when the power in the two orientation LP_{11} mode transfers into the other branch, some power in the LP_{01} mode also transfers into the other branch at the same time, thus the modes can not be easily separated. Consequently, there is an optimum diffusion value in the TEC fiber coupler process.

4.6   Discussion

In this chapter, four methods have been proposed to better realize adiabatic couplers and relax their fabrication conditions. Although each method requires preparation of the fiber, such as pre-etching, prepolishing, pre-aligning the semi-major axes, and pre-heating the fiber, the simulation results show that the couplers will be easier to fabricate thanks to increase tolerances. Best among these methods are couplers consisting of highly elliptical core fibers for simplifying the fabrication process. Unfortunately, so far all commercial elliptical core fibers are used to maintain polarization; therefore they have a depressed cladding that may cause much power loss during the tapering process [44]. So, new kinds of elliptical core fibers are required.

Chapter 5

Realization of Mode Separating Couplers

5.1 Introduction

The unique real mode separating coupler reported by Thursby *et. al.* [72] was realized by polishing a two-mode fiber and bonding it to a prism. The LP_{11} mode was coupled into the prism by its evanescent field and collected by another fiber glued to the other side of the prism. This kind of mode separating coupler has a high insertion loss and is difficult to assemble. In the previous chapters, mode separating couplers were simulated under various conditions. The numerical results show that it is possible to realize the mode separating coupler by the fusion and tapering method. Compared with the polishing method, mode separating couplers made by the fusion and tapering technique have low excess loss, thermal stability, and are easier to fabricate. In this chapter, the LP_{11} mode launching and stripping method, as well as confirmation of the LP_{11} mode transfer will be presented. The effect of fusion time and flame sweep distance on transmission that will be followed by a study of mode separating coupler fabrication process. This chapter will close with comparison between the calculated and experimental results. .

5.2 LP$_{11}$ Mode Launch

There has been much work done for efficient and selective launching of the LP$_{11}$ mode into a two-mode fiber. Approaches to launching can be classified into three methods; The first is the side launching method whereby a second waveguide structure is brought in close contact with a side polished or etched two-mode fiber. An exchange of power from the second waveguide to a particular fiber mode occurs via the evanescent field. The second is the body launching method by resonant coupling between the LP$_{01}$ and LP$_{11}$ spatial modes in a two-mode fiber. It involves the formation of a grating with spatial period equal to the intermodal beat length. The types of gratings include stress-induced index gratings formed by periodically squeezing a two-mode fiber [2], path-length gratings created by periodic microbending [3, 5, 120], and photo-induced index gratings [121]. The third approach is the end launching method which can be carried out by using a conventional optical lens, optical phase shifter [91] or offset beam [122, 123]. For this work, the latter method was used by offsetting the joint between a single mode fiber and two-mode fiber to launch the LP$_{11}$ mode. The theory and experimental results of this offset beam launch method follows.

We start by considering a single mode fiber joined to a two-mode fiber. We are interested in launching both the LP$_{01}$ and LP$_{11}$ modes into the two-mode fiber. For simplicity, we assume the fibers are aligned colinearly and without a gap. The fundamental mode propagating from the single mode fiber will excite guided modes and radiation modes of the two-mode fiber. The light reflected from the front face of two-mode fiber can be neglected.

The electric and magnetic fields of the incident fiber will be denoted E_i and H_i. The propagating electromagnetic field produced in the two-mode fiber is a superposition of the

fields E_{lm} and H_{lm} of the LP$_{1m}$ mode (l=0 or 1, m=1). Residual fields in the two-mode fiber are denoted as E_r and H_r and consist of cladding modes, radiation modes and possibly other guided modes. As is well known from electromagnetic field theory, the tangential component of the electric and magnetic fields must be continuous at the boundary between two regions. This continuity of the transverse field at the joint interface requires that

$$\mathbf{E}_i(x,y) = \sum_l a_{lm}\mathbf{E}_{lm}(x,y) + \mathbf{E}_r(x,y)$$
$$\mathbf{H}_i(x,y) = \sum_l a_{lm}\mathbf{H}_{lm}(x,y) + \mathbf{H}_r(x,y)$$

(5.1)

for all values of x and y, where the coefficients a_{lm} are the modal amplitudes. By the orthogonality condition of fiber modes, each guided mode is orthogonal to the radiation field and all other guided modes, so we deduced from (5.1) that

$$a_{lm} = \frac{\int_{A_-} (\mathbf{E}_i \times \mathbf{H}_{lm}^*) \cdot \hat{z} dA}{\int_{A_-} (\mathbf{E}_{lm} \times \mathbf{H}_{lm}^*) \cdot \hat{z} dA}$$

(5.2)

For a weakly guiding fiber , the transverse field is described by a normalized scalar mode, and expression (5.2) become

$$a_{lm} = \int_{A_-} \hat{\psi}_i \hat{\psi}_{lm} dA$$

(5.3)

where $\hat{\psi}_i$ and $\hat{\psi}_{lm}$ are the normalized scalar modes of the single mode fiber and two-mode fiber, respectively. The power P_{lm} propagating in each mode is

$$P_{lm} = |a_{lm}|^2$$

(5.4)

Usually, one is only interested in the P_{lm} power guided by the desired mode relative to the power P_i transmitted by the incident fiber, i.e. the launching efficiency ζ defined by

$$\varsigma = \frac{P_{lm}}{P_i}$$

(5.5)

Fig. 5.1 shows the launching efficiency of the LP_{01} and LP_{11} modes versus the transverse offset distance, and Fig. 5.2 shows the power ratio in the two-mode fiber versus the offset distance. The fibers used for the calculation were Flexcor™ for the single mode fiber, and SMF28™ for the two-mode fiber, operating with a light source of 0.9754 μm. The fiber parameters used in the calculation are listed in Table. 5.1.
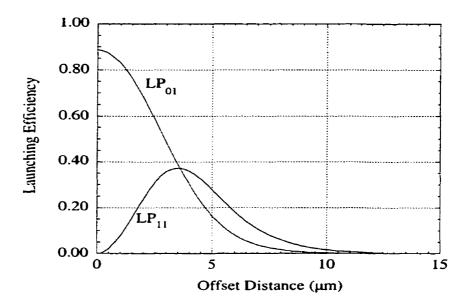
Figure 5.1 Launching efficiency of the LP_{01} and LP_{11} mode in two-mode fiber versus the transverse offset distance.

	ρ_{co} (μm)	ρ_{cl} (μm)	n_{co}	n_{cl}	Δn	V	N.A
SMF28™	4.5	62.5	1.45569	1.45113	0.0045	3.3	0.11437
Flexco™	1.7	62.5	1.45779	1.45113	0.0066	1.5	0.1385

Table 5.1 The parameters of the fibers to be connected at 0.9754 μm.
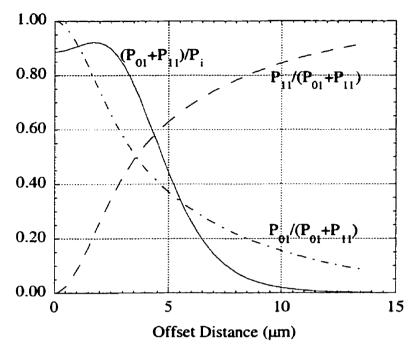
Figure 5.2 The power ratio in a two-mode fiber versus the transverse offset distance. The parameters used in the calculation are in Table. 5.1.

From Fig. 5.1, we found that there is an optimum offset distance for launching the LP_{11} mode. From Fig. 5.2, we found that the power ratio of the LP_{11} mode increased when the offset distance increase. At an offset of 3.6 μm the LP_{01} and LP_{11} mode have the same power. However, at an offset of 3.51 μm where the launched power has a maximum, the power ratios of the LP_{01} and LP_{11} modes are 51% and 49% respectively. It must be noted that although the power ratio of the LP_{11} mode increases when the offset increases, the total guided mode power decrease rapidly. So, to obtain sufficient light power, the offset should be less than 5 μm.

We have measured the total guided mode power and the LP_{01} mode power for various offset with a LP_{11} mode stripper. At the offset that produces the maximum LP_{11} mode

power, the power ratio of the LP_{01} and LP_{11} mode is 50.4% and 49.6% respectively, in excellent agreement with the calculation.

5.3 LP_{11} Mode Stripper

Mode strippers are devices that ideally transmit one particular fiber mode without losses and in which all other modes are suppressed. One kind of LP_{11} mode stripper consists of a biconical fiber taper [124]. At the taper waist, the fiber must be single mode. The biconical taper is immersed in index-matching liquid to eliminate cladding modes. The LP_{11} mode can also be removed from the fiber by etching down part of the cladding and surrounding the fiber with an external higher index medium [125]. Due to their larger transverse field extent, LP_{11} modes are attenuated by power leakage whereas the attenuation of the fundamental mode remains negligibly small.

A simple LP_{11} mode stripper consists of a fiber coil with several turns and a small radius of curvature [126]. Since the bend loss of the LP_{11} mode is much larger than that of the LP_{01} mode, the LP_{11} mode can be effectively removed by the fiber coil. The remainder of this section is devoted to calculating the bend losses of the LP_{01} and LP_{11} modes and to choosing the proper coil radius to strip the LP_{11} mode from two-mode fibers.

It is well known that bends modify the guiding properties of optical fiber and cause loss especially toward long wavelengths. Conventional theories [127, 128] assume a simplified model of fiber with an infinitely extended cladding and, consequently, predict a monotonous increase of the loss with wavelength or curvature. In recent years, it has been shown experimentally that the finite dimensions of the cladding and the presence of the coating can significantly affect the loss behavior. Oscillations of the loss versus both wavelength and bend radius were observed. The bend loss modulation can be attributed to

coherent coupling between the core-propagating field and the fraction of radiated field reflected by the cladding coating interfaced [129].

A bend loss formula that takes into account loss modulation was originally obtained [130] by modeling the bent fiber as five-layer slab waveguide. Different models have been proposed for the evaluation of the peak position of bend loss [131] and shape [132, 133]. Among them, the model of Renner leads to a simple bend loss formula that is based on a plane approximation of the curved cladding-coating interface of an equivalent step-index fiber. In some cases the Renner's method fits experimentally observed data well. Faustini and Martini [134] developed a more general and more complicated integral formula valid for a wider range of both wavelength and bend radius. Their derivation is based on the hypothesis of a weak perturbation of the propagating field and a plane cladding-coating boundary. For the restricted range of bend radius and fixed wavelength situation, Renner's formula is valid, so it will be used to estimate the bend losses.

The bend loss of a coated fiber is

$$\alpha_{BL} = \alpha_B \frac{2(Z_2 Z_3)^{1/2}}{(Z_3 + Z_2) - (Z_3 - Z_2)\cos(2\Theta)} \tag{5.6}$$

where α_B is the conventional bend loss for which an expression was given by Macuse [127],

$$\alpha_B = \frac{1}{e_v} \frac{1}{2} \sqrt{\frac{\pi}{\rho_\infty R}} \left(\frac{U}{V}\right)^2 \frac{1}{W^{3/2}} \frac{\exp\left[-\frac{2}{3}\left(\frac{W}{\rho_\infty}\right)^3 \frac{R_b}{\beta^2}\right]}{K_{l-1}(W)K_{l+1}(W)} \tag{5.7}$$

$$e_v = \begin{cases} 2 & l = 0 \\ 1 & l \neq 0 \end{cases}$$

where ρ_{co} and ρ_{cl} are the core and cladding radius respectively, $K_l(W)$ is the modified Bessel function, while U, V and W are the usual normalized parameters given by

$$V^2 = U^2 + W^2$$
$$U^2 = \rho_{co}^{2}(k^2 n_{co}^{2} - \beta^2) \tag{5.8}$$
$$W^2 = \rho_{co}^{2}(\beta^2 - k^2 n_{cl}^{2})$$

with $k=2\pi/\lambda$. Here λ is the wavelength, n_{co}, and n_{cl} are the core and cladding indices, and β is the axial propagation constant of a straight fiber. R_b denotes the effective bend radius, which differs from the actual bend radius R_{exp} by a material-dependent elastooptical correction factor [135]. Other parameters in Eq. (5.6) are listed as follows.

$$Z_2 = k^2 n_{cl}^{2}(1 + \frac{2\rho_{cl}}{R_b}) - \beta^2$$
$$Z_3 = k^2 n_{coat}^{2}(1 + \frac{2\rho_{cl}}{R_b}) - \beta^2 \tag{5.9}$$
$$\Theta = \frac{\gamma^3 R_b}{3k^2 n_{cl}^{2}}\left(\frac{R_o}{R_b} - 1\right)$$

where n_{coat} is the coating index and

$$R_o = \frac{2k^2 n_{cl}^{2}\rho_{cl}}{\gamma^2}$$
$$\gamma = (\beta^2 - k^2 n_{cl}^{2})^{1/2} \tag{5.10}$$

R_o is the critical bend radius. When R_b is larger than R_o, the oscillation in the bend loss curve disappears. We used SMF28™ fiber from Corning, the parameters for it are listed in Table. 5.1. The refractive index difference between cladding and acrylate coating is about 0.1. The cutoff wavelength for the LP_{11} mode is 1.35 μm. The bend loss spectrum for a bend radius of 10 mm is shown in Fig. 5.3. One can see that a slight increase in wavelength can increase the bend loss dramatically, and the bend loss of the LP_{11} mode is higher than that of the LP_{01} mode by many orders of magnitude. The bend loss as a

function of bend radius was also calculated for the case λ=0.9754 μm and the results are shown in Fig. 5.4. One can see that a slight decrease in bend radius can also increase the bend loss dramatically, and again the bend loss of the LP_{11} mode is higher than that of the LP_{01} mode by many orders of magnitude.
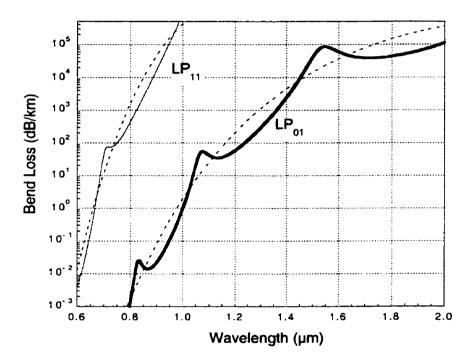
Figure 5.3   Bend loss of the LP_{01} and LP_{11} modes of SMF28™ versus bend wavelength for a bend radius of 10 mm. The dashed line is the conventional theory of Eq.(5.7), and the solid lines are Renner's formula of Eq. (5.6)
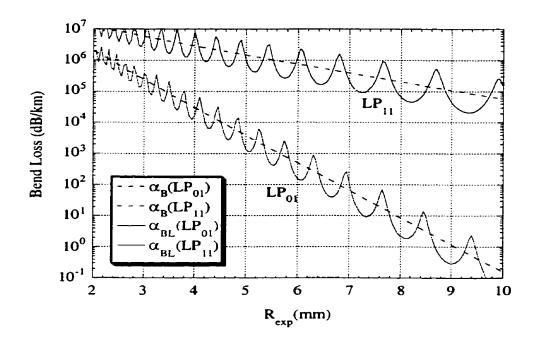
Figure 5.4   Bend loss of the LP_{01} and LP_{11} modes of SMF28™ versus bend radius for wavelength of 0.9754 μm. The dashed line is the conventional theory, and same legend as Fig. 5.3.

We may expect the power in the bent fiber to decay exponentially as

$$P(z) = P(0)\exp(-\alpha_{BL}z) \tag{5.11}$$

where $P(z)$ is the detected power, $P(0)$ is the power entering the bent fiber, and z is the light propagation length. If a fiber is wrapped around cylinder with a radius of R_{exp}, the expression of (5.11) can be rewritten as

$$P(z) = P(0)\exp(-2\alpha_{BL}\pi R_{exp}N) \tag{5.12}$$

where N is the number of turns around the cylinder. In practice, our concern is how many turns of the fiber loop can strip the mode power, so from the (5.12) we have

$$N = -\frac{1}{2\pi\alpha_{BL}R_{exp}}\ln\left(\frac{P(z)}{P(0)}\right) \tag{5.13}$$

We consider a mode stripper when its power decays to 1%, i.e., $P(z)/P(0)=0.01$. By this definition, the number of turns with a bend radius of 10 mm to remove the LP_{01} and LP_{11} modes versus the wavelength are shown in Fig. 5.5. We can see that for the bend radius of 10 mm, one turn of the fiber loop will strip out the LP_{11} mode when the light wavelength is longer than 0.938 μm and the LP_{01} mode when the wavelength is longer than 1.525 μm by Renner's formula. The number of turns to remove the LP_{01} mode of SMF28™ at a wavelength 1.55 μm and 1.30 μm was measured. The results show that the numbers of turn are 7 for 1.55 μm and 51 for 1.30 μm. The calculated results show that the number of turn is 3 for 1.55 μm and 65 for 1.30 μm by the conventional theory. However, the calculated results by the Renner formula are 1 turn for 1.55 μm and 252 turns for 1.30 μm. The experiment results shown that the conventional theory seems more suitable for estimating the actual number of turns.
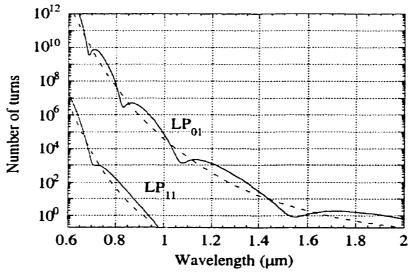
Figure 5.5 Number of turns at a bend radius of 10 mm for stripping out a mode versus wavelength. Same legend as Fig. 5.3.
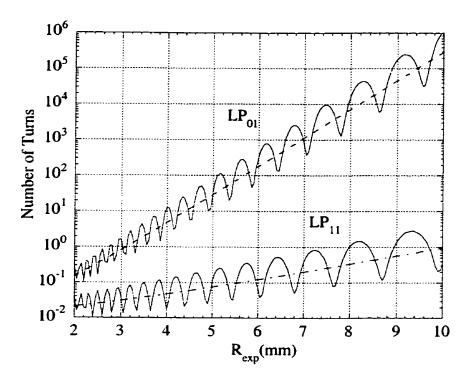
Figure 5.6 Number of turns at wavelength of 0.9754 μm for stripping out
a mode versus bend radius. Same legend as Fig. 5.3.

Fig. 5.6 shows that the number of turns at wavelength of 0.9754 μm to remove a mode versus bend radius. For a bend radius of 60 mm, to remove the LP_{01} and LP_{11} modes. One needs 182 and 1 turn respectively. While for a bend radius of 50 mm, to remove the LP_{01} and LP_{11} mode needs 30 and 1 turn respectively. In practice, the mode stripper was made of 10~15 turn loops at bend radius of 6 mm to remove the LP_{11} mode but not enough to cause the LP_{01} mode loss.

For bend loss calculation, R_b denotes the "effective" bend radius, which differs from the actual (experimental) bend radius R_{exp} by a material-dependent elastooptical correction factor. From Sharma et. al. [135], the correction factor is $R_b = f_R R_{exp}$, f_R depends on the

light source wavelength and the properties of the glass. They presented an empirical curve and lead to linear fitting expression.

$$f_R = 0.4\lambda + 0.69 \qquad (5.14)$$

where λ is in micrometers. For λ =0.9754 µm, the radius correction factor is *1.08*. In our set up, for SMF28™ and a operating wavelength of 0.9754 µm, the mode stripper was made of 10 turn loops with a radius of 6 to 8 mm.

5.4 Definition

In order to well describe the coupler, it is necessary to define some standard variables that can characterize the coupler. In Chapter 1, we gave the transmitted power expressions for an ideal lossless coupler, but in reality a power loss is inevitable. There are several reasons that cause the power loss. If the coupler is not adiabatic, the power of the guided modes will couple into higher order modes. Other reasons include dimensional imperfections of the fiber and a non-axial deformation of the coupler. Generally, the transmitted power at the output end of coupler can be written as

$$P_1 = (1 - \Gamma)\left[\xi\cos^2\frac{\alpha_i^x - \alpha_j^x}{2} + (1-\xi)\cos^2\frac{\alpha_i^y - \alpha_j^y}{2}\right]P_1(0)$$

$$P_2 = (1 - \Gamma)\left[\xi\sin^2\frac{\alpha_i^x - \alpha_j^x}{2} + (1-\xi)\sin^2\frac{\alpha_i^y - \alpha_j^y}{2}\right]P_1(0)$$

$$(5.15)$$

where the coefficient Γ represents the power loss, $P_1(0)$ is the power entering branch 1, P_1 and P_2 are the powers at the output. ξ is the polarization ratio in two perpendicular directions. From this expression, some definitions can be given.

Transmission:

$$T_1 = \frac{P_1}{P_1(0)}$$

$$T_2 = \frac{P_2}{P_1(0)}$$

$$(5.16)$$

Insertion loss:

$$\bar{T}_1 = 10\log(\frac{P_1}{P_1(0)})$$

$$\bar{T}_2 = 10\log(\frac{P_2}{P_1(0)})$$

(5.17)

Excess loss:

$$\bar{\gamma} = -10\log(1-\Gamma)$$

(5.18)

Coupling ratio:

$$P_{c1} = \frac{P_1}{(P_1+P_2)}$$

$$P_{c2} = \frac{P_2}{(P_1+P_2)}$$

(5.19)

Power transfer efficiency of LP$_{11}$ mode:

$$\eta = \frac{P_2^{11}}{P_1^{11}(0)}$$

(5.20)

where $P_1^{11}(0)$ denotes the LP$_{11}$ mode power at the entrance end, and P_2^{11} stands for the LP$_{11}$ mode power from branch 2 at output end.

Directivity:

$$\bar{D}_1 = -10\log(\frac{P_{R1}}{P_1(0)})$$

$$\bar{D}_2 = -10\log(\frac{P_{R2}}{P_1(0)})$$

(5.21)

The directivity is given in dB by the reflective power P_{R1} in branch 1 and P_{R2} in branch 2.

Isolation:

For a given wavelength λ_j, the isolation $I_1(\lambda_j)$ or $I_2(\lambda_j)$ are given by the insertion loss at this wavelength. Usually, the isolation is in decibels.

$$\bar{I}_1(\lambda) = \bar{T}_1$$

$$\bar{I}_2(\lambda) = \bar{T}_2$$

(5.22)

The isolation at a wavelength λ between branch 1 and 2 is given by

$$\bar{I}(\lambda) = \left| \bar{I}_1(\lambda) - \bar{I}_2(\lambda) \right| \tag{5.23}$$

When the loss is very small, $P_1(0) \cong P_1 + P_2$, one often uses the coupling ratio to replace the transmission.

5.5   Confirmation of LP_{11} Mode Transfer

So far, there have not been any reports about pure LP_{11} mode transfer in fusion and tapering couplers. Thus, the first step of this work was to confirm the LP_{11} mode transfer. The experimental set up for this step shown schematically in Fig. 5.7 was done according to the simulation of Chapter 3 and the preparation in section 5.2 and 5.3.

Figure 5.7   The experimental set up used to fabricate mode separating couplers. SMF, single mode fiber; S, light source; TMF, two-mode fiber; D1, D2, power detector.

The light source wavelength was 0.9754 μm and the source was pigtailed with a fiber(SMF28™) that is a two-mode fiber at that wavelength. The two-mode fiber connected directly with the light source was spliced to a single mode Flexcor™ fiber (parameters are listed in Table. 5.1). The core centers were aligned, so that only the LP_{01} mode is excited with minimum loss into the single mode fiber. Then, this single mode

fiber was spliced to a two-mode fiber(SMF28™) with a slight offset. The power ratio of the LP_{11} and LP_{01} modes was controlled by the offset distance. The power transmission was detected by a HP 81532A power sensor. The LP_{11} mode stripper (MS) consisted of a small fiber loop with a diameter of 1.6 cm, whose function was to strip out the power of the LP_{11} mode and to allow only the power of the LP_{01} mode be detected. In order to confirm LP_{11} mode transfer, we arranged three different ways to detect the output transmission. Their results are shown in Fig. 5.8 (a), (b) , Fig. 5.9 (a), (b) and Fig. 5.10 (a), (b). From Fig. 5.8, we find that the transmission of a two-mode fiber coupler is different from that of single mode fiber couplers. There are two small peaks before the usual oscillation in the transmission curve. This may be caused by LP_{11} mode transfer. In Fig. 5.9, we used a mode stripper to remove the LP_{11} mode power, so that only the power of LP_{01} was detected in branch 1. The experimental results show that the power of the LP_{01} mode did not change much when the elongation was less than 17 mm, while the two small peaks are still visible in the secondary branch. Thus, the two small peaks appear to be caused by power transfer of two orientations of the LP_{11} modes. This conclusion is reinforced by another experiment, depicted in Fig. 5.10. Two mode strippers were used in both branches simultaneously and only the power of LP_{01} mode was measured in both branches. The results show that the two small peaks disappear and the transmission curves are nearly identical to those of a conventional single mode fiber coupler. Thus, we can conclude that the two peaks in the transmission curves are caused by pure LP_{11} mode transfer. In subsequent fabrication of two-mode fiber couplers, mode strippers were no longer needed to evaluate the power transfer of the LP_{11} modes. Besides, having checked the far field of both branches at the second peak position, we found that in branch 1 the field distribution corresponds to an LP_{01} mode pattern, and in branch 2, to an LP_{11} mode pattern. Another way to check the output field is to turn branch

1 and branch 2 into a 1.6 cm diameter loop before detecting their respective powers. We found that the power in branch 2 becomes zero after 2 turns; whereas the power of branch 1 only reduces 4% after 30 turns. This verified that the power in branch 2 belonged to the LP_{11} modes and the power in branch 1 was in the LP_{01} mode.

(a)

(b)
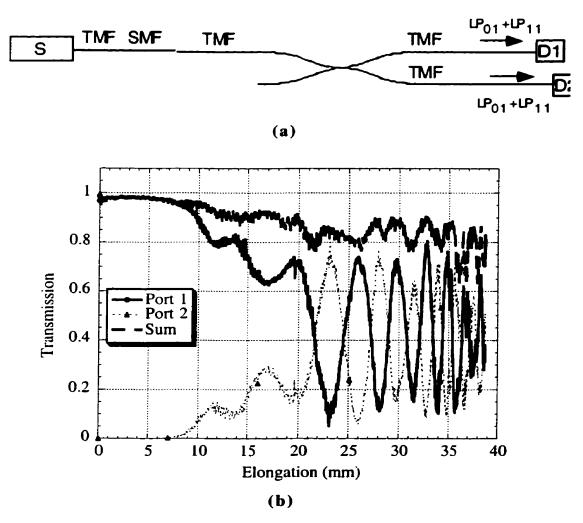
Figure 5.8 (a) The setup to measure the transmission without the mode stripper. (b) The experimental results with fusion time of 830 seconds, sweep distance of 11.0 mm and flame width of 4 mm.

(a)

(b)
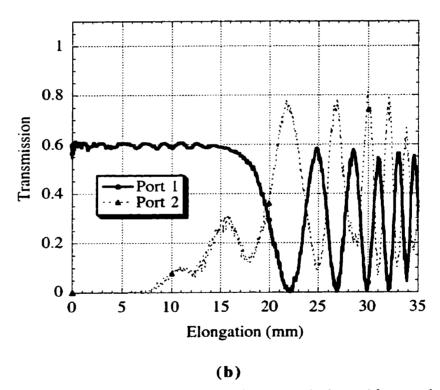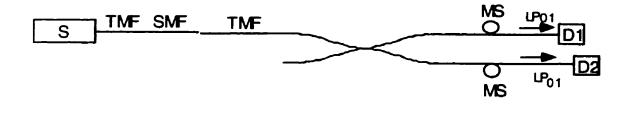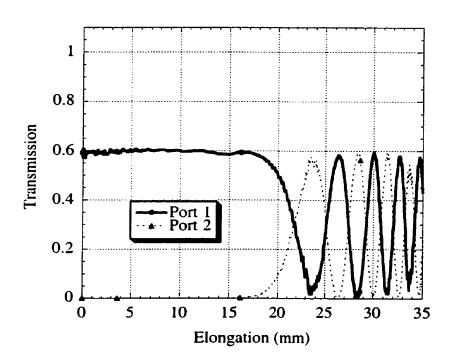
Figure 5.9 (a) The set-up to measure the transmission with a mode striper in branch 1. (b) The experimental results.

(a)

(b)

Figure 5.10 (a) The setup to measure the transmission with a mode stripper in each branch. (b) The experimental results.

5.6   Fabrication of Mode separating couplers

In the previous section, we observed the pure power transfer of the LP_{11} mode. Now the question becomes how to fabricate a coupler that is able to transfer all the power of the LP_{11} modes from branch 1 to branch 2, while all the power of LP_{01} mode still stays in branch 1.

First, it is necessary to present the coupler fabrication process. That includes fiber coating removal, fiber setting, fusion, elongation, coupling-ratio adjustment, and packaging. The power transfer between two fibers is caused by the decrease of the distance between the cores and the decreases of the diameters of the cores and the claddings. So, the fabrication parameters of the processes of (a) fusion, (b) elongation, and (c) coupling ratio adjustment are extremely important in determining the fiber coupler characteristics such as excess loss and coupling ratios. Steps (a-c) were automated.

The fiber coating can be removed by thermal or chemical etching method. In particular, coating materials such as acrylate, hytrol, PVC, and nenon can be etched by acetone, methanol, and chloroform. An other way to remove the fiber coating is the mechanical method with a fiber stripper. The latter is simple and fast, but it often causes micro-flaws in the bare fiber section. After removing the fiber coating, it is always necessary to further clean the bare fiber by wiping paper dampened with acetone, methanol or alcohol over the stripped area.

"Fiber setting" means that the fibers are properly placed on the fiber-hold stages. Two fibers were placed parallel on the stages and clamped so that the tension applied to the two fibers was the same. Then, alignment clamps were used to hold the fibers in contact on a horizontal plane, which was checked by a microscope.

After setting the normalization of the detector and system to record the transmission curve, the fusion process was started. The fiber fusion was realized by the narrow flame of a micro torch that was placed close to the fibers and to heat them. It is also possible to use a CO_2 laser or a microheater. To avoid too much deformation of the fibers, this flame is swept along parallel to the fibers. The sweep distance was determined by forming a smooth transition region from unfused to fused regions. The fusion degree was measured by the image of the fusion region on the monitor screen relayed by a microscope.
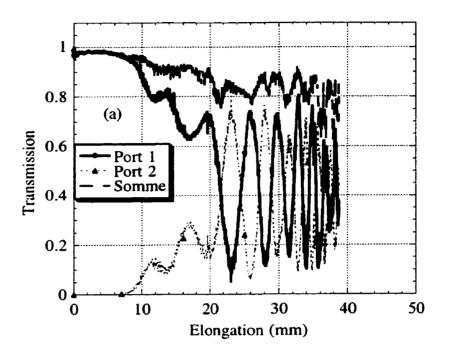
For the elongation process, it is important to utilize a wide flame to ensure that a coupler is finished with an adiabatic tapering region. The wide flame is obtained by using a large size of micro torch or a small size micro torch sweeping rapidly around the elongation points. The elongation speed was determined by the degree of fiber softening. The elongation process was finished when the coupling ratio was observed close to the vicinity of the prescribed coupling ratio. For the adjustment process, the fibers were heated weakly and elongated slightly with small steps until the target value of the elongation was obtained.
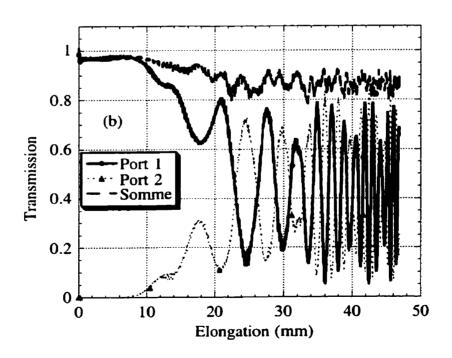
The final process was the packaging; a piece of quartz substrate was placed under the coupler while it was still held by the elongation stage. Then, the coupler was aligned in the middle of the substrate. Two drops of epoxy was placed outside of the coupler tapering region to glue the coupler onto the substrate, which served to fix the coupler form. The other two drops of epoxy covered the ends of the fiber jacket which served to release the strain caused by an external force and to avoid breaking the bare fiber section. When the epoxy was cured and the coupler was solidly fixed on the substrate, the coupler was removed from the elongation stage and inserted into a Kovar or Invar tube called enclosure. Finally, both ends of the metal tube were sealed by silicone which also
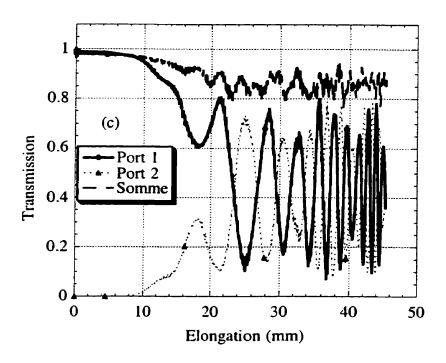
provides some strain relief for the fiber. The thermal expansion coefficient of Kovar (about 5 ppm/°C) or Invar (about 2 ppm/°C) is the smallest among metals and is a close to the quartz substrate. This avoids excessive insertion loss, coupling ratio shift and breakage of the coupler caused by thermal expansion strain. This packaging technique provided good stability and reliability. By properly attaching the fiber to the quartz substrate, the differential thermal expansion between the fiber and the substrate is minimized, producing good thermal stability during temperature cycling. The epoxy used here had the characteristics such as small thermal expansion coefficient, fast cure time and strong bonding force. The enclosure and booting material further aids the resistance to hot, humid environments. As a commercial product, the product packages should pass the Bellcore test criteria such as GR-1221-CORE, that include specific mechanic tests such as vibration, impact and fiber retention and so on. With long-term exposure to humidity, epoxies tend to soften and swell and the bond between fiber and substrate is weakened. This rarely leads to catastrophic failure, but the resulting variations in insertion loss may exceed the performance specification of the splitter. Recently, it has been reported that Gould Inc developed a new technique to attach the fibers on the substrate using a kind of glass solder powder and that is melted by a CO_2 laser. The test results have demonstrated that this new technique is better than that of epoxies.
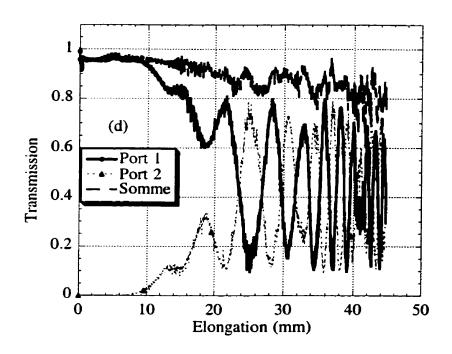
5.7 Experimental Results

Several samples were made using the fabrication processes described in previous sections. The characteristics of a mode separating coupler that concerns us are the LP_{11} mode transfer efficiency and the excess loss, which are affected by many factors, including the flame sweep distances and the fusion time.

(a)

(b)

(c)

(d)
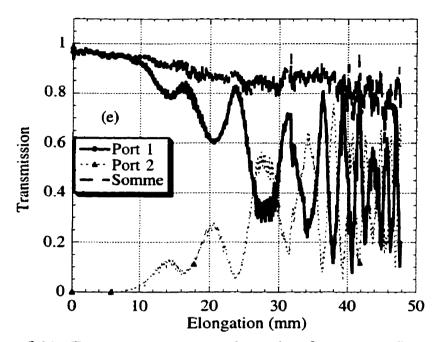
Figure 5.11 Transmission versus elongation for various flame sweep distances. (a) 11.0 mm. (b) 12.0 mm. (c) 12.3 mm. (d) 12.5 mm. (e) 13.0 mm.

		(a)	(b)	(c)	(d)	(e)
Initial Power (μW)	in branch 1	19.79	19.28	20.90	19.49	19.69
	in branch 2	21.10	19.16	20.67	18.63	19.20
Elongation value corresponding to second peak (mm)		17.10	17.67	18.23	18.80	20.58
Transmission at above elongation	in branch 1	62.87%	62.56%	61.46%	61.00%	60.52%
	in branch 2	29.57%	31.51%	33.44%	32.50%	27.98%
Total transmission		92.57%	94.17%	95.00%	94.50%	88.41%
Excess loss (dB)		0.34	0.26	0.22	0.25	0.53
LP_{11} mode power ratio in launched branch		40.0%	40.0%	40.0%	40.0%	40.0%
Sweep distance (mm)		11.00	12.00	12.30	12.50	13.00
LP_{11} mode transfer efficiency		73.9%	78.8%	83.6%	81.3%	70.0%

Table 5.2 The measured values of the characteristics of five short couplers.

5.7.1 The Influence of Flame Sweep Distances

In order to study the effect of the flame sweep distance on the transmission, five mode separating couplers were made by using the setup shown in Fig. 5.7 with the same fusion time of 850 seconds, and the same launching conditions (launching power ratios in branch 1 were 60.0% of the LP_{01} and 40.0% of LP_{11} modes), and various flame sweep distances. Fig. 5.11 (a), (b), (c), (d), and (e), shows the coupler transmissions corresponding to various flame sweep distances, and Table 5.3 gives the detailed measurement values for these five couplers.

From Fig. 5.11 we can see that all transmission curves in branch 2 have two small peaks that correspond to the LP_{11} mode power transfer. The first peak is a single orientation of the LP_{11} component power transfer and the second peak is the combination of both orientations of the LP_{11} mode. We are interested in the second peak; if both orientations of LP_{11} mode are synchronous, the peak value will be a maximum. The transfer efficiency of the LP_{11} mode is defined as the ratio between the power of the LP_{11} mode obtained in branch 2 and that launched in branch 1. From Table. 5.2, one finds the following:

(i) The elongation value corresponding to the second peak increases with the sweep distance. It is due to the coupler longitudinal profile that is determined by the flame sweep distance. For the same elongation, the ITR of the coupler waist for long flame sweep distance is larger than that for short flame sweep distance. This will cause the effective index difference between supermodes to have smaller values for a longer sweep distance. Consequently, to obtain the same accumulated phase difference, the supermodes need to propagate a longer distance, so that the elongation value is relatively longer.

(ii) There is an optimum sweep distance to obtain the maximum power transfer efficiency of the LP_{11} mode. The coupler with a sweep distance of 12.30 mm has the maximum transfer efficiency of the LP_{11} mode among the above five couplers. Its value reaches 83.6%.

(iii) All five couplers were not adiabatic. Although we carefully prepared the fibers during the coupler fabrication process, the excess losses were still about 0.2-0.5 dB. These losses are caused by the non-adiabatic tapering. To avoid this kind of loss, one should increase the sweep distance, this is discussed later in Section 5.7.3.
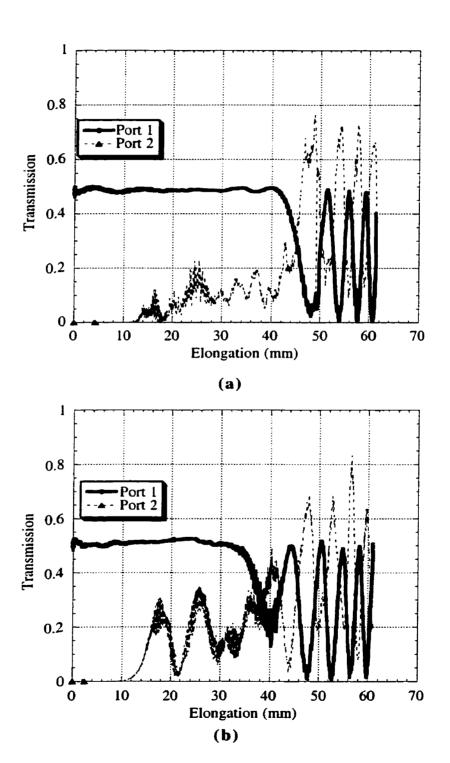
Another thing that needs to be mentioned is that each coupler had different small peak values. This demonstrates that both orientations of the LP_{11} mode have different ratios. The LP_{11} mode launched by the offset connection was prevalent in one orientation of the LP_{11} mode. However, during the propagation process, the other orientation was excited by a fiber twist or bend; this excitation is difficult to control. Fortunately, if both orientations of the LP_{11} mode are synchronous at the second peak, the different ratios of both orientations of the LP_{11} modes will not affect the result.

5.7.2 The Influence of the Fusion Time

In the previous section, we saw that the flame sweep distance influences the coupler transmission. Essentially, the different flame sweep distances determine the coupler longitudinal profile. During the coupler fabrication process, there is another factor, the fusion time, which also influences the coupler longitudinal profile. Fig. 5.12 shows the transmission as a function of the elongation for various fusion times. For clarity, an LP_{11} mode stripper was used in branch 1 to demonstrate that only the LP_{11} mode power was transferred. Except for the fusion time, all the couplers were fabricated under the same

conditions, with a flame sweep distance of 20 mm, and power ratio of 49.6% for the LP_{11} modes and 50.4% for the LP_{01} modes in the launching branch.

From Fig. 5.12. (a), (b), and (c), one finds the following results: (i) When the fusion time is 500 seconds, corresponding to a fusion small degree, the power transfer of the LP_{11} mode is weak. When the fusion time is 1000 seconds, the power transfer of the LP_{11} mode obviously increases. Nevertheless, when the fusion time is longer, e.g., 2000 seconds, the power transfer does not change significantly. Actually, the effect of a long fusion time is to reduce the refractive index difference between the fiber core and the cladding by dopant diffusion and cause the diameter of the fiber core to expand and change its shape. This phenomenon can be explained by the coupled mode theory. For the case of a short fusion time, the fusion degree is small and the distance between the two fiber cores is large; consequently, the field overlap of the LP_{11} modes between two individual fibers is very small, so, the power transfer is weak. With the increase of fusion time, the fiber core expands and more mode fields between the individual fibers overlap each other. The result is much more power transfer of the LP_{11} mode. However, when all the mode fields cover each other, the transfer power of LP_{11} mode no longer increases even if the fusion time increases. This is the case of 2000 seconds fusion time. (ii) The power transfer of the LP_{01} mode behaves as usual when the fusion time is short. However the power transfer of the LP_{01} mode is not complete when the fusion time is longer. This is due to the asymmetry of the coupler structure caused by narrow flame heating from one side. (iii) With the increase of fusion time, the elongation values (corresponding to the point at which the LP_{01} mode begins to transfer) become shorter, but these elongation values are still longer than those of the LP_{11} mode even if the fusion time is 2000 seconds. Therefore, the coupler asymmetric structure does not significantly affect the power transfer of the LP_{11} mode.

(a)

(b)
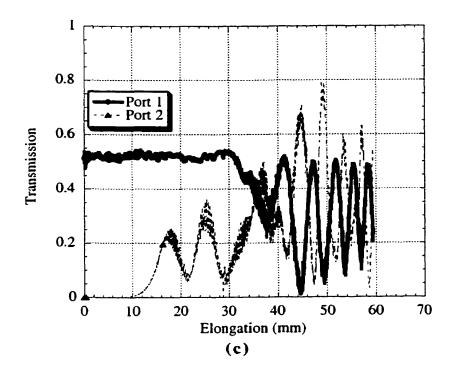
Figure 5.12 Transmission versus elongation for various fusion times. (a) 500 seconds. (b) 1000 seconds.(c) 2000 seconds.

The longer the fusion time is, the more the LP_{11} mode power is transferred, but very long fusion times cause another problem. The transmission versus fabrication time defined as the time between the beginning of the fusion process to the end of the elongation the process are shown in Fig. 5.13. The fibers were first fused for 3300 seconds and then were drawn by a pair of translation motors. It was observed that the transmission power suddenly dropped when the elongation process was started. The reason for this phenomenon is unclear, perhaps the mechanical properties of the fiber were changed after heating for such long time. Therefore, the proper fusion time is a factor one should consider in the coupler fabrication process.

In summary, the influence of fusion time on the transmission can be classified into two cases. When the fusion time is not long, its influence on the transmission can be described by the fusion degree. In general, the fusion time should be long enough to ensure the fibers reach a fusion degree of 1. When the fusion time is relatively long, although the fusion degree is already equal to 1, the fibers are still subject to heat, and so the effect of the fusion time on the transmission is then described by fiber core diameter, core shape and the refractive index difference between core and cladding. These changes can be measured by the refracted near-field method that will be described in Section 5.8.1.
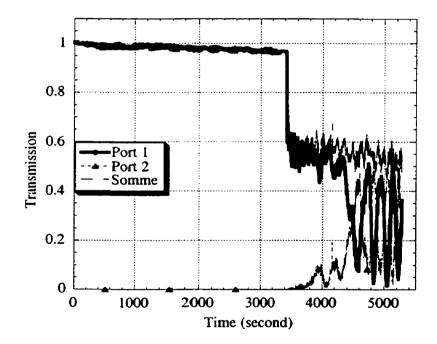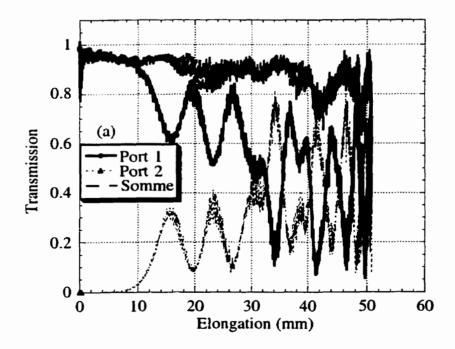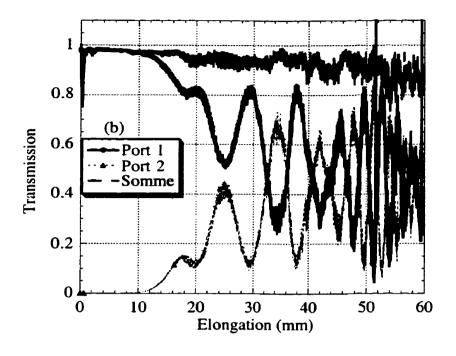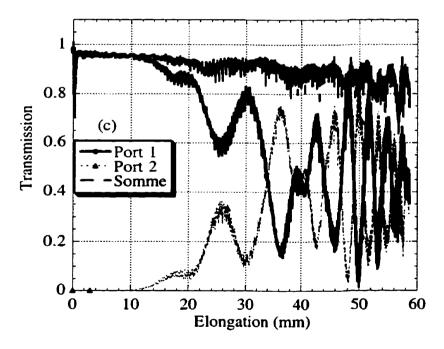
Figure 5.13 Transmission versus fabrication process time for a fusion time of 3300 seconds and a flame sweep distance of 20 mm.

5.7.3 Quasi Adiabatic Couplers

In section 5.6.1, the total transmission of all couplers decreased significantly with the increase of the elongation, meaning that the couplers were not adiabatic. As is well known, a small slope of tapering is the criterion to realize adiabatic couplers. In section 3.2.2, the simulation results showed that a longer flame sweep distance can reduce the taper slope. So, to obtain an adiabatic coupler, it is better to use a long flame sweep distance. However, as already discussed in section 5.6.2, longer fusion times favor the power transfer of the LP_{11} modes. Thus, we increased the flame sweep distance and fusion time to fabricate couplers which new parameters that should fit the mode separating conditions. The experimental results are shown in Fig. 5.14 and the details are given in Table 5.3.

(b)

Port 1
Port 2
− −Somme

Transmission

Elongation (mm)

(c)

Port 1
Port 2
− −Somme

Transmission

Elongation (mm)
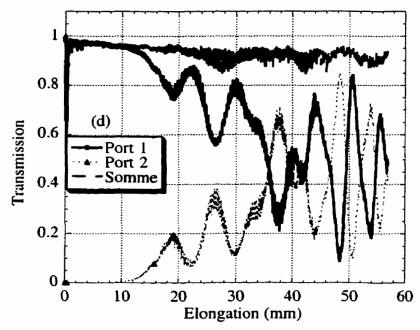
Figure 5.14 Transmission versus elongation for the following flame sweep distances and fusion time (a) 2000 seconds and 19 mm. (b) 1650 seconds and 20.0 mm. (c) 1800 seconds and 21.0 mm. (d) 2000 seconds and 22.0 mm. The details are listed in Table. 5.3.

From the experimental results, we found that there was 1-2% power loss during the fusion process that was caused by a non-uniform shape in the fused region. This kind of loss can be reduced by adjusting the fibers to be as parallel as possible, and ensure they are as clean as possible. Also, OH absorption of the fiber from the flame is another reason for the loss. Moreover, there is another 2-4% power loss during the elongation process, which is caused by shape fluctuation in the tapering region due to the gas flame instability. The excess losses of these four couplers ranged from 0.14 dB to 0.34 dB, so that this kind of coupler is almost adiabatic. Comparing the results with those in section 5.6.1 we find that the longer couplers are better than the previous ones. The power transfer efficiencies of the LP_{11} mode were around 90%, the best one reaches 92.3%.

		(a)	(b)	(c)	(d)
Initial Power(μW)	in branch 1	51.62	44.38	52.57	48.05
	in branch 2	48.33	43.00	49.27	48.86
Elongation value corresponding to the second peak (mm)		23.13	24.95	26.17	26.64
Transmission at above elongation	in branch 1	51.22%	51.05%	58.19%	56.60%
	in branch 2	41.34%	45.73%	36.19%	38.33%
Total transmission		92.56%	96.78%	94.38%	94.94%
Excess loss (dB)		0.34	0.14	0.25	0.23
LP_{11} mode power ratio in launch branch		46.3%	49.6%	39.8%	46.3%
Fusion time (second)		2000	1650	1800	2000
Sweep distance (mm)		19.00	20.00	21.00	22.00
LP_{11} mode transfer efficiency		89.3%	92.2%	90.9%	82.8%

Table 5.3 Measured values for the four long couplers of Fig. 5.14.

5.7.4 Packaging Samples

So far, there are two kinds of couplers classified by fabrication parameters. One has a relatively short flame sweep distance and fusion time. This kind of coupler is relatively easy and fast to fabricate, but the transfer efficiency of the LP_{11} mode is relative low,

about 80%. The other kind of coupler needs a relatively long flame sweep distance and a long fusion time, which leads to very restrictive requirements for fiber parallelism, tension equality and flame stability. However, this kind of coupler can reach a transfer efficiency for the LP_{11} mode of about 90%. Fig. 5.11(c) and Fig. 5.14 (b) represent these two kinds of couplers respectively. We fabricated and packaged a few couplers. The typical results are shown in Fig. 5.15 and Fig. 5.16 respectively. The epoxy used in the package was the EP30AOHT (supplied by Master Bond, Inc) which has a very good thermal stability and is cured in 20 minutes at a temperature of 300 °C.
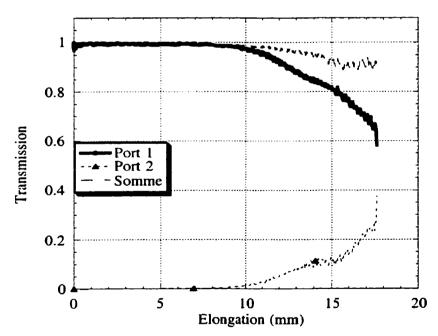
Figure 5.15 Transmissions versus elongation of a typical packaged coupler fabricated by the fusion time of 850 seconds and the flame sweep distance of 12.3 mm.
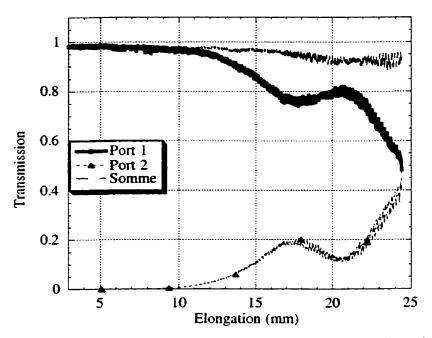
Figure 5.16 Transmission versus elongation of a typical packaged coupler fabricated by fusion time of 1650 seconds and flame sweep distance of 20.00 mm.

	Type I	Type II
Fusion time (second)	850	1650
Sweep distance (mm)	12.30	20.00
Elongation (mm)	17.62	24.40
Transmission in branch 1	58.17%	48.56%
Transmission in branch 2	37.72%	46.72%
Excess loss (dB)	0.18	0.20
Power ratio of LP_{11} modes in launching branch	46.3%	50.6%
Transfer efficiency of LP_{11} modes	81.5%	92.3%
Package length (mm)	65.0	95.0

Table 5.4 The parameters of the typical packaged samples.

5.8 Numerical Analysis

To deeply understand the experimental results, it is necessary to perform a the numerical analysis. In Chapter 3, the mode separating coupler model has already been built. Now, the question is how to obtain the practical parameters such as the expanded core radius, relative index difference after fusion, and the core shape. So, before doing the simulation, it is necessary to know the longitudinal geometrical and index profile of the fiber and coupler. These parameters can be measured by the refracted near-field refraction method.

5.8.1 The Measurement of the Parameters

The principle of operation of the refracted near-field refraction method is that the light rays entering the fiber through one end face and leaving through the core-cladding interface are dependent on the distance from the fiber core axis. The measurement set up is pictured in Fig. 5.17.
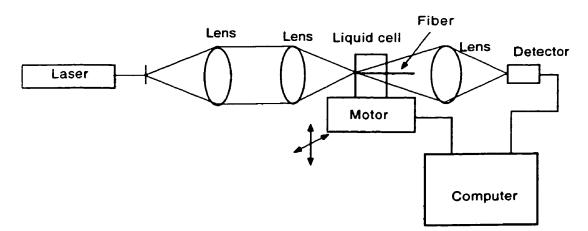
Figure 5.17 Apparatus used for the refraction near-field measurement.

A laser is used here because its coherent light can be focused to a small spot. The objective lens collimates the laser beam to provide approximately uniform illumination across the aperture of a lens that focuses the light onto the fiber end face. The fiber is mounted inside a cell filled with matching oil whose index is very slightly higher than the fiber cladding index. The cell has two windows. The entrance window consists of a microscope cover slide, because the fiber must be located very close to the focusing lens. The exit window is fitted with a hypodermic needle through which the fiber is admitted into the cell. The liquid filled cell is mounted on a stage that is moved in two dimensions via a micrometer drive by a constant speed motor controlled with a computer so that the fiber can be scanned across the laser beam. An opaque disk is centered on the output light cone. The light passing the opaque disk is focused onto a photo diode detector. In reality, the index profile is measured by detecting the refracted light from the fiber.

The reference [136] provides an expression for a square difference of the refractive indices of fiber and liquid in terms of the detected power $P_d(r)$.

$$n^2(r) - n_{cl}^2 = n_{cl}^2(\sin^2\theta_{max} - \sin^2\theta_{min})\frac{P_{cl} - P_d}{P_{cl}}$$

(5.24)

where $n(r)$ is the index profile of a fiber, r is the distance from the fiber core axis, n_{cl} is the refractive index of the fiber cladding, P_{cl} is the total power received by the detector when the laser beam is scanning the fiber cladding, θ_{max} is the maximum angle defined by the input aperture, θ_{min} is the minimum angle defined by the opaque disk in the output beam. Because the refractive index difference between the fiber cladding and the liquid is very small, the expression can be further approximated as

$$2n_{cl}(n(r) - n_{cl}) = n_{cl}^2(\sin^2\theta_{max} - \sin^2\theta_{min})\frac{P_{cl} - P_d}{P_{cl}}$$

(5.25)

Finally, we have

$$n(r) - n_{cl} = K(P_{cl} - P_d) \tag{5.26}$$

where K is constant. Therefore, the index profile is almost linear function of the detected power. The K value can be calibrated by the power P_{oil} detected when the laser beam is scanned in the liquid.

$$K = \frac{n_{cl} - n_{oil}}{P_d - P_{oil}} \tag{5.26}$$

The refractive index of a liquid n_{oil} is easy to be measured by an Abbe refracted meter, so, if the power difference between the laser beam scanning in liquid and fiber is detected, the refractive index profile will be obtained. In our experiment, the liquid in use is glycerin with a refractive index of 1.4697 for the laser wavelength 0.488 μm and the refractive index of silica is 1.4634. This method is available to measure the fiber refractive index profile of single mode or multimode and also available to make one and two dimensions measurements. Besides, since the power curve is a function of the scanning distance, if the diameter of the fiber cladding is known, the core diameter can be measured. The cladding diameter of standard fiber is 125 μm.

In section 5.6.2, we have observed that the fusion time influenced the power transfer of the LP_{11} mode. Eventually, during the fusion process, the temperature of the flame is about 1100 ^{0}C, so that the core diameter and the refractive index profile may change because of dopant diffusion. Accordingly, it is necessary to precisely know the variation of the index profile and of the core radius of the coupler after fusion and tapering. However, the measurement of the index profile and radius along the coupler longitudinal direction is very difficult. In order to evaluate the core dopant diffusion we only measured the index profile and the radius of a single fiber in the middle point of the fusion region before and after fusion using the refracted near-field method. The computer-controlled fusion process of the single fiber was the same as that of couplers shown in Fig. 5.11(c).

The results in Fig. 5.18 and Fig. 5.19 show how the index profile evolves from a step profile into a gradient profile and how the core radius extends radially. Fig. 5.20 gives the core refractive index and the variation of fiber radius with fusion time. The core refractive index is found to decrease almost linearly and the radius to increase quadratically with the fusion time by fitting the measurement values. In Fig. 5.21, the cross-section of a coupler before tapering is shown. Not only do the core dopant diffuses but their core shape also changes from circle to ellipse after fusion, which must be taken into account in the calculation of the coupler transmission.

(a)

(b)
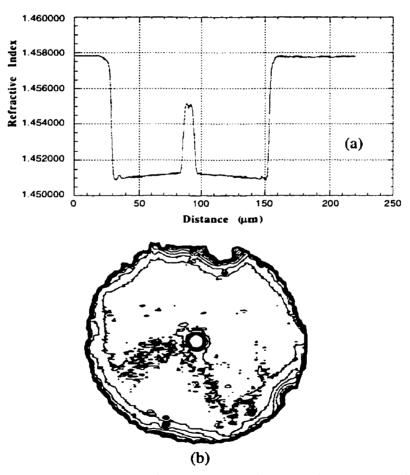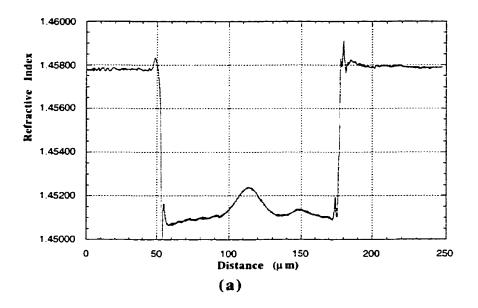
Figure 5.18 Measurements of (a) index profile and (b) cross section of a SMF28™ fiber before heating. n_{cl}=1.45112, n_{co}=1.45517, Δn=0.0041, ρ_{cl}=62.5 mm, ρ_{co}=4.5 mm, V=3.2.

(a)

(b)
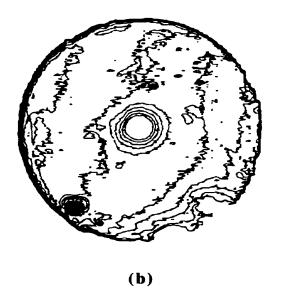
Figure 5.19 Measurements of (a) index profile and (b) cross section of a SMF28™ fiber after heating by a typical receipt of a complete fusion of a coupler. n_{cl}=1.45112, n_{co}=1.45240, Δn=0.0013, ρ_{cl}=62.5 mm, ρ_{co}=9.1 mm.
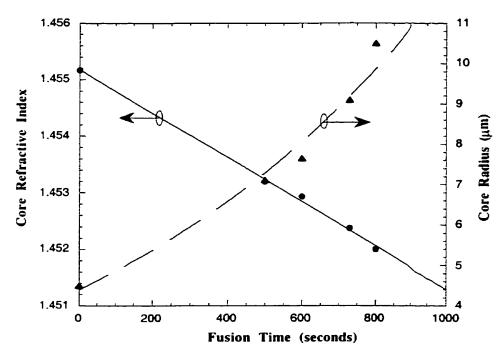
Figure 5.20 Core refractive index and core radius of the fiber as function of the fusion time.

Figure 5.21 Cross section of a fused coupler without tapering.

5.8.2 Numerical Results

The power transmission has been calculated by a numerical method based on the experimental parameters. To calculate the propagation constants of the coupler supermodes, we used the fiber mode expansion method (FMEM) that is discussed in Chapter 3. To simplify the calculation and reduce the computation time, we made four approximations. First, we assumed that the core radius is expanded uniformly after fusion, which means that the core radius has the same value along the fusion region, although the core radius in the middle region is larger than that in the two ends. Second, although the index profile along the transverse direction is nearly a Gaussian function, we still used the equivalent step profile. Third, we assumed that the index step along the longitudinal direction decreases linearly to the mid-point of the coupler. This assumption is supported by the measurement results shown in Fig. 5.20 that the step is a linear function of the heating time. During the fusion and drawing process, the heating time in the middle region is longer than that on either side, the core index thus decreases further in this region. Since the local effective indices of the supermodes are functions of the index step and cross section geometry, the longitudinal index profile will affect the supermode accumulated phase and further affect the power distribution at the output end. Finally, we neglected the effect of additional core expansion during the drawing process because the core loses its guiding role when the coupler cross section is sufficiently reduced. We used the parameters measured experimentally, such as fiber core eccentricity of 0.8, fusion degree of 1, index step between the core and cladding of 0.0013 after fusion, and the initial field includes 60% LP_{01}, 40% LP_{11}, and fitted the powers of the LP_{11} modes to 10% of $LP_{11}{}^o$ and 30% of $LP_{11}{}^e$. The effective indices of the supermodes are shown in Fig. 5.22, the transmission in Fig. 5.23, and the total normalized power in Fig. 5.24. The parameters chosen for the simulation are corresponding to the practical experimental

situation shown in Fig. 5.11(c), *i.e.*, the best result in type I mode separating coupler. In that case, the flame sweep distance is 12.30 mm, fusion time is 850 seconds, the core shape and radius, and the relative index difference shown in Fig. 5.19 and Fig. 5.21 respectively. For convenient comparison, the experimental result is shown in Fig. 5. 25. Although we used several simplifications, the essential features of the total power transmission are similar to the experimental result. According to the calculation there is still 3.0% power of LP_{11} in branch 1 at an elongation of 17.7 mm, and the transfer efficiency is 92.5%. From Figs. 5.23 and 24, we deduce that the limitation of the transfer efficiency is the separation of the two peaks of the LP_{11}^e and LP_{11}^o modes. By carefully choosing the proper flame sweep distance, flame width and fusion time, it is possible to obtain that the power of both LP_{11}^e and LP_{11}^o modes transfer into branch 2 at the same elongation value. Furthermore, the calculated amplitude of the output transmission is higher than the experimental one. This is because the calculations assume that the coupler is adiabatic when in fact this is not the case. If we etch or polish the fibers to reduce their cladding diameters before fusion, the adiabatic condition should be satisfied. In addition, the calculated power peak of the LP_{11} modes at elongation 17.70 mm (see Fig. 5.24) are somewhat different from that observed in the experiment at elongation 18.23 mm. This is probably caused by the longitudinal variation of the refractive index profile of the coupler, which is not accurately described by a linear function.

In brief, through the simulation, it is clearly shown that the two peaks that appeared in branch 2 are caused by the power transfer of both orientation LP_{11} modes and the first peak is caused by the odd LP_{11} mode. To increase the power transfer efficiency, it is very important to let the two power transfer peaks of LP_{11} modes completely overlap, which could be done by adjusting the geometrical and index profiles.
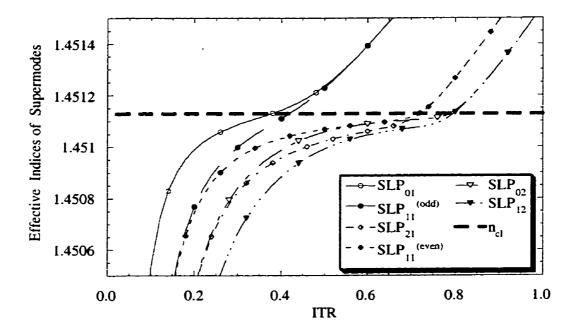
Figure 5.22 Effective index of the scalar supermodes as function of the Inverse Taper Ratio (ITR) in the fusion and tapering coupler.
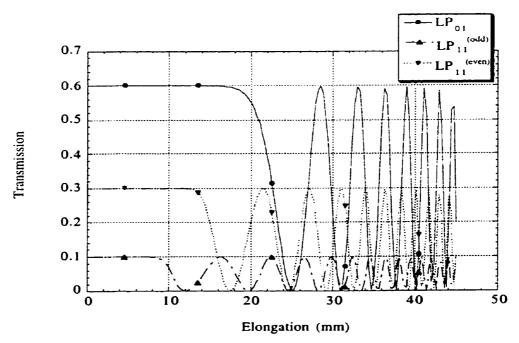
Figure 5.23 Theoretical transmission of three individual modes in one fiber branch.
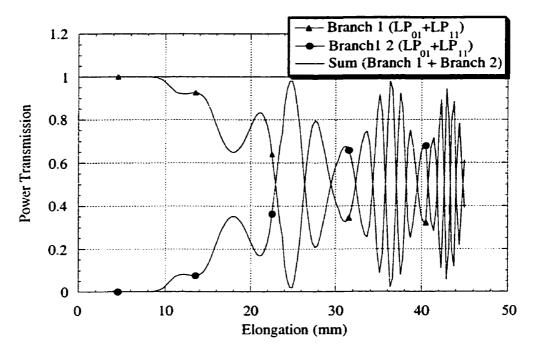
Figure 5.24 Theoretical power transmission as function of elongation in both branches of the coupler. The parameters in use are the same as that in experiment shown in Fig. 5.25.
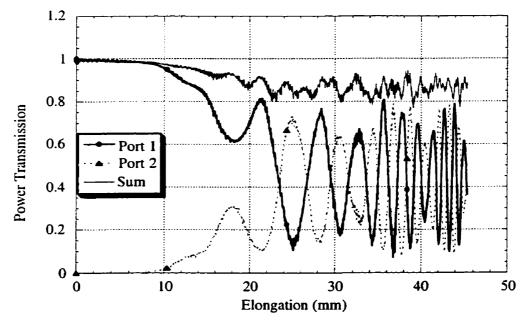
Figure 5.25 Experimental power transmission as function of elongation in both branches of the coupler.

5.9 Discussion

The mode separating couplers are first realized by the fusion and tapering method. Both types of samples have been packaged, the power transfer efficiency of LP_{11} mode reached as high as 81.5% and 92.3%, and the excess losses are as low as 0.18 dB and 0.2 dB respectively. The numerical results agree well with the experimental results, which confirms our numerical analysis and helps us understand the basis on the mode separating couplers.

The detailed studies on the influence of fusion time and flame sweep distance show that there is an optimum value for these two parameters. To increase the power transfer efficiency of LP_{11} modes, it is necessary to properly choose the parameters.

To further increase the power transfer efficiency of LP_{11} mode and decrease the excess loss, the improvement method such as prepolishing, pre-etching, high elliptical core fiber and the thermally expanded core fiber discussed in Chapter 4 might be the solution.

Conclusion

The existing MSC is an in-line device that was constructed by polishing a two-mode fiber and stacking it in a prism. This kind of MSC has some drawbacks such as high insertion loss, sensitive to the coupling length, and complicated fabrication. The existing theoretical study of MSC was for the uniform structure coupler with the perturbative method. This model is too simple to use in the design of the MSC. In this dissertation, the first step was to develop the supermode analysis for two-mode fiber couplers. Then, the transmissions of two-mode couplers were obtained by using the transfer matrix method. Furthermore, the mode separating conditions were derived. The numerical techniques such as the finite difference method and FMEM were used to design the MSC made by the polishing method, fusion and tapering method, and other various methods. Finally, the all-fiber mode separating coupler was realized by the fusion and tapering method.

For the MSC made by the polishing method, simulation results show that it is possible to realize the mode separation with a uniform or parabolic structure but the fabrication requirements are very strict. The fibers used in the polishing method could be circular or elliptical core. Relatively, using an elliptical core fiber has some advantages such as large precision tolerance on the coupler length.

For the MSC made by the fusion and tapering method, the first step was to model the coupler longitudinal profiles under various flame widths and flame sweep distances. Then the effective indices of six supermodes were calculated with the fiber mode expansive

method, and the transmissions were obtained by the transfer matrix method. Finally, the mode separation conditions were designed for the MSCs made by circular or elliptical core fibers. In addition, the beat lengths, the birefringence and the adiabatic criteria for two-mode fiber coupler case were studied. In order to depict the transmission precisely, three hypotheses based on the experimental measurements were taken during the simulation process. First, the cross section of fiber core evolves from a circle into an ellipse after heating the two parallel fibers; second, the refractive index difference between the core and the cladding decrease as a linear function of ITR; Third, after heating, the index profile evolves from a step to a graded profile. However, for simplicity, the equivalent step profile was used. Simulation results show that the MSC made by elliptical core fibers has a shorter elongation and a shorter flame sweep distance than that made by circular core fibers. Unfortunately, the adiabatic criterion is broken down for the elliptical core fiber case, so the alternative method is proposed.

For the MSC made by the pre-etching and prepolishing methods, the simulation results demonstrated that the pre-etching and prepolishing methods could reduce the elongation and flame sweep distances, so that the adiabatic conditions could be more easily satisfied. In addition, the highly elliptical core and thermally expanded core fibers were considered to be used in the fabrication of the MSC. The numerical results show that these kinds of fibers are good at the fabrication of MSCs, especially, the highly elliptical core fibers making the mode separation conditions much simpler due to only the even LP_{11} mode propagating in it.

This dissertation reports the MSC was realized for first time by the fusion and tapering method. Compared with the one made by the polishing method, the fusion and tapering coupler demonstrates a good mechanical stability, short fabrication time and less cost. The

transfer efficiency of the LP_{11} mode depends on the beat synchronism of both orientation LP_{11} modes at certain elongation points. This beat synchronism can be adjusted by fusion time and flame sweep distance and the latter is more sensitive. The best packaged samples show this kind of mode separating coupler having a high transfer efficiency of 92.3% and low excess loss of 0.2 dB. The calculation results (shown in Fig. 5.24) match well with the experiment results (shown in Fig. 5.25); therefore the numerical analysis based on the experimental parameters and the three hypotheses proposed in this thesis was validated.

Although successful modeling and fabrication of mode separating couplers were reached in this dissertation, the deep potential and sophisticated features of these devices are presently far from being exhausted. Some improvements could be considered in the future. First, the refractive index difference between core and cladding variation with fusion time is very critical to the transmission. This variation is caused by the diffusion of the dopant in the core region. So far, there is no suitable way to obtain an accurate solution for various situations. In this dissertation, the index difference used was a typical value measured in experiment. In general, to design the mode separating coupler, it is necessary to know precisely the index difference value. Such a study could be very interesting. Second, the cross sectional shape of the fiber core after fusing is another factor affecting the transmission. The core shapes measured as an ellipse may be effected by the flame position and fusion time, but the physical mechanism and the possibility of shape-controlling still need to be investigated. Third, the fiber used in the fabrication of mode separating couplers in this dissertation was SMF28™, that is a circular core fiber, However, the simulation showed that the elliptical core fibers have better properties than circular ones in making mode separating couplers. Although the circular core could become an elliptical core after fusion, the ellipticity is still small. If the mode separating

coupler could be made directly by a highly elliptical core fiber, especially one which only supports the LP_{01} and even LP_{11} modes, the separation of the modes will be easier.

In conclusion, mode separating couplers made by the fusion and tapering method introduce many advantageous features for the improvement of optical fiber sensing systems and will play an increasingly important role in the future of optical communication systems. Following this progress, modeling and fabrication of mode separating couplers will become even more challenging.

References

[1]   B. Schmauss. (1992). Transmission of two mode coded channels in one fibre using optical directional couplers as mode selective elements. Opt. Quantum Electron., 24, 603-609.

[2]   R. C. Youngquist, J. L. Brooks, and H. J. Shaw. (1984). Two-mode fiber modal coupler. Opt. Lett., 9, 177-179.

[3]   C. D. Poole, C. D. Townsend, and K. T. Nelson. (1991). Helical-grating two-mode fiber spatial-mode coupler. J. Lightwave Technol, 9, 598-604.

[4]   B. Y. Kim, J. N. Blake, S. Y. Huang, and H. J. Shaw. (1987). Use of highly elliptical core fibers for two-mode fiber devices. Opt. Lett., 12, 729-731.

[5]   J. N. Blake, B. Y. Kim, and H. K. Shaw. (1986). Fiber-optic modal coupler using periodic microbending. Opt. Soc. Am., 11, 177-179.

[6]   F. A. Castro, S. R. M. Carneiro, O. Lisboa, and S. L. A. Carrara. (1992). Two-mode optical fiber accelerometer. Opt. Lett., 17, 1474-1475.

[7]   S. Y. Huang, J. N. Blake, and B. Y. Kim. (1990). Perturbation effects on mode propagation in highly elliptical core two-mode fibers. J. Lightwave Technol, 8, 23-33.

[8]   B. Y. Kim, J. N. Blake, H. E. Engan, and H. J. Shaw. (1986). All-fiber acoustic-optic frequency shifter. Opt. Lett., 11, 389-391.

[9]   O. Lisbou and S. L. A. Carrara. (1992). In-line acoustic-optic frequency shifter in two-mode fiber. Opt. Lett., 17, 154-156.

[10]   C. D. Poole, J. M. Wiesenfeld, and A. R. McCormick. (1992). Broadband dispersion compensation by using the higher-order spatial mode in a two-mode fiber. Opt. Lett., 17, 985-987.

[11]   S. Y. Huang, H. G. Park, and B. Y. Kim. (1989). Quadrature phase detector using two-mode waveguides. Opt. Lett., 14, 1380-1382.

[12]   J. N. Blake, S. U. Huang, B. Y. Kim, and H. J. Shaw. (1987). Strain effects on highly elliptical core two-mode fibers. Opt. Lett., 12, 732-734.

[13]   K. A. Murphy, S. Miller, A. M. Bengsarkar, and R. O. Claus. (1990). Elliptical-core two-mode optical-fiber sensor implementation methods. J. Lightwave Technol, 8, 1688-1695.

[14]   A. M. Vengsarkar, J. A. Greene, and K. A. Murphy. (1991). Photoinduced refractive-index changes in two-mode elliptical-core fibers: sensing applications. Opt. Lett, 16, 1541-1543.

[15]   W. J. Bock and T. R. Wokinski. (1990). Hydrostatic pressure effects on mode propagation in highly birefringent two-mode fibers. Opt. Lett., 15, 1434-1436.

[16]   K. Bohnert, G. C. Wit, and J. Nehring. (1995). Coherence-tuned interrogation of a remote elliptical-core, dual-mode fiber strain sensor. J. Lightwave. Tech., 13, 94-103.

[17]   T. Wilson and C. Sheppard. (1984). Theory and Practice of Scanning Optical Microscopy. London: Academic Press Inc.

[18]   J. W. B. Spillman, B. R. Kline, L. B. Maurice, and P. L. Fuhr. (1989). Statistic-mode sensor for fiber optical vibration sensing uses. Appl. Opt., 28, 3166-3176.

[19]   S. K. Sheem and J. G. Giallorenzi. (1979). Single-mode fiber-optical power divider: encapsulated etching technique. Opt. Lett., 4.

[20]   S. K. Sheem and J. H. Cole. (1979). Acoustic sensitivity of single-mode optical power divider. Opt. Lett., 4, 322-324.

[21]   F. J. Liao and J. T. Boyd. (1981). Single-mode fiber coupler. Appl. Opt., 20, 2731-2734.

[22]   D. C. Tran, K. P. Koo, and S. K. Sheem. (1981). Single-mode fiber directional couplers fabricated by twist-etching techniques (stabilization). IEEE J., QE-17, 988-991.

[23]   D. C. Tran and K. P. Koo. (1981). Stabilizing single-mode fiber coupler by using gel glass. Electron. Lett., 17, 187-188.

[24]   R. A. Bergh, G. Kotler, and H. J. Shaw. (1980). Single-mode fiber optical directional coupler. Electron. Lett, 16, 260-261.

[25]   O. Parriaux, S. Gidon, and A. A. Kuznetsov. (1981). Distributed coupling on polished single-mode optical fibers. Appl. Opt., 22, 2420-2423.

[26]   M. J. F. Digonnet and H. J. Shaw. (1982). Analysis of a tunable single-mode optical fiber coupler. IEEE. J., QE-18, 746-752.

[27]   B. K. Nayar and D. R. Smith. (1983). Monomode-polarization-maintaining fiber directional couplers. Opt. Lett., 8, 543-545.

[28]   S. Georgiou and A. C. Boucouvalas. (1985). Low-loss single-mode optical couplers. Pro. Inst. Electr. Eng., 132.

[29]   Z. Mao, X. Feng, and B. Li. (1986). Mode excitation theory and experiment of single-mode fiber directional coupler with strong coupling. J. Lightwave Tech., LT-4, 466-472.

[30]   J. D. Beasley, D. R. Moore, and D. W. Stowe. (1983). Evanescent wave fiber optic couplers: three methods. Pro. SPIE, 417, 36-43.

[31]   S. T. Nicholls. (1985). Automatic manufacture of polished single-mode fiber coupler. Electron. Lett., 21, 825-826.

[32]   C. D. Hussey and J. D. Minelly. (1988). Optical fiber polishing with a motor-driven polishing wheel. Electron. Lett., 24, 805-807.

[33]   M. J. F. Digonnet, J. R. Feth, L. F. Stokes, and H. J. Shaw. (1985). Measurement of the core proximity in polished fiber substrates and couplers. Opt. Lett., 10, 463-465.

[34]   O. G. Leminger and R. Zengerle. (1985). Determination of single-mode fiber coupler design parameters from loss measurements. J. Lightwave Tech. LT-3, 864-867.

[35]   C. A. Villarruel and M. R.P. (1981). Fused single-mode fiber access couplers. Electron. Lett., 17, 243-244.

[36]   B. S. Kawasaki and K. O. Hill. (1981). Biconical-taper single-mode fiber coupler. Opt. Lett., 6, 327-328.

[37]   M. H. Slonecker. (1982). Single-mode fused biconical taper coupler. Conf. Opt. Fiber Commun. (OFC'82). 36-37.

[38]   M. Kawachi, B. S. Kawasaki, and K. O. Hill. (1982). Fabrication of single-polarization single-mode fiber couplers. Electron. Lett., 18, 962-964.

[39]   C. A. Villarruel, M. Abebe, and W. K. Burns. (1983). Polarization preserving single-mode fiber coupler. Electron. Lett., 19, 17-18.

[40]   B. S. Kawasaki, K. O. Hill, and R. G. Lamont. (1983). Configurations, performance, and applications of biconical taper optical fiber coupler structures. Canadian J. Phys., 61, 352-360.

[41]   C. M. Ragdale and M. H. Slonecker. (1984). Review of fused single-mode coupler technology. Pro. SPIE, 479, 2-8.

[42]   J. Bures, S. Lacroix, and J. Lapierre. (1983). Analyse d'un coupleur bidirectionnel à fibres optiques fusionnées. Appl. Opt., 22, 1918-1921.

[43]   J. Bures, S. Lacroix, C. Veilleux, and J. Lapieere. (1984). Some particular properties of monmode fused fiber couplers. Appl. Opt., 23, 968-969.

[44]   F. de Fornel, C. M. Ragdale, and R. J. Mears. (1984). Analysis of single-mode fused tapered fiber couplers. Pro. Inst. Electr. Eng., 131, 221-228.

[45]   J. V. Wright. (1985). Variational analysis of fused tapered couplers. Electron. Lett., 21, 1064-1065.

[46]   A. W. Snyder. (1985). Polarizing beam splitter from fused-taper couplers. Electron. Lett., 21, 623-625.

[47]   J. M. P. Rodrigurez, T. S. M. MacLean, B. K. Gazey, and J. F. Miller. (1986). Completely fused tapered couplers: comparison of theoretical and experimental results. Electron. Lett., 22, 402-404.

[48]   K. S. Chiang. (1986). Analysis of fused couplers by the effective-index method. Electron. Lett., 22, 1221-1222.

[49]   M. H. Slonecker and J. C. Williams. (1983). Recent advances in single-mode fused taper coupler technology. Pro. SPIE, 412, 50-53.

[50]   T. Bricheno and A. Fielding. (1984). Stable low-loss single-mode couplers. Electron. Lett., 20, 230-232.

[51]   M. S. Yataki, M. P. Varnham, and D. N. Payne. (1985). Fabrication and properties of very-long fused taper couplers. Conf. Opt. Fiber. Commun. (OFC'85). 108-110.

[52]   D. C. Johnson and K. O. Hill. (1986). Control of wavelength selectivity of power transfer in fused biconical monomode directional couplers. Appl. Opt., 25, 3800-3803.

[53]   P. M. Kopera, H. H. A. Krueger, V. J. Tekippe, and D. L. Wuensch. (1984). Performance evaluation of single-mode couplers. Pro. SPIE., 479, 9-15.

[54]   I. Yokohama, J. Noda, and K. Okamoto. (1987). Fiber-coupler fabrication with automatic fusion-elongation processes for low excess loss and high coupling-ratio accuracy. J. Lightwave Techol., LT-5, 910-915.

[55] Y. Takeuchi and J. Noda. (1992). Novel fiber coupler tapering process using a microheater. IEEE Photon. Techol. Lett., 4, 465-467.

[56] Y. Takeuchi and M. Horiguchi. (1994). Microheater control of wavelength-flattened fiber coupler properties. Appl. Opt., 33, 1029-1034.

[57] Y. Takeuchi. (1996). Thermodynamic analysis of WDM fiber couplers fabricated by using a microheater. J. Non-Crystalline Solids., 202, 272-278.

[58] S. Donati, L. V. Annovazzi, and F. Picchi. (1998). Ultr-low insertion loss fused couplers fabricated by a long furnace. Pro. Workshop on Fiber Optics Passive Components (WFOPC'98). 161-164.

[59] M. Eisenmann and E. Weidel. (1988). Single-mode fused biconical couplers for wavelength division multiplexing with channel spacing between 100 and 300 nm. J. Lightwave. Technol., LT-6, 113-118.

[60] F. Gonthier, S. Lacroix, X. Daxhelet, R. J. Black, and J. Bures. (1989). Broadband all-fiber filters for wavelength-division-multiplexing application. Appl. Phys. Lett., 54, 1290-1292.

[61] J. Bures, D. Ricard, and S. Lacroix. (1994). All-fiber dense Wavelength Division Multiplexes. Opto-electronic science and engineering (ICOESE'94). 455-457.

[62] T. Bricheno and V. Baker. (1985). All-fibre polarisation splitter/combiner. Electron. Lett., 21, 251-252.

[63] Y. Namihira. (1986). Polarisation beam-splitter and combining characteristics of fused-taper single-mode fiber couplers. Electron. Lett., 22, 715-716.

[64] I. Yokohama, K. Okamoto, and J. Noda. (1985). Fiber-optic polarisation beam splitter employing birefringent-fibre coupler. Electron. Lett., 21, 415-416.

[65]   I. Yokohama, K. Okamoto, and J. Noda. (1986). Analysis of fiber-optic polarizing beam splitters consisting of fused-taper couplers. J. Lightwave Technol., LT-4, 1352-1359.

[66]   F. Bilodeau, S. Faucher, K. O. Hill, and D. C. Johnson. (1986). Wavelength, polarization and mechanical properties of compact, low-loss fused fiber beam splitters: fabrication and overcoupled operation in many orders. ECOC'86. 129-132.

[67]   J. D. Love and M. Hall. (1985). Polarization modulation in long couplers. Electron. Lett., 20, 784-785.

[68]   F. P. Payne, C. D. Hussey, and M. S. Yataki. (1985). Modeling fused single-mode fiber couplers. Electron. Lett., 21, 461-462.

[69]   A. W. Snyder and X. Zheng. (1985). Fused couplers of arbitrary cross-section. Electron. Lett., 21, 1079-1080.

[70]   W. V. Sorin, B. Y. Kim, and H. J. Shaw. (1986). Highly selective evanescent modal filter for two-mode optical fibers. Opt. Soc.Am., 11, 581-583.

[71]   A. Kumar, U. K. Das, R. K. Varshney, and I. C. Goyal. (1990). Design of a mode filter consisting of two dual-mode highly elliptical core fibers. J. Lightwave Technol., LT-8, 34-38.

[72]   G. Thursby, D. Walsh, W. C. Michie, and B. Culshaw. (1994). An in-line mode splitter applied to a dual polarimeter in elliptical core fiber. Tenth International Conference on Optical Sensors. 339-342.

[73]   S. Barcelos, M. N. Xervas, and P. S. J. Russell. (1995). Selective excitation of fiber-modes using surface plasmons. IEEE Photon. Technol. Lett, 7, 1051-1053.

[74]   R. D. Pechstedt, P. S. J. Russell, and F. D. Lioud-Lucas. (1995). Selective coupling of fiber modes with use of surface-guided Bloch modes supported by dielectric multilayer stacks. Opt. Soc. Am., 12, 2655-2659.

[75]   M. S. Whalen and T. H. Wood. (1985). Effectively nonreciprocal evanescent-wave optical-fiber directional coupler. Electron. Lett., 21, 175-176.

[76]   A. W. Snyder and J. D. Love. (1983). Optical Waveguide Theory: Chapmanand Hall.

[77]   M. S. Saad. (1985). Review of numerical methods for the analysis of arbitrarily-shaped microwave and optical dielectric waveguides. IEEE Trans.Microwave Theory Tech., MTT-33, 894-899.

[78]   D. Marcuse. (1991). Dielectric Optical Waveguides: Academic, San.Diego, Calif.

[79]   C. Vassallo. (1991). Optical Waveguide Concepts: Elsevier, Amsterdam.

[80]   K. S. Chiang. (1994). Review of numerical and approximate methods for the modal analysis of general optical dielectric waveguides. Opt. Quantum Electron., 26, s113-s134.

[81]   M. D. Feit and J. J. A. Fleck. (1981). Propagating beam theory of optical fiber cross coupling. J. Opt. Soc. Am, 71, 1361-1372.

[82]   W. Huang, C. Xu, S. Chu, and S. Chaudhuri. (1992). The finite-difference vector beam propagation method: analysis and assessment. J. Lightwave Technol., 10, 295-305.

[83]   E. E. Kriezis and A. G. Papagiannakis. (1995). A joint finite-difference and FFT full vectorial beam propagation scheme. J. Lightwave Technol., LT-13, 692-700.

[84]   S. Lacroix, F. Gonthier, and J. Bures. (1994). Modeling of symmetric 2X2 fused-fiber couplers. Appl. Opt., 33, 8361-8369.

[85]   C. H. Henry and B. H. Verbeek. (1989). Solution of scalar wave equation for arbitrary shaped dielectric waveguide by two-dimensional Fourier analysis. J. Lightwave Techol., LT-7, 308-313.

[86]   T. F. Jablonski and M. J. Sowinski. (1989). Analysis of dielectric guiding structures by the iterative eigenfunction expansion method. IEEE Trans. Microwave Theory Tech., 37, 63-70.

[87]   C. Chang and H. Chang. (1996). Analysis of modal cutoffs of radially inhomogeneous two-core optical fibers by circular harmonics expansion method. J. Lightwave Techol., LT-4, 2804-2812.

[88]   X. Daxhelet, S. Lacroix, and F. Gonthier. (1997). Fibre mode expansion for 2-D waveguide calculations. Opt and Quantum Electron, 29, 139-150.

[89]   M. S. Stern, C. L. Xu, F. Ma, and W. P. Huang. (1995). The use of a sparse matrix eigenmode solver in semivectorial finite difference modeling of optical waveguides. Integrated photonics Research

[90]   H. A. Van der Vorst. (1992). BI-CGSTAB a fast and smoothly converging variant of BI-CG for the solution of nonsymetric linear systems. SIAM J. of Sci. Stat. Comput., , 631-644.

[91]   W. Q. Thornburg, B. J. Corrado, and X. D. Zhu. (1994). Selective launching of higher-order modes into an optical fiber with an optical phase shifter. Opt. Lett., 19, 454-456.

[92]   C. D. Hussey and T. A. Birks. (1988). Fabrication of wavelength-flattened tapered couplers using polishing for cladding removal. Electron. Lett., 24, 1072-1073.

[93]   L. Eyges and P. Wintersteiner. (1981). Modes of an array of dielectric waveguides. J.Opt.Soc.Amer., 71, 1351-1360.

[94]   C. V. Cryan, K. P. Oakley, and C. D. Hussey. (1993). Wavelength-insensitive fused polished couplers. Electron. Lett., 29, 1163-1165.

[95]   R. P. Dahlgren and N. H. Katis. (1993). Computer-controlled technique for cutting curved grooves in polished fiber-optic coupler substrates. IEEE Photon. Technol. Lett, 5, 1227-1230.

[96]   R. J. Black, F. Gonthier, S. Lacroix, and J. Bures. (1987). Tapering fiber: an overview. Pro. SPIE. 2-19.

[97]   W. K. Burns, M. Abebe, and C. A. Villaruel. (1985). Parabolic model for shape of fiber taper. Appl. Opt., 24, 2753-2755.

[98]   T. A. Birks and Y. W. Li. (1992). The Shape of Fiber Tapers. J. Lightwave Technol., 10, 432-438.

[99]   F. Gonthier. (1993). "Conception et réalisation de coupleurs multi-fibres intégrés à des fibres optiques unimodales," Ph.D thesis in Ecole Polytechnique. Montréal Universite .

[100]   C. P. Botham. (1988). Theory of tapering single-mode optical fibres by controlled core diffusion. Electron. Lett., 24, 243-244.

[101]   C. P. Botham and J. S. Harper. (1989). Design of adiabatic tapers by controlled core diffusion. Electron. Lett., 25, 1520-1522.

[102]   M. N. Mclandrich. (1988). Core dopant profiles in weakly fused single-mode fibres. Electron. Lett., 24, 8-10.

[103]   K. Shiraishi, Y. Aizawa, and S. Kawalami. (1990). Beam expanding fiber using thermal diffusion of the dopant. J. Lightwave Technol., 8, 1151-1161.

[104]   K. Shiraishi, T. Yanagi, and S. Kavakami. (1993). Light-propagation characteristics in thermally diffused expanded core fibers. J. Lightwave Technol., 11, 1584-1591.

[105] F. Gonthier, S. Lacroix, and J. Bures. (1994). Numerical calculations of modes of optical waveguides with two-dimensional refractive index profiles by a field correction method. Opt. Quantum Electron, 26, s135-s149.

[106] C. Yeh. (1976). Modes in weakly guiding elliptical optical fibres. Opt. Quantum Electron., 8, 43-47.

[107] L. Eyges, P. Gianino, and P. Wintersteiner. (1979). Modes of dielectric waveguides of arbitrary cross sectional shape. J. Opt. Soc. Am, 69, 1226-1235.

[108] S. R. Rengarajan and J. E. Lewis. (1980). First higher-order mode cutoff in two-layer elliptical fiber waveguides. Electron. Lett., 16, 263-264.

[109] J. K. Show, W. M. Henry, and W. R. Winfrey. (1995). Weakly guiding analysis of elliptical core step index waveguides based on the characteristic numbers of mathieu's equation. J. Lightwave Technol., 13, 2359-2371.

[110] J. D. Love, W. M. Henry, W. J. Stewart, R. J. Black, S. Lacroix, and F. Gonthier. (1991). Tapered single-mode fibres and devices Part 1: Adiabaticity criteria. IEE Proc. Pt. J., 138, 343-354.

[111] R. J. Black, S. Lacroix, F. Gonthier, and J. D. Love. (1991). Tapered single-mode fibres and devices Part 2: Experimental and theoretical quantification. IEE Proc. Pt. J., 138, 355-364.

[112] R. G. Lamont, K. O. Hill, and D. Johnson, C. (1985). Tuned-port twin biconical-taper fiber splitters: fabrication from dissimilar low-mode-number fibers. Opt. Lett., 10, 46-48.

[113] C. V. Cryan and C. D. Hussey. (1992). Fused polished single mode fibre couplers. Electron. Lett., 28, 204-205.

[114] C. V. Cryan and C. D. Hussey. (1992). Bending of fused polished couplers. Electron. Lett., 28, 2104-2106.

[115] N. M. O'sullivan, T. A. Birks, and C. D. Hussy. (1992). Wavelength-flattened response in bent fibre couplers'. Electron. Lett., 28, 204-205.

[116] J. T. Krause, W. A. Reed, and K. L. Walker. (1986). Splice loss of single-mode fiber as related to fusion time, temperature, and index profile alteration. J.Lightwave Technol., LT-4, 837-840.

[117] J. S. Harper, C. P. Botham, and S. Hornung. (1988). Tapering single-mode optical fibres by controlled core diffusion. Electron. Lett., 24, 245-246.

[118] H. Hanafusa, M. Horiguchi, and J. Noda. (1991). Thermally-diffused expanded core fibers for low-loss and inexpensive photonic components. Electron. Lett., 27, 1968.

[119] M. Kihara, S. Tomita, and M. Matsumto. (1992). Loss characteristics of thermally diffused expanded core fiber. Photon. Technol. Lett., 4.

[120] H. F. Taylor. (1984). Bending Effects in Optical Fibers. J. Lightwave Technol., LT-2, 617-628.

[121] H. G. Park and B. Y. Kim. (1989). Intermodal coupler using permanently photoinduced grating in two-mode optical fiber. Electron. Lett., 25, 797-799.

[122] M. Imai and E. H. Hara. (1975). Excitation of the fundamental and low-order modes of optical fiber waveguide with Gaussian beams.2: offset beams. Appl. Opt., 14, 169-173.

[123] M. A. Arbore, M. J. F. Digonnet, and R. H. Pantell. (1996). Analysis of the insertion loss and extinction ration of two-mode fiber interferometer devices. Opt. Fiber Technol., 2, 400-407.

[124] T. Ozeki, T. Ito, and T. Tamura. (1975). Tapered section of multimode cladding fibers as mode filters and mode analyzers. Appl. Phys. Lett, 26, 386-388.

[125] Y. Suematsu and K. Furuya. (1975). Quasi-guided modes and related radiation losses in optical dielectric waveguides with external higher index surroundings. IEEE Trans., MTT-23, 170-175.

[126] Y. Katsuyama. (1979). Single-mode optical propagation in 2-mode region of optical fiber by using mode filter. Electron. Lett., 15, 442-444.

[127] D. Marcuse. (1976). Curvature loss formula for optical fibers. J. Opt. Soc. Am., 66, 216-219.

[128] A. W. Snyder, I. White, and D. J. Mitchell. (1975). Radiation from bent optical waveguides. Electron. Lett., 11.

[129] R. Morgan, J. S. Barton, P. G. Harper, and J. D. C. Jones. (1990). Wavelength dependence of bending loss in monomode fibers: effect of the buffer coating. Opt. Lett., 15, 947-949.

[130] Y. Murakami and H. Tsuchiya. (1978). Bending losses of coated single-mode optical fibers. IEEE J. Quantum Electron., 14, 495-501.

[131] A. J. Harris and P. F. Castle. (1986). Bend loss measurements on high numerical aperture single-mode fibers as a function of wavelength and bend radius. J. Lightwave Technol., LT-4, 34-40.

[132] I. Valiente and C. Vassallo. (1989). New formalism for bending losses in coated single-mode optical fibers. Electron. Lett., 25, 1544-1545.

[133] H. Renner. (1992). Bending losses of coated single-mode fibers: A simple approach. J. Lightwave Technol., 10, 544-551.

[134] L. Faustini and G. Martini. (1997). Bend loss in single-mode fibers. J. Lightwave Technol., LT-15, 671-679.

[135] A. B. Sharma, A.-H. Al-Ani, and S. J. Halme. (1984). Constant-curvature loss in monomode fibers: an experimental investigation. Appl. Opt., 23, 3297-3301.

[136]   D. Marcuse. (1981). Principles of optical fiber measurements. New York: Academic Press.